PolyCMUTs for ultrasonic nondestructive testing of carbon fiber reinforced plastic – a feasibility study

B.Sc. Jonas Welsch

17.12.2019

Prof. Dr. Ing. Heinz Voggenreiter

Institut für Flugzeugbau
Universität Stuttgart
Institut für Leichtbauproduktionstechnologie
Deutsches Zentrum für Luft- und Raumfahrttechnik

Prof. Dr. Edmond Cretu

Electrical and Computer Engineering
University of British Columbia

Kurzfassung

In der nachfolgenden Thesis wurde untersucht ob die Technologie der PolyCMUTs, neuartige Ultraschallsensoren, für die zerstörungsfreie Werkstoffprüfung verwendet werden kann. Hierfür wurden zuerst die theoretischen Werte errechnet, danach wurden mit Hilfe einer Testplatte aus CFK und einem herkömmlichen Ultraschallprüfkopf erste Tests durchgeführt und im Anschluss wird erklärt wie die ersten Prototypen gefertigt wurden. Nach etlichen Problemen in der Fertigung wurde schließlich ein funktionierender luftgekoppelter Prototyp entwickelt. In der nachfolgenden Charakterisierung traten allerding unvorhergesehene Resonanzphänomene auf. Diese wurden untersucht und schließlich erklärt. Des Weiteren wurde untersucht ob und wie diese Phänomene die Fabrikation weiterer Prototypen verbessern kann. Als Ergebnis wird festgestellt das die Technologie gewaltiges Potential besitzt, allerding aktuell noch viel weitere Forschung von Nöten ist um ein kommerziell nutzbares System zu entwickeln.

Abstract

The following thesis describes the research conducted in between May and October of 2019 on the topic of PolyCMUTs and their usability for nondestructive evaluation of carbon fiber reinforced plastics. The first step was to calculate the acoustic and mechanical material properties of a provided CFRP test plate and the test of those values with a commercially available CMUT probe. The next part is the explanation of the manufacturing process of new prototypes and the many difficulties that occurred during this process. After several trials a working air coupled ultrasonic transducer was fabricated and then thoroughly characterized. The characterization showed some unexpected behaviour which was then investigated and contributed to a so-called Helmholtz resonance. The resonance phenomena was further explained and the possible benefits in PolyCMUT fabrication were evaluated. The last step was to evaluate these phenomena for further improvement to the technology. The result is that PolyCMUTs can indeed be used for NDE but they need further research and development. A commercial usage is not yet possible.

Table of contents

Nomenclature

CFRP	carbon fiber reinforced plastic
CMUT	Capacitive micromachined ultrasonic transducer
DLR	Deutsches Zentrum für Luft und Raumfahrttechnik
ECE	Electrical and Computer Engineering department
LDV	Laser doppler vibrometer
NDE	Nondestructive evaluation
NDT	Nondestructive testing
PolyCMUT	polymer based capacitive micromachined transducer
UBC	University of British Columbia
UT	Ultrasonic transducer

A	membrane surface area
a	hole radius
C	fiber stiffness coefficient
c	speed of sound
e	element size
E_L	longitudinal Youngs modulus
f	frequency
h	cavity height
n	number of holes
p	output pressure
Q	magnitude mass source
R	membrane radius
S	surface area of all holes
T	Transmission coefficient
t	membrane thickness
V	volume of the cavity
Z	acoustic impedance
δ	end correction of the membrane

λ	wavelength
ν	poisson ratio
ρ	density
σ_L	longitudinal tensile strength
ω	circular frequency

List of figures

List of tables

1. Introduction

With rise of environmental consciousness and the hunt for ever more cost savings in the last few decades new challenges for engineering have arisen: Vehicles like cars and airplanes are required to use less and less fuel to save cost and to reduce emissions and this can mainly be achieved by one design change. They need to be lighter.

The necessary reduction in weight has instigated a rise of new manufacturing materials and on the forefront of these materials is a century old concept: Composites. Composites have been used throughout history in many different variants, but the main principle is still the same. A mechanically softer but more flexible matrix is used to secure a bundle of stiffer but more brittle fibers. This combination leads to strong, lightweight materials. Modern composites include materials like glass fiber composites, aramid fiber composites and especially carbon fiber reinforced plastics (CFRP). CFRP nowadays is used in everything from cars to rockets to airplanes but it is inherently hard to manufacture. The layering of different plies, the infiltration with resin and the curing process can all produce defects inside the material not visible from the outside.

Another problem is that design safety factors have become smaller and smaller as our understanding of fracture mechanics and lifetime fatigue grew. Both problems lead to a need to test those materials and components without destroying them. Nondestructive evaluation methods were first used in aircraft production in the second world war for quality control and the very first of these methods was the testing with ultrasound. In modern times NDE is not only used for quality assurance but also for life cycle management of critical components. The idea of damage tolerant design instigates the need for NDE to asses how critical a discovered damage is and how much fatigue damage occurred over a certain life time.

Over the decades more and more NDE methods have been developed. X-ray, thermography, magnet resonance tomography and many more but none could replace the classic method of ultrasound testing. It is still cheaper and faster than most of the other techniques.

The way to produce ultrasound has been the same for nearly a century: piezoelectric crystals are cut in a way that they produce a desired frequency if excited by an electric signal. This method is expensive, and the resulting images are not very precise. However, in the early 90s a revolution started: Capacitive micromachined ultrasonic transducers were developed, promising new and exciting possibilities with lower fabrication cost, better resolution and nearly unlimited possibilities in geometries. Just as the first CMUT probes become commercially available another evolution surfaced: a research group at the University of British Columbia under Professors Robert Rohling and Edmond Cretu and with the work of then PhD student Carlos Gerardo developed a CMUT made of polymer. The new material meant a decrease in manufacturing cost by a factor of 10 and a significant increase in energy efficiency.

The question for this thesis now is: Can this new ultrasonic transducer be adapted for the use in nondestructive testing? The following pages give at least a glimpse at an answer and the challenges facing the project.

2. Current state of technology

2.1 Ultrasonic history

The history of ultrasound research is a long, sometimes glorious, sometimes frustrating one. It is marked by massive improvements caused by extensive sharing of research during the last half of the 19th century and 2 world wars but also considerable drawbacks through lack of funding and several legal battles.

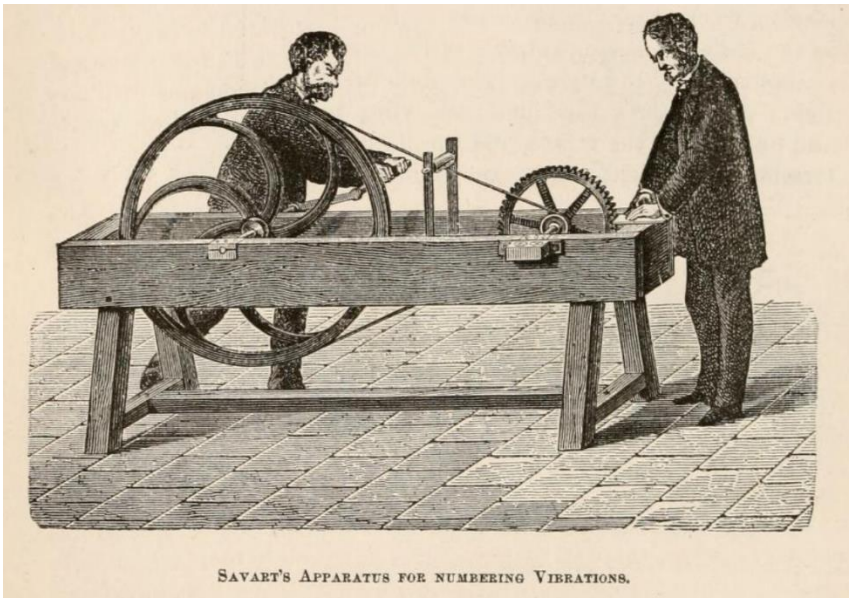

FIGURE 1: THE FIRST ULTRASONIC GENERATOR, THE SAVART WHEEL, ILLUSTRATED IN THE POPULAR SCIENCE MONTHLY IN 1873

The basis for ultrasonic research was contributed to by observations and theories published by some of the biggest names in science including Newton, Laplace and Lagrange but the real first work on actual ultrasonics was undertaken to find the audible limit of human hearing. Felix Savart is generally acknowledged for building the first ever ultrasonic generator, a wheel with a toothed cog (Fig. 1,[1]) being able to produce frequencies up to 24,000 Hz in 1830 [2]. Further improvements in ultrasonic generators and the general acoustic theory were made by Helmholtz (1860) [3] and Kundt (1867) both researching vibrations in open air tubes [4] amongst others. Probably the most important generator of ultrasound for the 19th century was invented by Sir Francis Galton who, by filling a whistle he developed himself with hydrogen, was able to reach frequencies up to 80.000 Hz as early as 1883 [2, 5]. Although James Prescott Joule in 1847 discovered the magnetostriction effect, and the piezoelectric effect was also discovered in the 19th century by the Curie brothers [6] both were extensively researched in the following decades but were not utilized as generators for other applications as the needed electronics and the materials themselves were quite expensive at the time. [7].

To conduct scientifically accurate research in the field of acoustics one not only needs a frequency generator, but also a device to measure and check the excited acoustic waves. The standard until the age of electroacoustics used to be the sensitive flame first described by Dr. John LeConte in 1858 [2, 8] seen in *Fig. 2* [9]. Another, although at the beginning rarely used detector, was developed by Kundt in 1866 and used a sealed glass tube with very fine dust particles. If the tube got excited by an acoustic wave, the volume of the glass tube could be changed, creating a standing wave and so frequency dependent dust figures would form [2, 10].

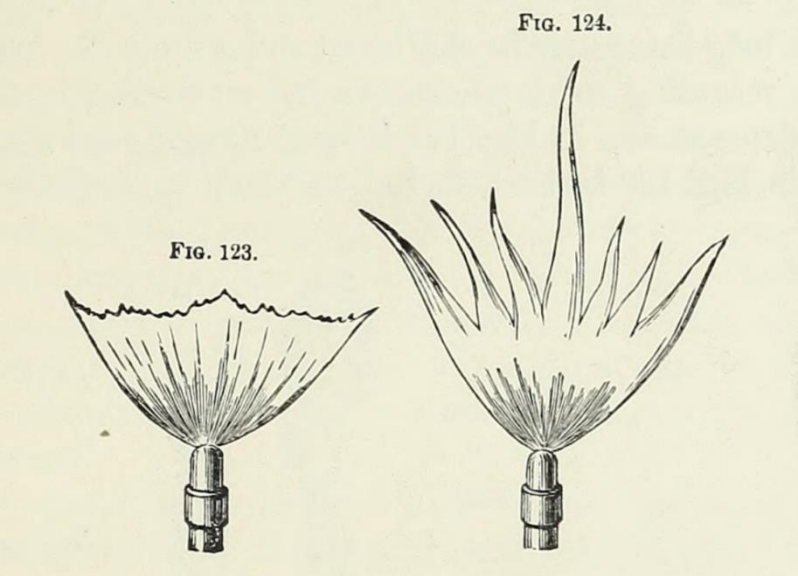

FIGURE 2: THE SENSITIVE FLAME OF A GAS BURNER, FIRST DISCOVERED BY DR. JOHN LECONTE, ILLUSTRATED IN JOHN TYNDALL'S BOOK FROM 1903

The remaining subject for the history of ultrasound in the 19th century is the theory behind it all. After the aforementioned research by Newton, Laplace and many others there were still some inexplicable phenomena especially in the propagation of waves, their absorption and the insignificant influence of the media viscosity on wave velocity. Major work in these theoretical topics were done by Stokes in 1845 but because sufficient experimental equipment was not available yet. In 1865 Helmholtz [11] and Kundt in 1968 [3] both started investigations on the velocity of sound in narrow tubes and, although using nearly similar experiments, received completely different results. Kundt concluded that the discrepancies could not only be attributed to frictional effects and suggested a major influence of heat exchange. Kundt's conclusion led Kirchhoff to further investigate heat conduction and his results showed both mechanisms were of comparable importance to attenuation but only of second order influence on sound velocity [2]. All of this culminated in Lord Rayleighs book The Theory of Sound in 1877 [12] and several following papers [13–18]. These theories and papers were so fundamental that they are cited, used and even sometimes reprinted to this day. For our case especially his paper on surface waves [18] laid the fundamentals for modern nondestructive testing. The surface waves he discovered were named Rayleigh waves in his honour and it is a testament to their relevance to this day that the reader will find them time and time again in this thesis.

At the start of the 20th century research mostly continued where it left the 19th century with most of the investigations conducted with the old methods of creating acoustic waves. Sirens, Galton whistles and other mechanical devices seemed to be the standard generators for years to come but significant improvement in electronics led to several different new concepts, all introduced in rapid succession. Tesla, Poulson, Alexanderson and Fessenden all developed high frequency generators for

communication but the most notable invention at the time was made by Lee deForest in 1907. His "Device for amplifying feeble electric currents" [19] was a compact vacuum tube that could be used as an amplifier in all kinds of electric circuits. In the beginning it was used exclusively as a sensitive detector for radio waves, its true potential unrecognized until years later. The first use as an amplifier occurred in 1912 and with improvements in vacuum pump technology from 1913-1915 it finally allowed for the development of high-power amplifiers, rendering the inventions of Tesla, Poulson and a lot of others obsolete [2]. Another major contribution was Voigt's 1910 "Lehrbuch der Kristallphysik" [20], a thorough investigation of crystals, their dielectric constants and most importantly the differential equations describing their vibrational behavior. It became a standard book for piezoelectrics in the next decades, even though he never managed to build a piezoelectric transducer himself.[2]

The next step in ultrasonic development was started by a tragedy that impacted the whole western world at the time. In 1912 the ocean liner RMS Titanic, on its maiden voyage, hit an iceberg and sunk claiming the lives of over 1500 people. Apart from new maritime regulations a lot of researcher started to focus their work on iceberg and collision detection with the most promising being acoustic ranging devices. Other investigations were focussed on underwater communication and submarine detection. The work of Lewis Fry Richardson in 1912, who patented an underwater ultrasonic ranging device, the predecessor of the later developed sonar, was probably the most important from this period [2]. Based on Richardson's work the Submarine Signaling Company (now Raytheon) under the leadership of R. A. Fessenden developed a coil activated membrane oscillator, capable to produce frequencies of 540 Hz or 1100 Hz [21–23]. Tests in 1914 showed a capability of detecting icebergs up to 2 miles away. The now renamed Fessenden oscillators were used for depth finding, iceberg warning and submarine detection throughout the entire first world war [2, 24]. An interesting fact is that this is basically an electrically activated device that produces and receives ultrasound through moving a membrane, a concept we will see again 70 years later.

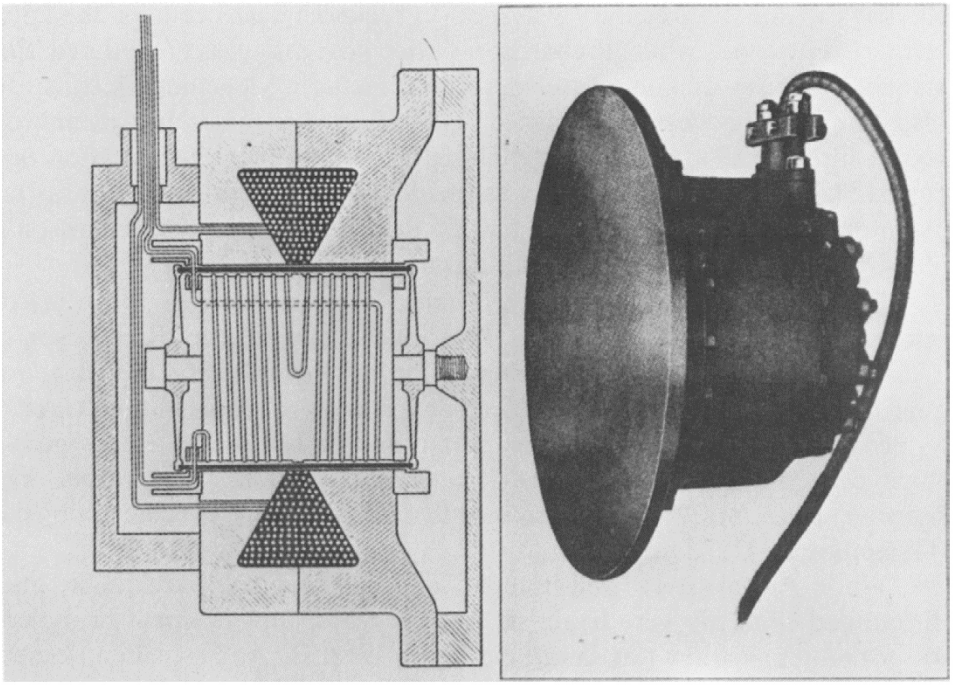

FIGURE 3: IMAGE FROM "A HISTORY OF ULTRASONICS" BY KARL F. GRAFF

Even though the Fessenden oscillator became the standard equipment for thousands of ships, research in the acoustic detection area picked up a lot of momentum especially after Germany declared the

unrestricted submarine warfare in 1915. The extensive share of research between allied Britain, the United States, Russia and France culminated in the development of the first real sonar by the French scientist Paul Langevin with the help of Russian electrical engineer M. Constantin Chilowsky. Langevin developed a steel quartz sandwich transducer with an output power of about 1 kW and for the very first time got clear echoes from submarines up to 8 km away [25]. Although the French findings were reported to their allies in June 1917 it was already too late for war time application of the apparatus [2].

After the armistice in 1918 researchers quickly reoriented their efforts and most turned to civil applications. The following 2 decades saw the use of ultrasound as a tool in scientific research, the invention of mechanical manufacturing methods using ultrasound, the improvement of piezoelectric materials and especially the development of frequency control via quartz crystals. The development mentioned last was part of the great electrical revolution and was used for decades for radio frequency control, timekeeping, telephony and other applications that need stabilized frequencies. What followed was one of the biggest legal battles over patent rights. Alexander Nicolson of AT&T and Walter Cady disputed over who developed the idea first and although Cady filed the first patent in 1921, Nicolson won the lawsuit in 1940. It took another 13 years until 1953 for Cady to be finally recognized as the true inventor [26]. Another setback produced was the legal battle between the US Army and Paul Langevin over compensation for the war time development which led the latter to abandon his research on submarine detection and to strictly follow civil applications [27].

In the years immediately before World War 2 some significant progress appeared. From 1928 to 1930 a lot of high-power ultrasonics and their effects on organic materials were investigated, with the idea of using ultrasound to heat up tissue for medical appliances. Another most important development was made in Soviet Russia. S. Ya. Sokolov published the first paper on the use of ultrasound for flaw detection in materials, effectively creating the field of ultrasonic nondestructive testing (NDT) [2, 28, 29]. With the outbreak of the war and Germanys extensive use of submarine warfare allies Britain, the US and even the Soviet Union once again started sharing results. The main focus was again submarine detection but with the introduction of ever more complex machines which considerable numbers of lives were dependent on, new technologies in NDT were desperately needed [2, 30]. Early NTD generators, or nondestructive evaluation (NDE) as it became known later, all used continuous, transmissive methods that would register decreases in radiation intensity and therefore material flaws. The many problems with this technique were, amongst others, that the tests always required geometry access from both sides, standing waves could develop and render certain parts untestable and the general sensitivity and robustness of the system was not very high. Although pulse-echo methods were mentioned pretty early into the development of NDE they were not feasible as the electronics were not yet able to detect the very fast response echoes. Their response time for submarine detection was more than sufficient with the distances usually being several kilometers but the extremely fast response of metals and other thin geometries was just to fast. The revolution came with the development of new electronics for radar detection and so in 1942 Floyd Firestone in the US applied for the first patent using a pulse echo mechanism [31]. Donald Sproule in the UK and Sokolov filed similar patents at about the same time but because this research was deemed top secret it was not shared between those nations and even the patents stayed secret until years later [2, 32, 33].

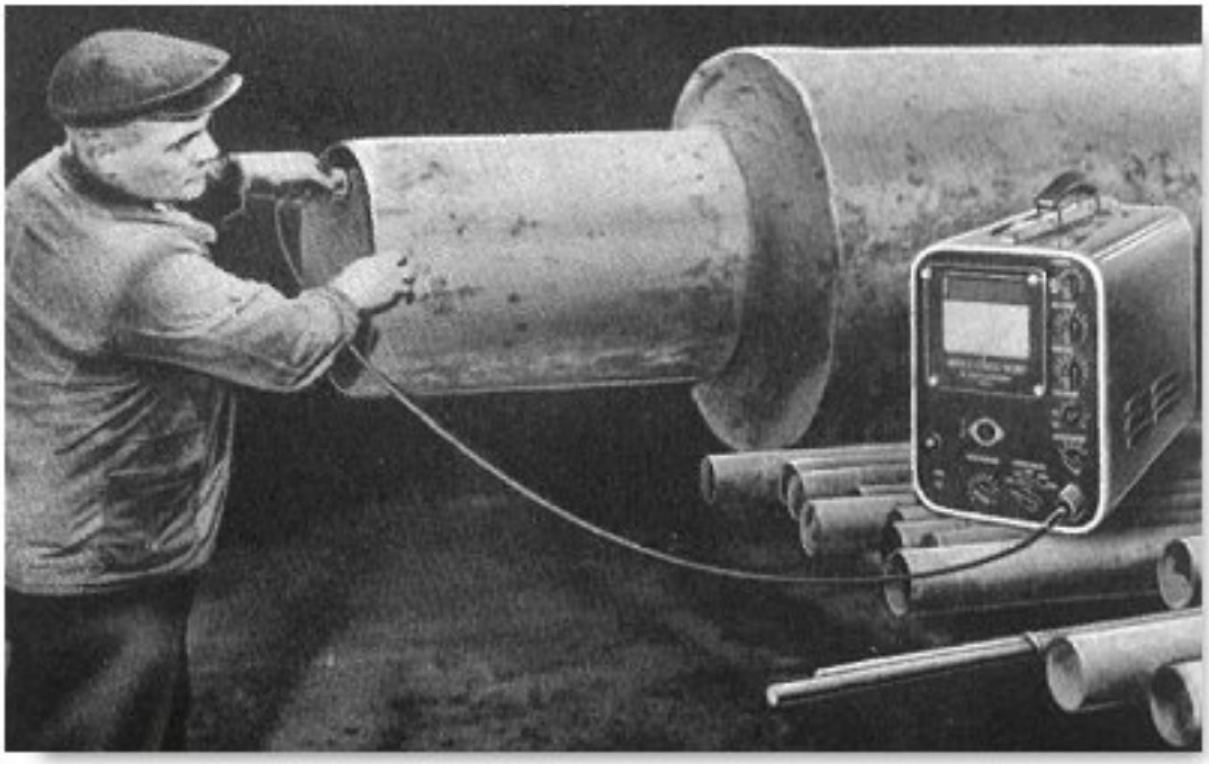

FIGURE 4: EARLY NDE TRANSMISSION TESTING WITH A KRAUTKRÄMER APPARATUS AROUND 1950. IMAGE TAKEN FROM WWW.OB-ULTRASOUND.NET

All these first NDT machines used an oscilloscope to display the frequency response (Fig. 5,[34]), a displaying technique that in modern ultrasonics is called an A-Mode, or amplitude mode, image. The first B-Mode image was developed by Donald Erdman in 1952, after also developing the now widely used immersion techniques in 1948 [2, 29]. The brightness mode (B-Mode) produces a 2D image out of several single scans, mostly from arrays. Immersion NDE means that the ultrasonic transducer (UT) and the part one wants to test are immersed in water. This significantly reduces the needed power as the impedance mismatch between transducer and water is not as grave as between air and transducer. More on both topics will follow later on. Because of the ever increasing demand for piezo crystals, mainly quartz, meant that soon the supply in high quality crystals became sparse. The discovery of easily producible piezo ceramics helped to insure a steady supply for the quickly rising demand. Other topics researched at the time included medical imaging, ultrasonic cleaning, welding, flow meters, liquid sensors burglar alarms and flame sensors. Not everything was practical but the early 50s were a golden age for new ultrasonic inventions [2].

With the basics set, the next decades saw mostly improvement of the aforementioned applications. Transducers became smaller and smaller, the increased computational power meant better and better images and new coupling materials between UT and piezo ceramics meant a constantly increasing efficiency. For decades some of the problems could not be solved though: the prices for better and smaller ceramics kept rising and air coupled energy efficient pulse echo methods seemed to be unattainable due to the high impedance mismatch [30, 33, 35, 36]. The current piezoelectric transducers will in the following chapters be named PMUTs or piezoelectric micromachined ultrasonic transducers.

The next real step in UT development was the invention of capacitive micromachined ultrasonic transducers or CMUTs. Named subminiature condenser microphones by their inventors Dietmar Hohm

and Gisela Hess in 1989 [37] it is a vibrating membrane that is activated by its capacitance as seen in Fig. 6. Interestingly the basic working principle is not far of to a Fessenden oscillator, developed nearly 90 years earlier, just a lot smaller. CMUTs offer cheaper production cost, higher bandwidth, more flexibility for array geometries and a naturally better impedance match with air. A big drawback however is that CMUTs are not really viable for high power ultrasound. This is due to the gap size between the electrodes in the range of μm, which is necessary because otherwise the needed voltages for the electric fields activating the vibrations would be too high. [38] Ultrasound today is used in a wide range of fields, including Medicine, Aerospace manufacturing, Naval sensors, distance sensors for cars and machinery and many others.

2.2 Ultrasound in general

Ultrasound, as mentioned earlier, is usually defined as being an acoustic and therefore mechanical wave with a frequency above the hearing threshold audible by humans. This threshold lies in between 20 Hz to 20,000 Hz, making 20 kHz the lowest ultrasonic frequency. To fully understand the phenomena and physical limitations described in this master thesis, we first must understand what a mechanical wave is, how it's created and what the general rules of propagation are. A good description is given by one of the pioneers of ultrasound research, J. D. Achenbach in his 1993 book "The Evaluation of Materials and Structures by Quantitative Ultrasonics":

'Mechanical waves originate in the forced motion of a portion of deformable medium. As elements of the medium are deformed, the disturbance is transmitted from one point to the next and the disturbance, or wave, progresses through the medium. In this process the resistance offered to motion offered by inertia must be overcome. As the disturbance propagates through the medium it carries along amounts of energy in the forms of kinetic and potential energies. Energy can be transmitted over considerable distances by wave motion. The transmission of energy is effected because motion is passed on from one particle to the next. Mechanical waves are characterized by the transport of energy through motions of particles about an equilibrium position.' [39]

This admittedly rather lengthy definition mentions most of the must know phenomena and especially the boundaries of ultrasound. The forced motion described in the first sentence is what creates the wave. These forced motions can either be induced purely mechanical, through magnetostriction or piezoelectric effects. Examples of these excitation methods were given in chapter 2.1. Another piece of information in this sentence is the deformable medium itself. This mentions the main difference between electromagnetic and mechanical waves: they can not travel in vacuum.

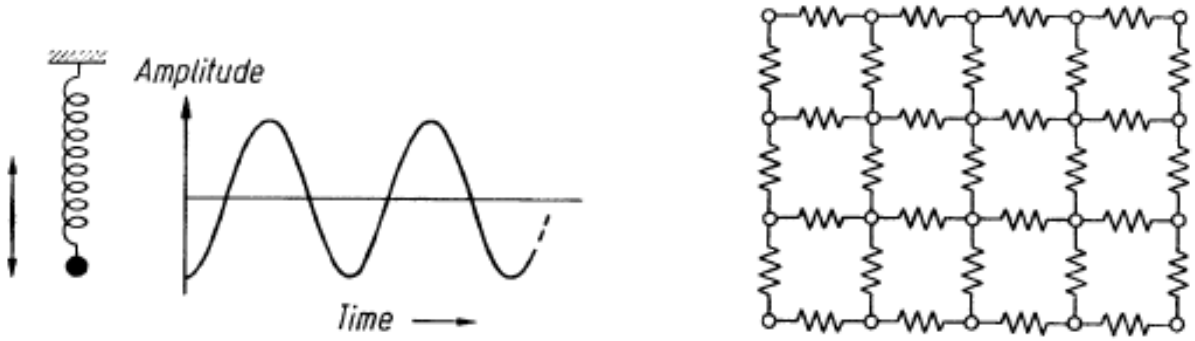

FIGURE 5: MODELS OF AN ELASTIC BODY TAKEN FROM ULTRASONIC TESTING OF MATERIALS, KRAUTKRÄMER & KRAUTKRÄMER 1990.

The second sentence of Achenbach's definition focuses on the mechanism of wave propagation. The mentioned deformation or disturbance can also be described as a forced motion out of the element's equilibrium position. This forces all neighboring elements to follow as to create a new equilibrium position. The simplest mathematical approximation for this, is a model of single elements with springs fitted in between as shown in Fig. 6 [29]. Although this model is not entirely correct as it neglects thermal and nonlinear phenomena, for this case it is a good enough approximation, as the very small excitations from ultrasound do not facilitate any nonlinear deformations in the micromechanical model [30].

The mentioned moment of inertia that must be overcome is the physical background of what is called acoustic impedance (Z). It describes the resistance offered to mechanical waves while traveling in a medium and especially while transferring from one medium to the other. It is dependant on the specific speed of sound and the density of the medium it travels through. When a sound wave travels from one material to the other and the have very different impedances it is called an impedance mismatch. If the mismatch is big enough (e.g. air and CFRP) most of the radiation will not be transferred but reflected. This is the biggest issue for airborne ultrasound today [40, 41]. Following is an example of the transmission coefficients from a piezo crystal to air and to water:

$$Z_{\text{piezo}} = 30\ \text{MRayl}$$

$$Z_{\text{air}} = 420\ \text{Rayl}$$

$$Z_{\omega\text{ater}} = 1{,}48\ \text{MRayl}$$

$$T_{\text{piezo/air}} = \frac{2 \cdot Z_{\text{air}}}{Z_{\text{air}} + Z_{\text{piezo}}} = 0.0028\%$$

$$T_{\text{piezo/water}} = \frac{2 \cdot Z_{\text{water}}}{Z_{\text{water}} + Z_{\text{piezo}}} = 9.4\%$$

The transportation of energy from one element to another also explains the impedance problems. The smallest element one can use in this is a single molecule. In dense materials the molecules are a lot closer to each other, so it is easier to transport the energy between the elements hence the high impedance and speed of sound of, for example, metal (high means low resistance) and the low impedance for air or water.

In liquids and gases waves can only travel by compressing the element in front of them because the elements are not connected via a crystalline structure. In solids however the propagation works different. Here waves can travel in different, so called modes as the particles can move in different patterns. The most common of these modes are the longitudinal and shear waves. Longitudinal waves work in the same way as in gases or liquids, they travel through compression and decompression. Shear waves travel through transverse displacement of the elements. Compared to longitudinal waves, shear waves are usually relatively weak. For easier understanding those two modes can be seen in Fig 7 [42].

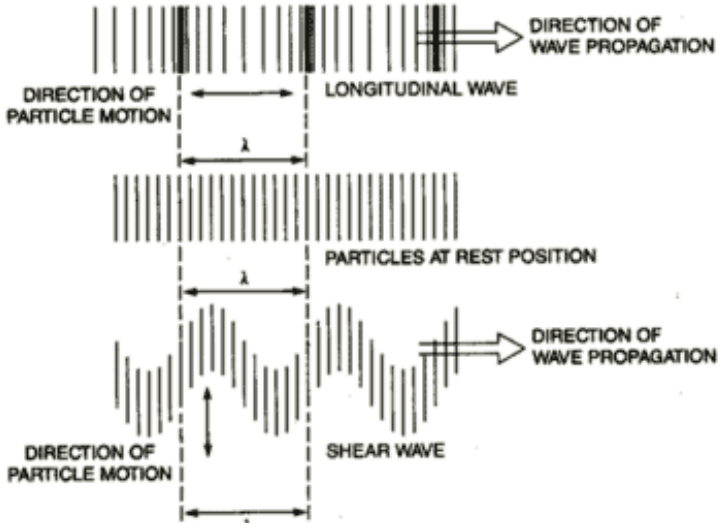

FIGURE 6: GRAPHIC DISPLAY OF LONGITUDINAL AND SHEAR WAVES

There are several different other modes, although only some of them are important for NDE so only these will be mentioned. First are the Rayleigh waves. Here the particles don't move along one axis as they do with longitudinal and shear modes but in an elliptic orbit around their equilibrium. The vibration is a combination of the first two modes with the main axis of the ellipsis perpendicular to the surface. Although they only reach a depth of about one wavelength (thus only effectively scanning near the surface), they are very useful for NDE as they are not only very sensitive to defects, but they also follow the geometry of the part reaching parts of the geometry other inspection methods can not. The last mode mentioned here are the so-called Lamb waves. The elements also move in elliptical orbits and the waves propagate along a plate or composite laminate, causing particle displacement throughout the whole thickness of the structure. Because these waves follow the part geometry, they are also called guided waves and belong to the group of waves only observable in plates or boundary layers. Both waves do excite further ultrasound waves at the adjacent medium, hence they are right now the only proven way to use ultrasound in a one sided, airborne constellation as one can use two transducers with the receiver shielded from the surface reflection of the transmitter [43–45].

When a wave propagates in a theoretically ideally elastic material, it will propagate without ever changing, but as materials are usually not ideal every propagated wave is subjected to changes. These are either changes to the waveform itself or changes to the amplitude of the wave (called attenuation or gain). Attenuation is caused by two mechanisms: First, in viscoelastic media, energy is dissipated as heat during deformation. Secondly, if the waveguide is surrounded by a medium other than vacuum, energy is transferred into that medium through the emission of ultrasound. Both mechanisms cause a continuous decrease in amplitude with growing propagation distance. Aside those material inherent mechanisms, sudden changes in the waveform and amplitude can be induced by the scattering of ultrasonic waves on macroscopic flaws, thereby enabling their detection in an ultrasonic detection process. Attenuation is usually measured in decibel (dB) which is defined as follows [46]:

$$A(\mathrm{dB}) = 20 \log_{10} \left(\frac{a}{a_0}\right) \qquad 1.1$$

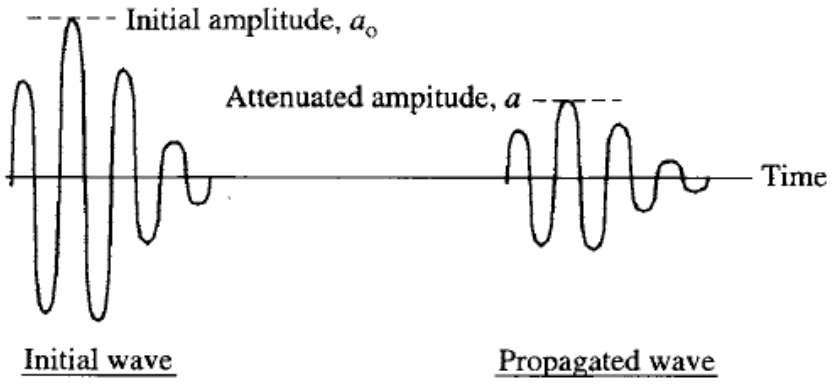

FIGURE 7: ATTENUATED WAVE. GRAPHIC TAKEN FROM ULTRASOUND AND ELASTIC WAVES- FREQUENTLY ASKED QUESTIONS

2.3 Nondestructive evaluation

With the rapid development of new technologies in the 2nd World War machines became more and more complex and ever more lives depended on them. The need to test the parts produced without limiting their load bearing capabilities became evident. The first major field was the aerospace industry as newer planes needed to be lighter to adhere to the increasing performance demand and so their critical parts could no longer be designed much stronger then actually needed as this would not allow for the needed weight reduction [30]. Early methods included dye penetrants, x-rays, eddy currents, magnetic particles and ultrasound. As mentioned in chapter 2.1 ultrasound methods were developed by all major war parties but it was still a rather prototype technique even at the end of the war.

The normal design approach would be the “safe life” design. A part must be designed in a way that over its expected lifetime no damage should occur. With NDE techniques being able to detect smaller and smaller defects, a lot of parts that were still fine for use were classified as damaged or unusable. The development of the field of fracture mechanics allowed for the first time to calculate the severity of a defect. With known material properties and a known expected lifecycle fracture mechanics allows the user to calculate if the part will fail under a certain load. This development in the early 1970s meant that parts were no longer designed with the save life approach but damage tolerant. Especially with composites and their very complex manufacturing processes, small damages and defects are nearly impossible to avoid [29, 30, 33].

The NDE methods in use today include:

Liquid penetrants: The simples and most used NDE method of this list is the use of liquid penetrants. Nearly everybody has seen the effect of the discoloring of a tiny crack in the surface of a porcelain mug. The technique is widely used in nearly every manufacturing field. Its advantages are the simplicity of the process, it is fast and very portable, it inspects nearly the complete surface at once and it shows the size and location of the defect. Drawbacks are the dependency on the skill of the operator, coatings have to be removed, poor performance on hot, cold or rough surfaces and it only detects defects on the surface [47].

Magnetic Particle Inspection: Another very simple method that works by magnetizing the part the user wants to test and the flow very fine ferromagnetic particles over the surface. The magnetic field will show disturbed patterns at the location of defects. Training for this method is easy, it is accurate and reliable, it works through thin coatings and it is very low cost. Problems include that it requires ferromagnetic test material, large parts need large currents to be magnetized and most of the test objects need demagnetization after the test [47].

Eddy Current Inspection: The best example for an eddy current inspection device is the generally known metal detector. Using two coils that produce electromagnetic fields, the materials response to said fields can be measured and thus changes in it through defects and cracks can be detected. The following Figure 9 [47] shows the interaction of the fields with a test object. It is a safe, rapid, relatively low cost and very sensitive test method. The biggest disadvantage is that it is only viable for conductive test materials and that it can only detect defects relatively close to the surface [47].

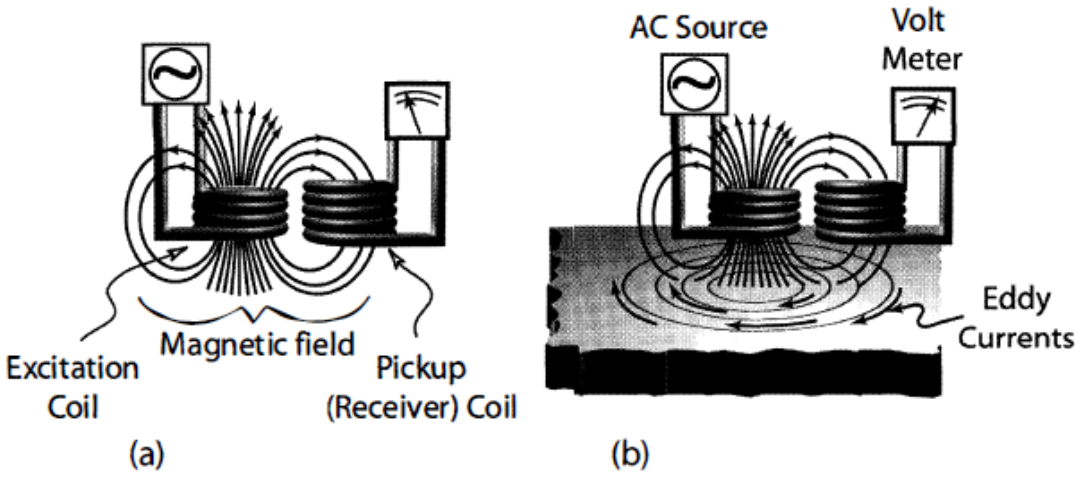

FIGURE 8: THE ELECTRIC FIELDS OF THE TWO COILS WITHOUT (A) AND WITH (B) INSPECTION MATERIAL.

Acoustic Inspection: Every material and geometry have their very own resonance frequency in which it rings when mechanically excited in a very short burst. Like a bronze bell that sounds unpleasant after it develops a crack, nearly every material can be tested that way. In older times the human ear was the detector of choice, but today hypersensitive microphones are used. The biggest drawback of this is that one needs a reference spectrum taken before the part was damaged. Another method is the nonlinear measurement which, through excitation with high energy pulses, detects the nonlinear parts of the vibration with a laser doppler vibrometer (LDV). It is currently the only method to detect closed cracks. The drawback is the very high energy needed to excite nonlinear vibration elements at the defects [48].

Radiographic Inspection: This topic includes methods using electromagnetic radiation, more accurate x-rays and computed tomography. X-rays are high energy waves fired at the part that is to be tested. Because of their high energy x-rays can easily penetrate all materials and then the attenuation of the wave by the defects can be made visible with a detector behind the test object. This technique can detect internal damages, it gives material properties such as the type of material and its density and it is usable for all materials. The problems are the very dangerous radiation, the high skill required by the operator and the very high price of the tests themselves [47].

Active Thermography: Although there are different approaches the basic parts are the same: an external heat source heats up the specimen, a thermographic camera images the resulting temperature distribution and the images should show different distributions for areas with defects. Although thermography can show defects inside of the material it is not always viable as not every specimen can cope with the thermal stresses associated with the heating. Another problem is the rather expensive equipment needed and the high skill required by the user.

There are several more methods, but these are the most widely used in modern NDE. If the reader wants to learn more on NDE the book Nondestructive Evaluation by Peter J. Shull [47] gives an excellent overview.

With the rise of welding in nearly all manufacturing fields and especially the aerospace industry it became vital to assure the quality of a weld as even critical parts are welded today. Apart from welds the biggest other field for testing are materials that are mostly anisotropic and which production processes are prone to error because of their complexity. Examples are most large composite structures as they usually need to be as light weigh as possible and monocrystalline turbine blades. As

the blades are produced, they are grown out of a single crystal and the slightest disturbance of the process will render the blade useless although it looks undamaged from the outside.

The one method not described in the list above is the one most important to this thesis. Ultrasonic NDE, as already mentioned, has been around since the 1940s and there are quite a few ways to archieve a scan. Generally we can classify in two categories:

Contact methods: In these test methods the transducer has direct contact to the specimen. Because of the high impedance mismatch there is usually a coupling medium between transducer and specimen as to get rid of the air in between. Usually it is either water, ultrasonic gel or some other kind of fluid. Transducers are ussually either single transducers in pulse echo mode, dual transducers in one casing (reciever and sender) or angle beam transducers. Dual transducers are usually used for thin materials or when the defects are expected to be close to the surface. Angle beam transducers excite shear waves, as they need to be reflected they are usually used to inspect welds. Normal contact transducers canbe used for all kinds of testing. A good example for a contact pulse echo scan is shown in Fig 10. With one scan very high resolution A, B and C-scans can be aquired. The specimen was a testplate of 7 mm thickness and is explained in greater detail later on. The used scanner was the water coupled pulse echo scanner OLYMPUS Omniscan SX.

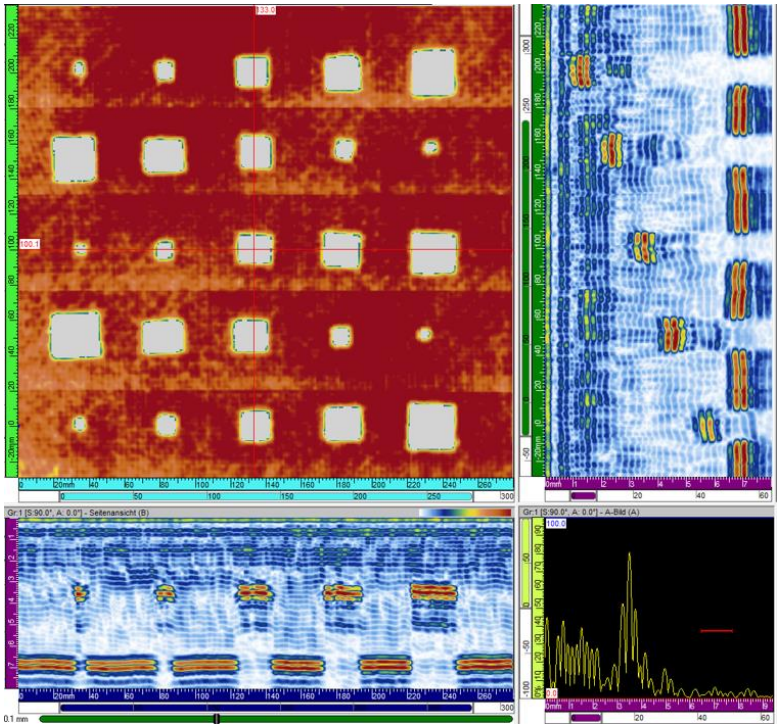

FIGURE 9: A ULTRASOUND SCAN ACQUIRED IN CONTACT MODE WITH WATER AS A COUPLING AGENT. THE BOTTOM RIGHT CORNER IS AN A-SCAN AT A CERTAIN POINT, THE BLUE PICTURES ARE B-SCANS SHOWING THE DEPTH OF THE DEFECTS AND THE LARGE RED PRINT IS THE RESULTING C-SCAN.

Non contact methods: The noncontact analysis is usually of great use when geometries are complex, surfaces are very rough or very sensitive. Usually transducer and specimen are either completely submerged in an immersion tank or they use the spray method were a laminar stream of water is sprayed against the specimen in the direction of wave propagation. Immersion test can be either in pulse echo mode or, if very high resolution is needed, in transmissive mode. Water coupled ultrasound

can use higher frequencies (as they are not absorped into air) and therefore archieves higher resolution then air coupled test methods. Air coupled test methods are either transmission scanning or lamb wave detection. Both are no pulse echo modes although lamb wave scanning is done from one side. Transmission and lamb wave scanning have the drawback that they only show the location of the defect on the 2D surface, but they can not detect it's depth. Fig. 11 shows differnet air coupled ultrasonic testing (ACUT) methods with B and C beeing Lamb wave methods, and Fig. 12 shows a comparison between lamb wave and transmission testing resoltion. Both scans were aquired from the same testplate as mentioned before.

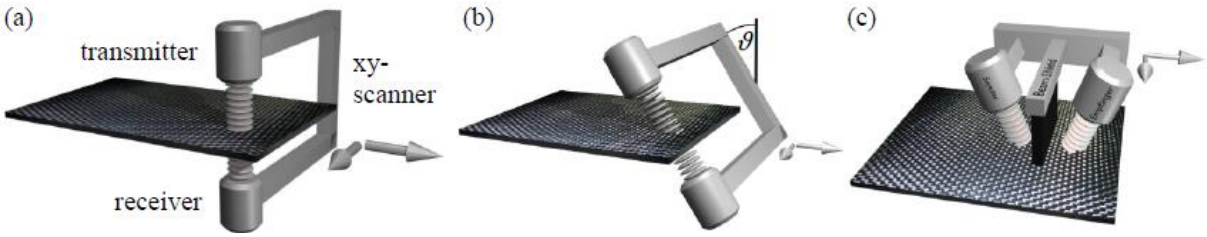

FIGURE 10: DIFFERENT ACUT METHODS: (A) TRANSMISSION (B) FOCUSED SLANTED TRANSMISSION MODE (C) FOCUSED SLANTED REFLECTION MODE

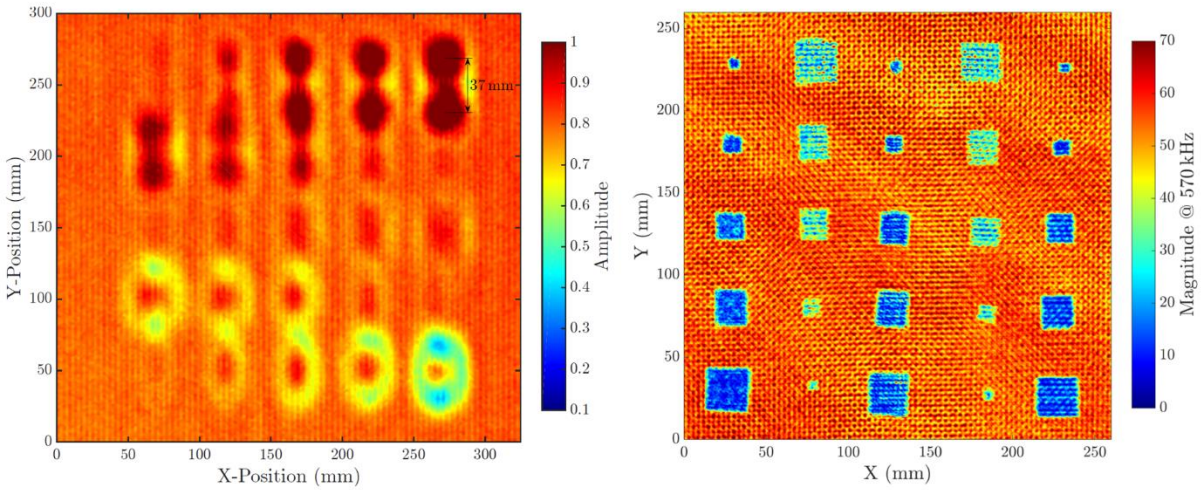

FIGURE 11: A COMPARISON BETWEEN A LAMB WAVE SCAN ON THE LEFT AND AN ACUT SCAN ON THE RIGHT

Overall the future goal of ultrasound NDE is to eliminate contact and immersion testing as both require complex and expensive hardware, are very complex to automize and not every specimen is suitable to be immersed in water [48]. Transmissive testing is sharing the same fate as in modern test requirements as acces to both sides of the specimen is not always given and 3D locating of the defect is sometimes necessary. A good example for a very recent automated testing stand was built by Airbus Helicopters München, Germany in 2011 to test their new tail rotor boom [49]. It still uses transmission mode but it is air coupled, saving all the infrastrucutre for the immersion. Otherwise industrial use is mostly limited to immersion or contact tests [45]

Special regognition should go to the lamb wave method as, although still in the prototype phase, is currently the only one sided ultrasound NDE method proven to be working. Lamb wave testing is researched by a lot of insitutions but special regocnition has to go to the German Aerospace Center

(DLR) and their automated testing process developed in their Center for Leightweight Production Technology in Augsburg Germany. To further understand how it is done and what the positive and negative aspects are a more detailed explanation of the process is needed.

In lamb wave NDE one ultrasonic transducer (UT) is used as a transmitter sending ultrasound into the specimen. This has to be done at a certain excitation angle as to actually excite lamb waves strong enough to produce the necessary signal. The receiving transducer is angled the same way to better catch the signal leaking from the surface of the plate. Both UTs are seperated by a beam shield as to not detect just the surface echo and the direct wave. As lamb waves can travel quite far and absorbtion in CFRP is not very high the focus points of the transducers on the surface should have some spacing. This can range from a few mm to several cm [44]. The following pictures show the general assembly of the 2 transducers and a automated test cell built up at the DLR in Augsburg.

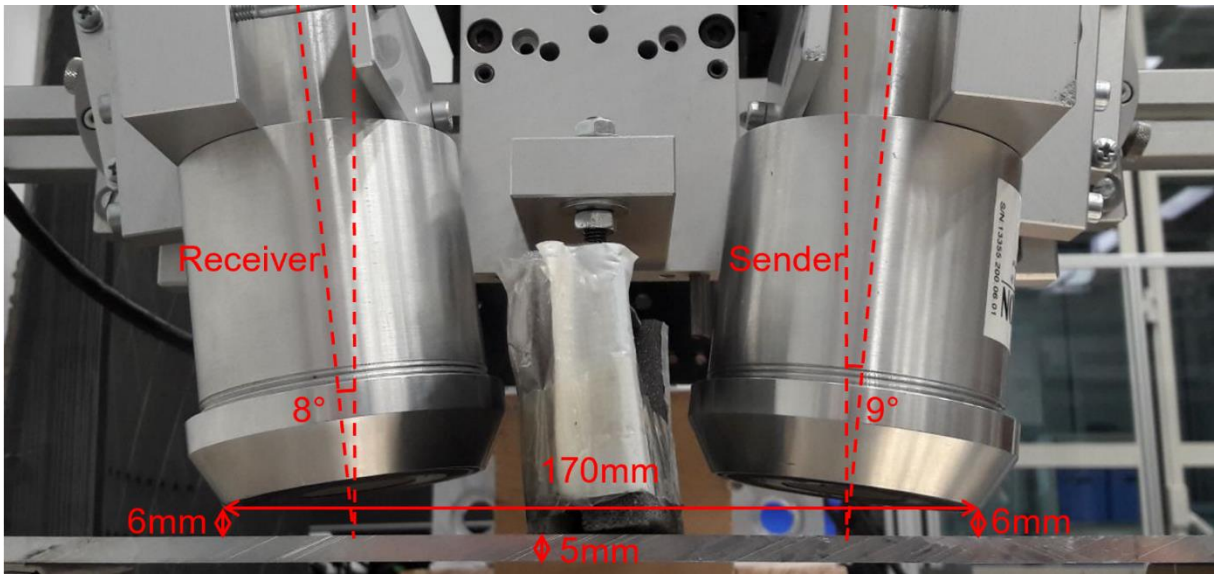

FIGURE 12: LAMB WAVE SCANNING SETUP WITH THE PROPER EXCITATION ANGLE FOR THE LAMINATE

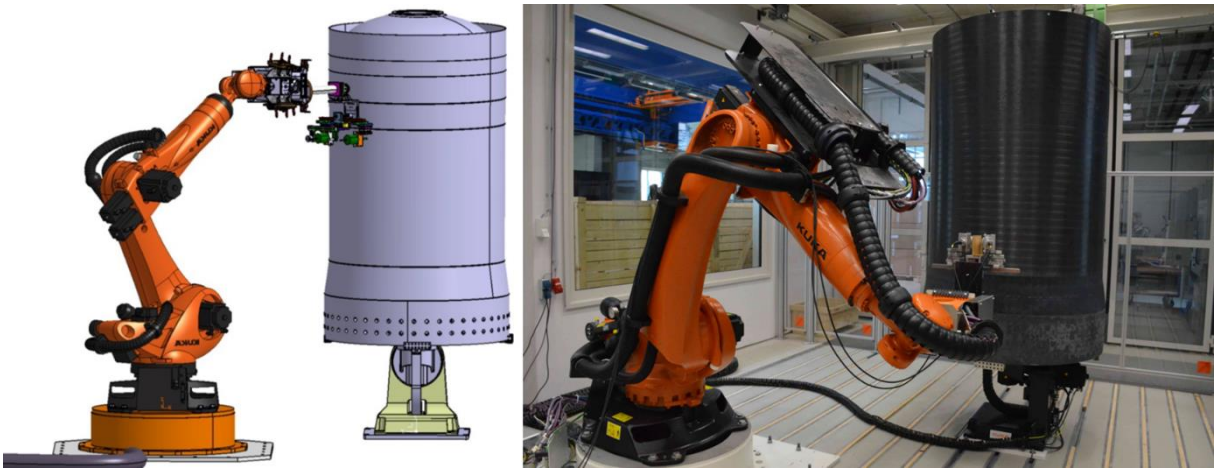

FIGURE 13: ROBOT SCANNING CELL AT DLR AUGSBURG SCANNING A ROCKET BOOSTER DEMONSTRATOR

To summarize the mentioned ultrasound testing methods and their use with composites:

Contact pulse echo:

- Very high resolution, fast, proven technology and easy to use, low power
- Produces A, B, and C-scan
- Contact to surface not always possible, coupling agent can damage specimen
- Used mostly for plates of very dense material, not usable for very porous specimen
- Good standalone automatization possibilities but not possible inline due to danger of damage to the specimen through the coupling medium

Transmission squirting/immersed:

- high resolution, proven technology, no contact with surface needed, medium power
- access to both sides necessary
- slow
- can not produce B-scan
- expensive hardware as water tanks are needed and components have to be waterproof
- good standalone automatization possibilities but no inline due to the need of water spray

Transmission ACUT:

- medium resolution, proven technology, contactless
- high power transducer needed
- access to both sides necessary
- slow
- can not produce B-scan
- Automatization possible but inline limitations due to double sided access

Lamb wave ACUT:

- One sided method, fast scanning speeds, contactless
- high power transducer needed
- Low resolution
- Can not produce B-scan
- Inline and standalone automatization possible
- For complex geometries and with changing layup the excitation angle has to be adjusted constantly

Pulse Echo ACUT:

- A, B and C-scan, one sided, contactless
- Very high automatization potential
- Not yet possible as impedance gap between air and specimen is too high

As can be seen above pulse echo ACUT would be the holy grail of NDE but the impedance gap between piezoelectric materials and air is just too big. This brings us to a recent development, the CMUTs.

2.4 The revolution – capacitive micromachined ultrasonic transducers

In 1989 Hohm and Hess developed what is nowadays recognised as the first CMUTs [37]. CMUTs are classified as micro-electro-mechanical systems (MEMS). MEMS devices are usually devices that use electrical and mechanical features but are built in the sizes of micrometers. This allows for cheap production, low power usage and a low use of space. Devices can be accelerometers, gyroscopes, flowmeters, microphones, speakers and more.

MEMS production has several processes that can be categorized as following:

Deposition: One of the first steps in nanofabrication is always the deposition process in which a building material for the structure (mostly metal, silicon, polymers or ceramics) is placed and bonded with the chosen substrate. A substrate mostly is a silicon waver, but it can basically be everything that is flat enough and that it is linking with the chosen building material. After deposition the whole substrate is covered in a uniform, even layer of the chosen building material. This can be achived via many different processes like physical vapor deposition, spin coating or chemical vapor deposition.

Patterning: Patterning is usually accomplished by a process called lithography. In lithography different forms of radiation are projected onto a radiation sensitive material (the mentioned even film). The projection creates microstructures on the substrate where, in the following process, either the exposed or non-exposed structures can be removed (depending on the material used). The radiation used can be X-rays, electron beams, ion beams, UV-light and several others. The material exposed is called a photoresist, or simply resist. The projection is achieved with so called photomasks (glass sheets with the geometry lasered on top) or maskless lithography systems.

Etching: In the process of etching the unwanted parts of the photoresist coating are removed thus creating the desired 3D structure on the substrate. Etching is generally classified in two groups: wet etching and dry etching. Wet etching usually uses some kind of fluid chemical which the sample has to be immersed into to etch away the unhardened photoresist. The chemicals can be strong acids like Hydrofluoric acid, solvents like acetone or electrochemical fluids. Dry etching is used when the desired structure can not be immersed in a fluid. It uses vapors or plasma to etch away the material.

Dicing: If a silicon waver was used as a substrate one usually produces more then one sample on its surface as wafers come in fixed sizes (150mm to 400mm). To separate the samples from each other it can be either mechanically sawn apart or cut by a laser.

The processes named above are the essential steps in microfabrication. There are some other rare processes, but these are the ones important to this thesis and they will be explained in greater detail at a later point. The first three, deposition, patterning and etching can be repeated on the same substrate several times as to create more complex, layered structures. To only selectively etch parts the sample has to be heated up (baked) several times in the processes but as before more will be explained at a later point.

Now that fabrication is explained how does a CMUT actually work? As already stated in its name a CMUT is a plate capacitor that can either act as a transmitter or a receiver. If an electrical signal is applied the capacitor will charge up and the resulting electric field will pull the top electrode towards the substrate acting as the bottom electrode. If the signal is then removed or weakened the membrane will snap back in its original state due to the stiffness of the material of the membrane. If one wants to excite a continuous signal or an ultrasonic wave, the excitation signal should be sinusoidal. If the

applied AC signal is just at a random frequency the CMUT output will be fairly limited but if the signal frequency happens to be the same as the resonance frequency of the membrane it will actually amplify

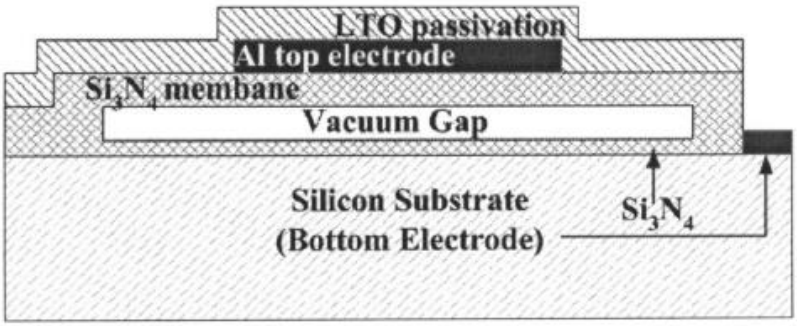

FIGURE 14: CROSS SECTION OF A CLASSIC CMUT WITH THE TOP ELECTRODE ON TOP OF THE MEMBRANE AND A PASSIVATION LAYER TO ALLOW USAGE IN FLUIDS. (TAKEN FROM ERGUN ET AL.)

the induced movement, thus increasing output pressure.

These vibration modes can be calculated, and they are dependant on the diameter, radius and thickness of the membrane and the material constants of the different components (electrode, sealant and membrane). One of the best sources on the equations in question is the book Vibration of Plates by Arthur W. Leissa [50]. The following figure shows the different vibration modes measured by a laser doppler vibrometer (LDV) on PolyCMUTs.

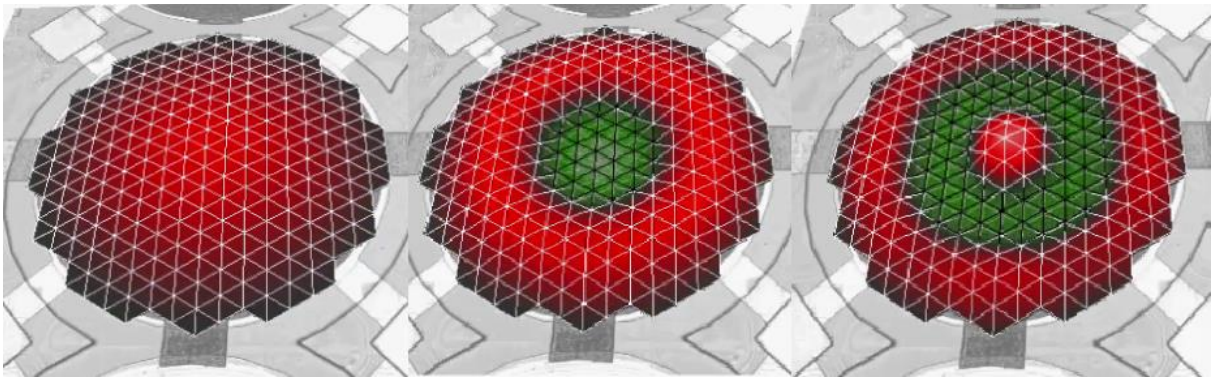

FIGURE 15: FIRST, SECOND AND THIRD VIBRATION MODE MEASURED ON A POLYCMUT WITH AN LDV

For the CMUT to work in linear operation and to be able to receive signals the plates of the capacitor, the electrodes must be charged. This is done via a DC biasing voltage. If the CMUT is biased arriving ultrasound will excite the membrane, therefore changing the distance between top and bottom electrode and thus changing the capacitance. This creates an electronic signal that can be detected [51].

After CMUTs were first developed their phenomenal performance when coupled with water was discovered. This led to a neglection of the air coupled operation regimes. Even water coupled CMUTs are still a somewhat prototype technology with the first free market products only arriving a few years ago in the medical sector [52]. In recent years the research into air coupled variants has gained more momentum as the composites market saw rapid growth and with it the demand for cheap and easy to use NDE equipment [53]. Other researchers focussed on increasing the bandwidth, output pressure, electrical efficiency or optimizing fabrication methods [35, 36, 54, 55]

2.5 The evolution – PolyCMUTs

As one can see from the mentioned manufacturing processes and materials used in CMUT production it can be very expensive and time consuming. In 2014 a research group at the Electrical and Computer Engineering department (ECE) at the University of British Columbia (UBC) under the leadership of professors Dr. Edmond Cretu and Dr. Robert Rohling were frustrated with the waiting time and cost associated with the outsourcing of prototype manufacturing of MEMS devices. Then graduate student Carlos Gerardo started looking into possibilities to produce UTs in house and at a cheaper and faster rate. The decision was made to focus on a polymer as a base material for the structures as it is printable thus faster and cheaper [56]. Several generations of prototypes later a workable PolyCMUT was produced and a paper on the development was published in Nature magazine [57] in 2018. The following description is a summarised version of said paper.

Although Gerardo et al. were not the first using a polymer to produce CMUTs, the first devices had very high operating voltages (hundreds of volts) as the effective gap between the electrodes was too high and they could not be properly sealed to be used in fluids [58]. These rendered them ineffective for uses in the medical field which the MINA group at ECE was focussing on at the time. A new fabrication process was needed.

The material chosen for the membranes was SU8 2000, a photopolymer readily available and widely used in microfabrication. It was selected due to its unique dielectric and thermal properties, its low density, optical transparency and mechanical flexibility. The next material needed was the sacrificial layer. In classic SU8 based manufacturing several different polymers, resist and even metals have been used but to stay true to the idea of developing an easy and cheap manufacturing process, the well-known OmniCoat was chosen. Although it has excellent selectivity while etching and it even enhances the adhesion of some photoresists to the substrate it is not photosensitive and it usually only results in a 5 to 15nm layer when spin coated (a 1µm layer is needed for the wanted gap size). To create a thicker layer around 85% of the solvents were evaporated, creating a thicker fluid and thus a coating thickness of 300nm at 1000RPM was achieved [57].

The processes shown in Fig. 15 [57] are the following:

First the concentrated OmniCoat is spin coated onto the substrate (a clean low resistant silicon wafer) and baked at 150°C to create a 320nm sacrificial layer. A layer of positive photoresist was then deposited on top and patterned by using a SF-100 maskless lithography system. The positive photoresist (S1813) was used to be able to selectively remove the non photosensitive OmniCoat. After etching the sample with developer (MF319) and removing the resist with acetone the structure left on the sample is the desired sacrificial layer. Plasma edging is used to remove possible residues of Omnicoat and increase adhesion to the substrate.

The second step is the spin coating of a layer of SU8 2000.5 as to create a mechanical support for the membranes and to act as an insulation between the top and bottom electrode to avoid short circuits should the membranes collapse. The membranes and etch channels are patterned onto the SU8 again using the maskless system. The sample is then postexposure baked and developed.

Step 3 starts with the deposition of AZP 4110, a photoresist used as a metal lift-off layer for the top electrode. It is again exposed and developed covering the areas that are supposed to be not covered by metal in the final product. Chromium is deposited on top at a thickness of 570nm. It was chosen because of its good adhesion to SU8 as other materials with lower electrical resistivity are harder to

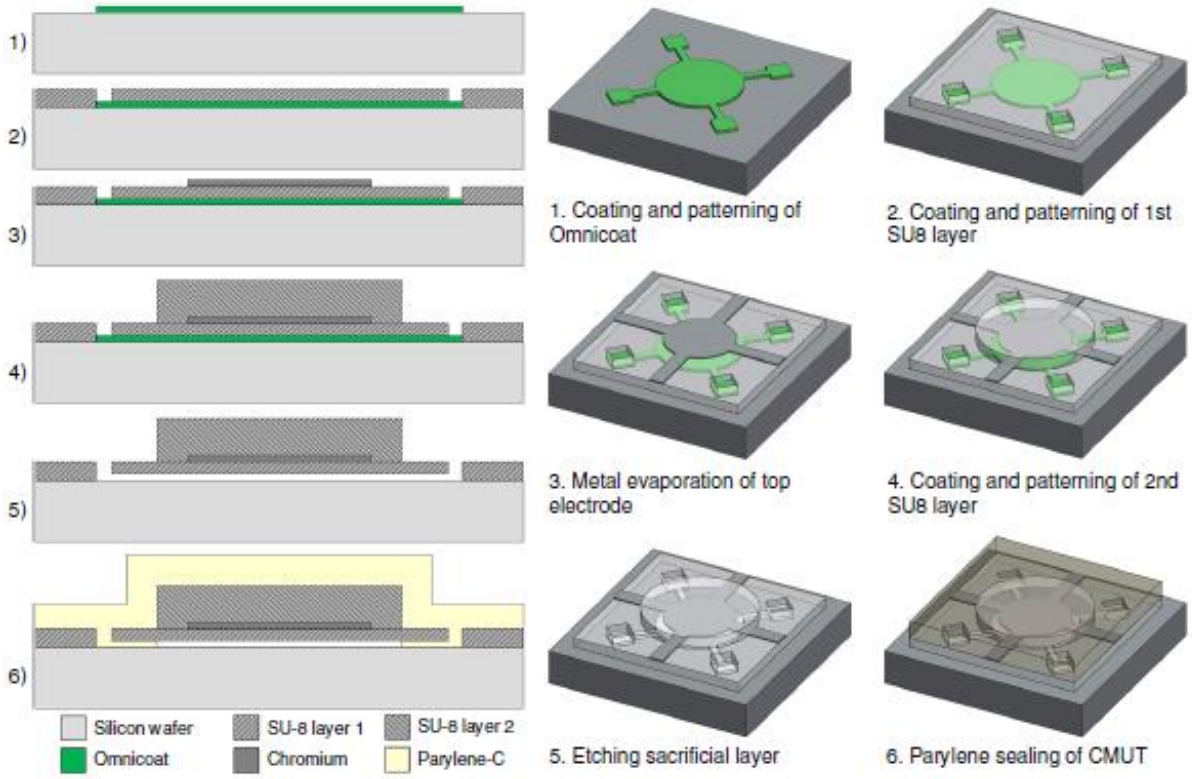

FIGURE 16: THE DIFFERENT MANUFACTURING STEPS FOR A POLYCMUT AS OUTLINED IN THE PAPER BY GERARDO ET AL.

bond with SU8. The deposition was made with a metal evaporation process and the additional material was removed by removing the photoresist.

The fourth step is to coat another layer of SU8 and patterning it to create the membranes. While developing the etch holes are again left open and the excess SU8 is removed. After development the sample is hardbaked at 150°C to increase the Young's modulus and potential cracks created by residual stresses in the multilayered sample.

Step 5 is the etching of the underlying sacrificial layer of OmniCoat by immersing the sample in MF319 developer. After the etching is finished the sample is first immersed in water for several hours and then in isopropanol to replace the leftover developer. To properly release the membranes and avoid any stiction problems with the substrate underneath the sample is put in a critical point dryer where the isopropanol is replaced by liquid CO_2 which evaporates after the sample is taken out.

The last step is to cover the sample with Parylene-C in a low-pressure chamber, making the sample watertight and creating a sealed vacuum cavity underneath. This step is essential for the use of the PolyCMUTs with a fluid which is again used as a coupling agent to decrease the inherent impedance mismatch. A side effect is that the atmospheric pressure around presses onto the membranes with their vacuum gap underneath, deflecting them in the direction of the substrate further decreasing the needed voltage. This step, although essential for water coupled use of the UTs, is not necessarily needed in the air coupled PolyCMUTs investigated in this thesis but this is shown later on.

Component	Dimension
Membrane radius	50 µm
Sacrificial layer thickness	0.30 µm
Membrane SU-8 layer 1 thickness	0.67 µm
Top electrode thickness	0.57 µm
Membrane SU-8 layer 2 thickness	2.40 µm
Passivation layer thickness	3.67 µm

TABLE 1: LAYER THICKNESSES OF THE POLYCMUT MENTIONED BY GERARDO ET AL.

The measurements of the different layers from the prototypes in the paper are given in Table 1 [57]. Each of them has different effects on the resulting properties of the membranes. A thicker passivation or sacrificial layer necessitate a higher pull in voltage as the electrodes are further apart. The thickness of the electrode itself on the one hand regulates how much electrical energy can be used before it is damaged but a thicker electrode also means a higher rigidity for the membrane thus again resulting in a higher pull in voltage and decreasing sensitivity. If the electrode is too thin however resulting resistive interconnection paths in combination with the capacitance of the CMUTs will result in a natural RC filter, degrading the excitation signals. The thickness of the membrane itself is then dictated by the second SU8 layer. With the thickness of the membrane the bandwidth, sensitivity, output pressure and quality factor, with the drawback of also increasing the needed voltage. Figure 16 shows the theoretical dependencies calculated with a MATLAB model used to design PolyCMUTs (programmed by Carlos Gerardo). It is mainly based on a paper on CMUT calculation by Wygant et al. [55]

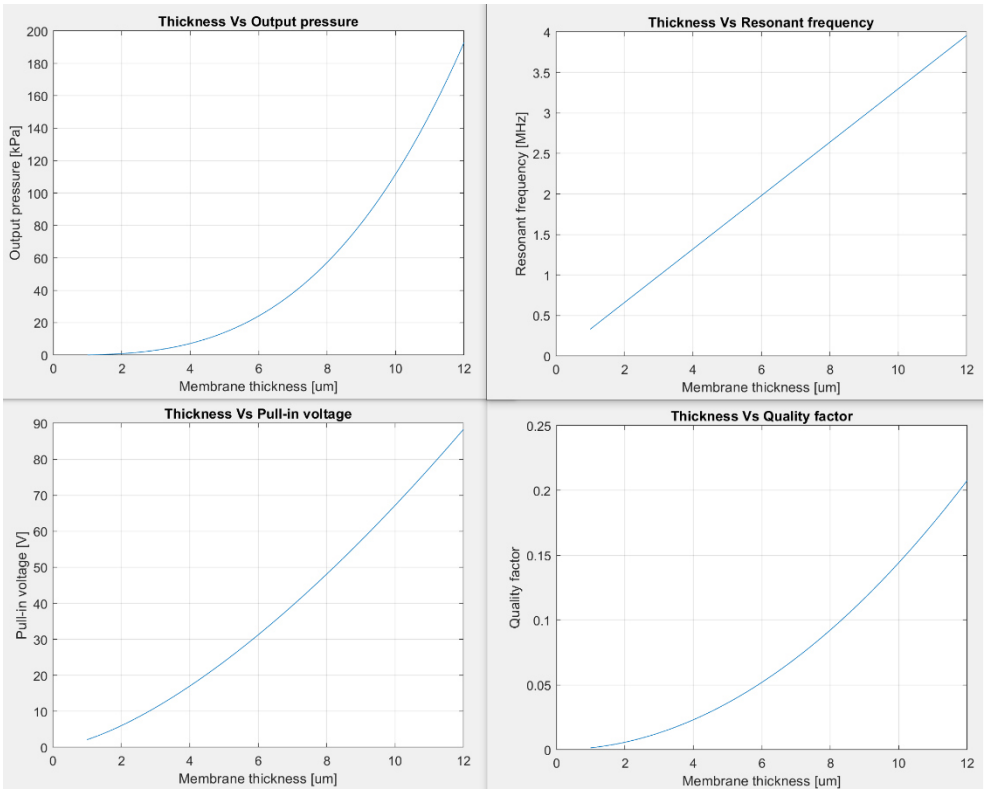

FIGURE 17: VARIATION OF THE MENTIONED PROPERTIES DEPENDANT ON MEMBRANE THICKNESS

If the changes by thickness variations are combined with changes in cavity height the PolyCMUT shows another fundamental difference to normal CMUTs: a whole range of high and low frequency devices can be produced all with the same pull in voltage as those two parameters are varied. The resonant frequency of the device, although also influenced by the thickness, is mainly determined by the radius of the membrane. As the first PolyCMUTs were produced for MHz water coupled applications another question was if the membranes are even producible in the needed size for the air coupled, kHz NDE transducers.

To summarize the advantages of a PolyCMUT:

- The impedance of a PolyCMUT is in the area of 3,4MRayl severely decreasing the impedance mismatch compared to traditional CMUTs (~ 20MRayl) or even piezoelectrical transducers (~30MRayl). It can be decreased even further with a matching layer.
- The total production cost of the prototypes is below US $100 with the cost in mass production potentially even lower. This is due to the used materials but also the comparably cheap manufacturing techniques. A classic UT currently is in the area of thousands of dollars.
- Excitation voltages are very low (around 22V for the water coupled model) and if the membranes are pre-biased, they become passive receivers working without supply voltage. This is considerably lower as the usual CMUT voltages. (60V to potentially hundreds of Volts) [59]
- Temperatures in the manufacturing process don't exceed 150°C so they can be built upon pre-existing electronical circuitry.
- The processes and materials in manufacturing have a low toxicity and the top layer of Parylene-C is even biocompatible.
- The total manufacturing time for the prototypes are under 24hrs total, allowing for a high number of prototypes and an even higher number of tests.
- The dielectric layer preventing short circuits makes them very safe to voltage spikes. The membranes collapse onto the substrate and return to normal operation once the spike is over.
- PolyCMUTs can be fabricated on a wide variety of substrates so they can also be flexible for use in special geometries or as wearables.

Each of these advantages on its own could be considered ground breaking for the field of CMUTs and ultrasonics in general and some of them have been achieved on their own, but the combination of all of these plus the advantages CMUTs generally posses is nothing short of revolutionary [56].

3. The study

3.1 The original task

The plan when this study was first started was to first evaluate the general feasibility of a PolyCMUT as a device for NDE. Several indicators already existed: As mentioned before Ergun et al. used their first CMUTs in 2003 for an air coupled transmission test with a 3mm sheet of Aluminum in between the two transducers and they did receive a signal with a loss of 87dB [60]. Kolo Medical also produces and sells CMUT probes for medical imaging so the basic technology is already tested and proven.

The plan that emerged was the following: Use a CFRP test plate provided by the DLR in Augsburg, calculate its exact material properties and therefore its impedance, calculate they theoretical loss for a distance of 3mm in air (a number given by the DLR to be able to safely use the transducer in robot assisted testing) and test the Kolo probe with it for a first general image. Simultaneously Carlos Gerardo would produce a sample with large membrane sizes to test if the frequency could be decreased to the kHz area without the need to increase the thickness of the membrane too much and therefore increasing the needed voltage to an unpractical level.

The next step would have been to use said sample to first do transmission and then pulse echo tests and try to get an A-mode signal of a delamination in the plate. However, it never cam to this point as the physical phenomena that where discovered while testing the first sample were unexpected and needed a lot of research on their own to fully understand their impact on the design of an air coupled PolyCMUT. The following chapters explain what happened and how everything discovered let to the final result.

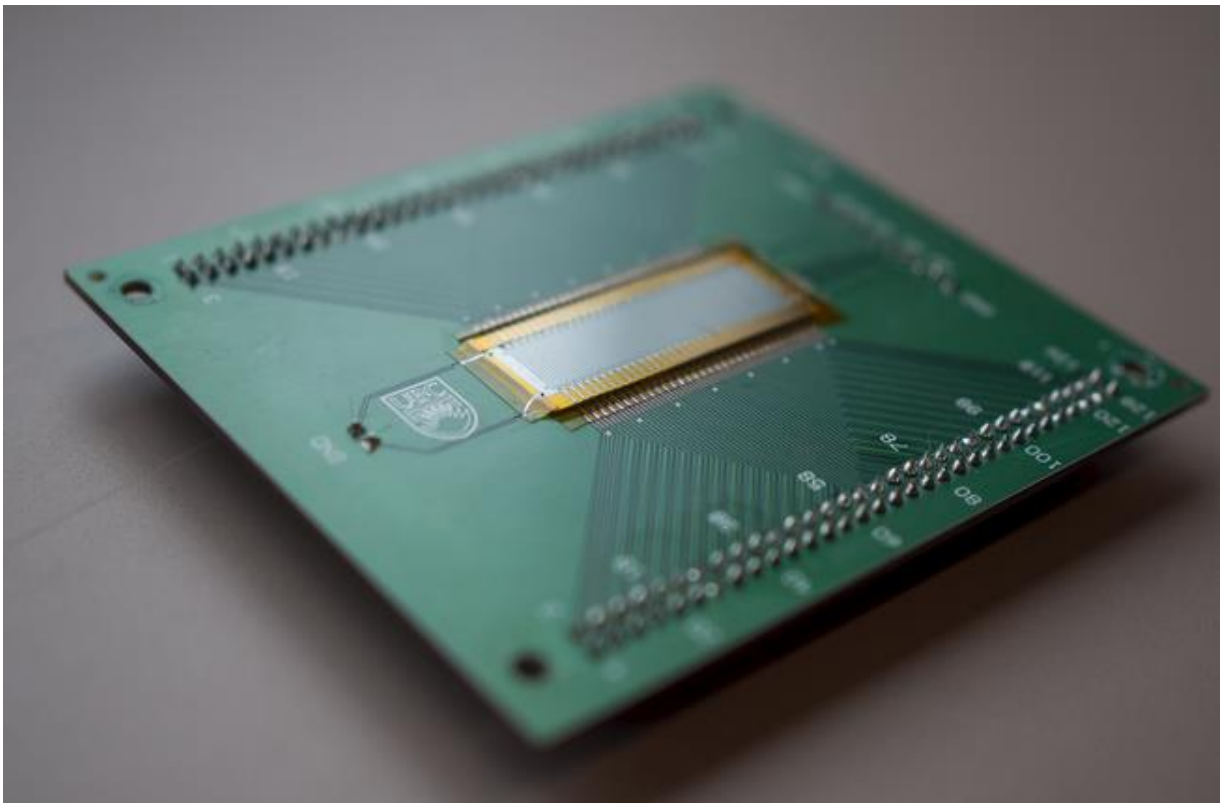

FIGURE 18: THE DESIRED FINAL RESULT: A WORKING POLYCMUT ARRAY FOR AIR COUPLED NDE IN THE KHZ RANGE. SHOWN HERE IS THE WATER COUPLED VARIANT.

3.2 The DLR test plate

The DLR provided a CFRP test plate for the tests but sadly not all parameters were known so there was some work to be done to calculate its mechanical and acoustical properties. CFRP itself is, because of its layup of different fiber directions, a very anisotropic material and the acoustic properties have to be calculated for every specimen separately. The plate itself was used for ultrasonic testing before, but it was used for lamb wave testing [45] so different properties were needed than the ones for our pulse echo experiments.

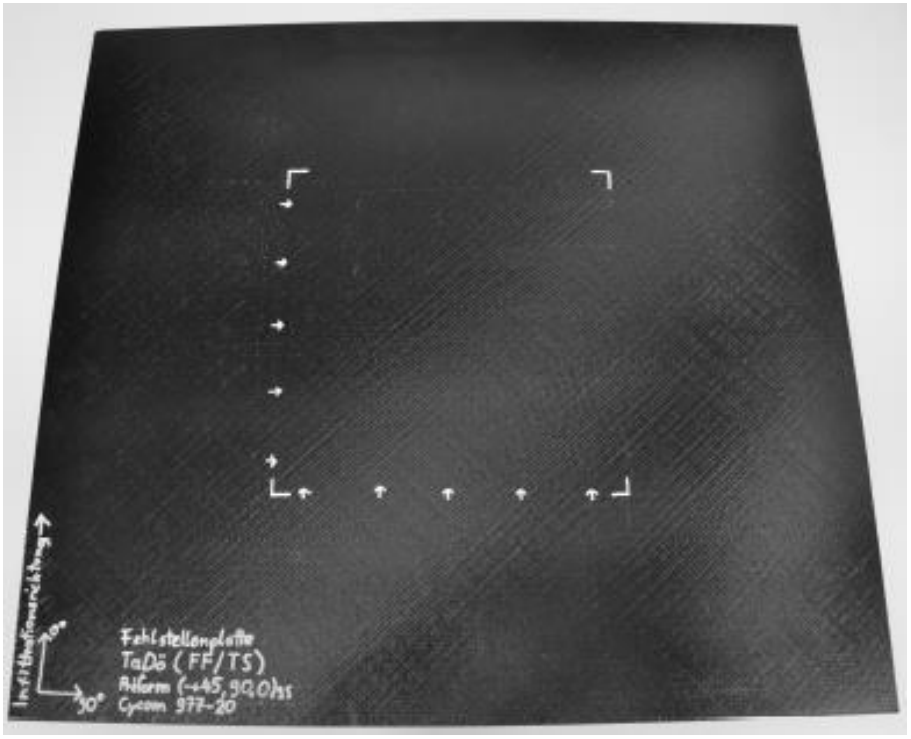

FIGURE 19: THE TEST PLATE PROVIDED BY DLR WITH ARTIFICIAL FLAWS IN THE WHITE SQUARE IN THE MIDDLE

The known properties of the plate were the following:

Fiber properties	
Name	Toho/Tenax IMS60 E13 24K 830tex
σ_L	5800 Mpa
E_L	290 Gpa
ρ	1.79 g/cm^3

Resin properties	
Name	Cycom 977-20
σ_L	-
E_L	-
ρ	1.3 g/cm^3

TABLE 2: THE PROVIDED MATERIAL DATA

Otherwise known was that it was a biaxial fabric, it was vacuum infiltrated, the fiber volume content was 54.5%, it had 12 layers biaxial fabric so 24 layers in total and the resulting Tensile modulus of one unidirectional layer should be 163GPa (data for Cycom 24K IMS UW 200gsm) [61]. The layup is:

$[(+45°; -45°; 90°; 0°)_3]_S$

For the calculation the use of eLamX 2.5 (24th August 2018) was chosen, an open source software developed by the Technische Universität Dresden. It was chosen because of its availability for free, its easy user interface and its of the shelf usability.

The sound waves in the pulse echo mode measurements only travel perpendicular to the layup angles so actually only the material properties of one layer needs to be calculated. This can easily be done by hand but because it was aimed at creating a somewhat robust process for future experiments (in different angles) it was decided to use eLamX and calculate the whole plate. The biggest challenge was the many missing material properties in transversal fiber direction. As these properties are very expensive to find out experimentally and they are not very useful in normal design steps they are often times not even known by the manufacturers. For our missing information data from similar materials mentioned in the book Process and Mechanical Modelling of Engineering Composites by Anthony K. Picket were used [62, pp. 58–59].

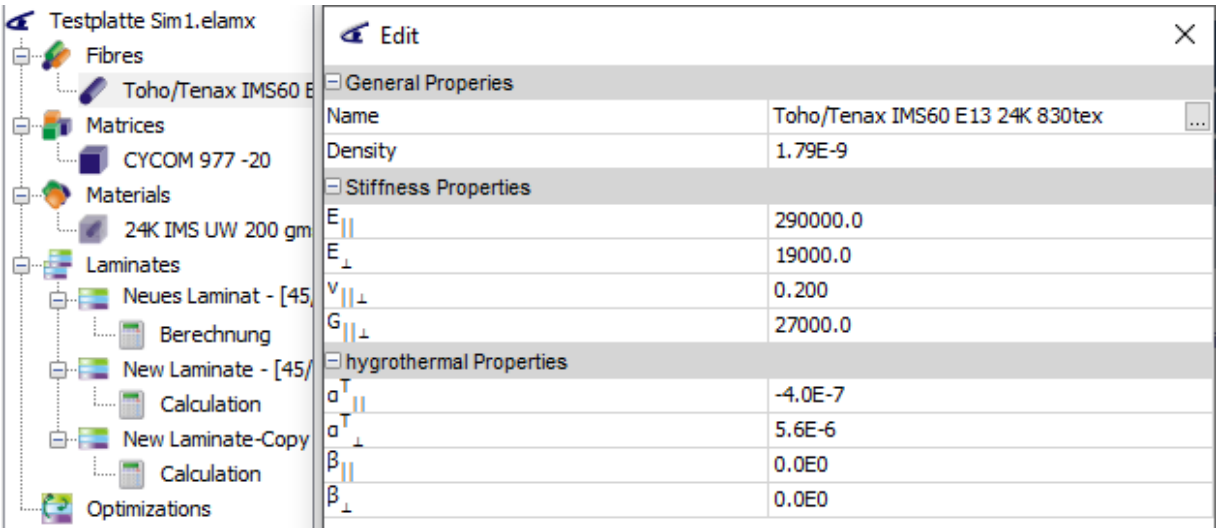

FIGURE 20: THE FIBRE PROPERTIES ENTERED INTO ELAMX

The properties seen in Fig 19 are the density and longitudinal Young's Modulus given by the original data sheet (seen in the appendix) and the transversal Young's Modulus, transversal Poisson ratio and the transverse sheer modulus. All are from the IM7-carbon entry in the book.

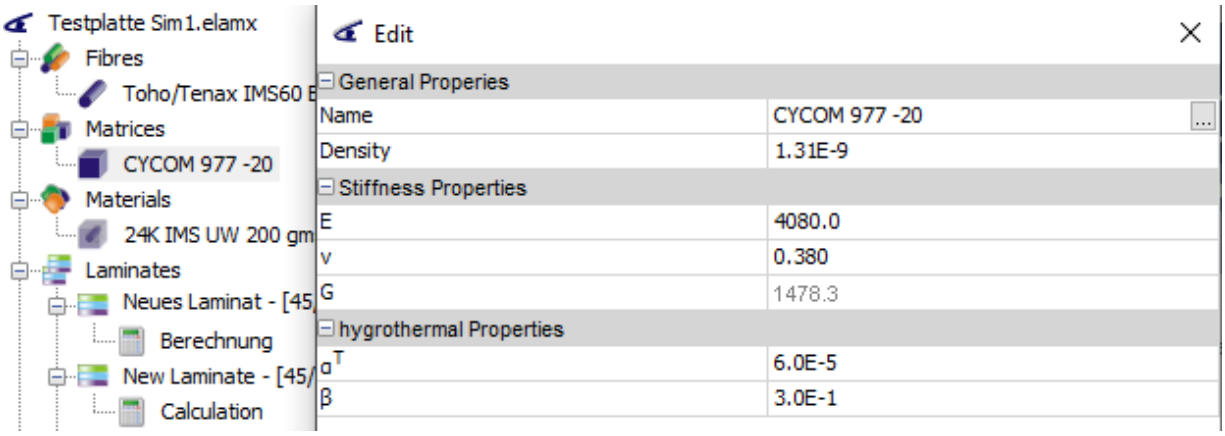

FIGURE 21: THE RESIN PROPERTIES ENTERED INTO ELAMX

The properties for the resin (Fig. 20) were the density given by the data sheet and the Young's modulus and Poisson ratio given by the book for the 8551-7 epoxy. Both fibre and resin in the book were chosen because they were described as being used mainly for aircraft design and their other properties were reasonably close to the given values. The used micromechanical models were the Rule of Mixture for the density and Halpin Tsai for the other values.

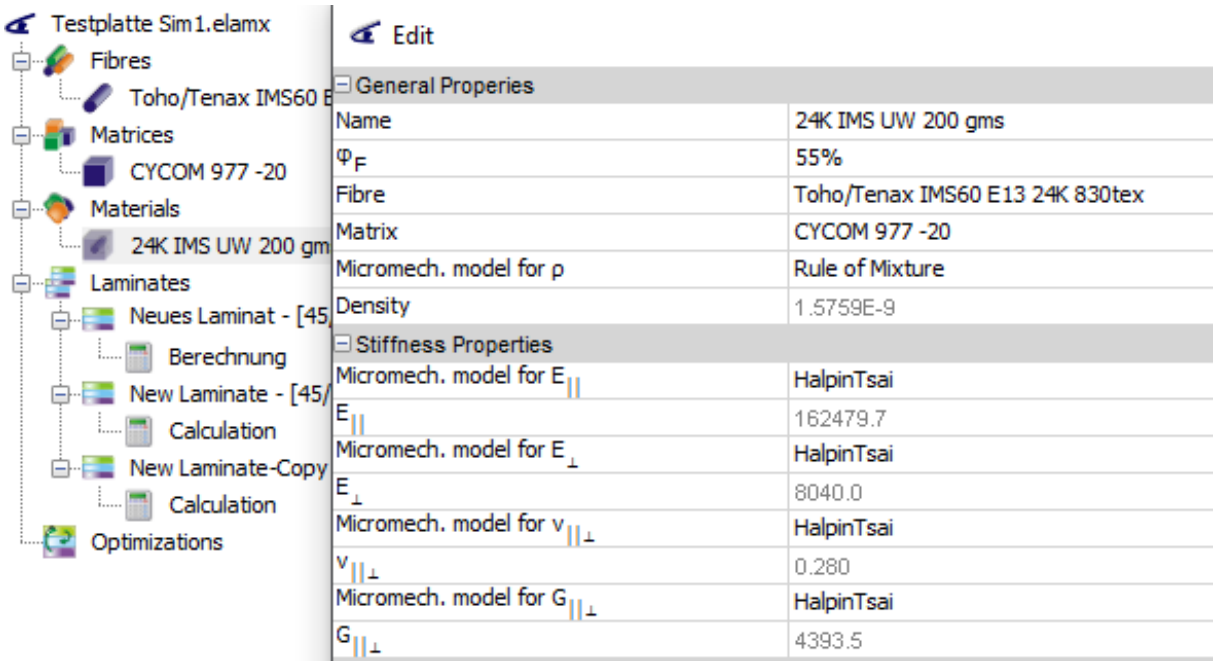

FIGURE 22: RESULTING MATERIAL PROPERTIES IN ELAMX

The resulting longitudinal Young's modulus perfectly fits with the given value of 163GPa, being calculated as 162.479GPa. The results can now be used to calculate the phase velocity of longitudinal waves travelling normal to the fibers (in following parts called speed of sound for easier reference) according to the formulas in Physical Ultrasonics of Composites [30]. The coordinate system used follows the usual notation shown in Fig. 22.

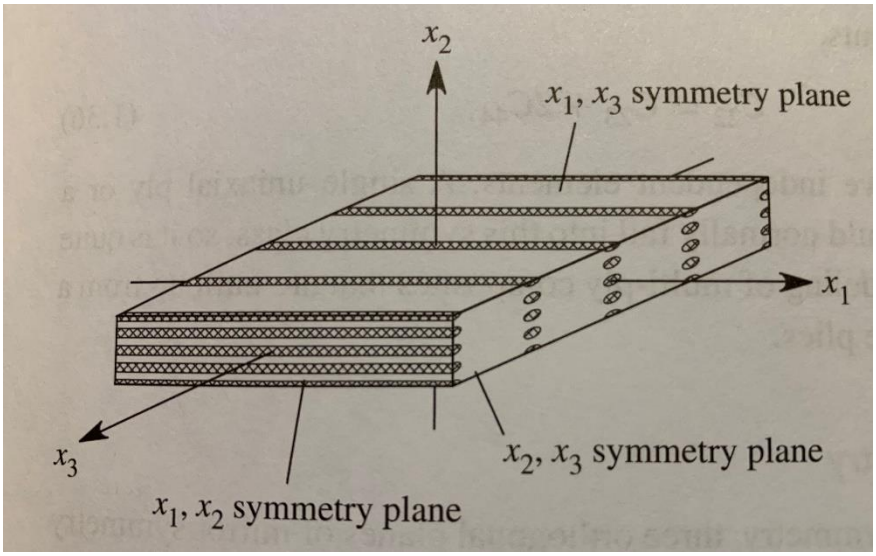

FIGURE 23: COORDINATE SYSTEM FOR A UNIDIRECTIONAL COMPOSITE [30]

The first calculation is the Poisson ratio ν_{21} with $E_{11,}$ being the Young's modulus parallel to the fibers, E_{22}, the Young's modulus perpendicular to the fibers and the Poisson ratio ν_{12}.

$$\nu_{21} = \frac{E_{22}}{E_{11}} * \nu_{12} = 0.013855 \tag{3.1}$$

The next step is to calculate the stiffness coefficient perpendicular to the fibers C_{22}.

$$C_{22} = (1 - \nu_{21} * \nu_{12}) * \frac{E_{22}}{D} = 10.8467 \text{ GPa} \tag{3.2}$$

With:

$$D = 1 - \nu_{23}^2 - 2 * \nu_{12} * \nu_{21} - 2 * \nu_{12} * \nu_{23} * \nu_{21} = 0.73836 \tag{3.3}$$

The step left is the calculation of the longitudinal phase velocity, the needed speed of sound c_L.

$$c_L = \sqrt{\frac{C_{22}}{\rho}} = 2623.44 \ \frac{\text{m}}{\text{s}} \tag{3.4}$$

The result itself already seems to be realistic as literature usually states a speed of sound between 2500 and 3000 $\frac{\text{m}}{\text{s}}$ [63]. The next step is to validate this calculation in an experiment so the model can be used for future research.

3.3 Verasonics and the Kolo probe

The next step was to find a way to validate the speed of sound. The easiest way to achive this is by actually scanning the plate via ultrasound, entering the suspected speed of sound and see where the machine shows the received echo of the backplate. If the backplate echo would be at 7mm depth, the speed of sound would be correct as the time of travel for the soundwaves was correctly measured by the ultrasound machine.

FIGURE 24: THE VERASONICS VANTAGE SYSTEM WITH THE COMPUTER ON THE LEFT AND THE SIGNAL PROCESSING UNIT IN THE MIDDLE.

The system used is the Verasonics Vantage system. The Vantage system is built specifically for research and thus it has many great advantages. Its software is an open MATLAB environment, making for easy programming. A large package of toolboxes for different probes, kinds of testing and other applications are included. All transmit parameters for the ultrasound wave can be controlled and the receiving signal can be obtained in B-mode images or as individual RF data for each element [64].

The probe used was another although small test: The Kolo L 22-8 is one of the very first developed CMUT probes for water coupled medical imaging. Although it is not optimized for NDE, with an acoustic matching layer optimized for soft tissue and a center frequency at 12 MHz (a high frequency meaning good resolution but low penetration depth), obtaining images with the Kolo probe would proof that even non optimized CMUTs can be used for NDE and that the Verasonics is the right System to test future PolyCMUT prototypes. The probe itself is an array of 256 elements, which for our tests were only creating a planar wave although a focused beam might result in even better resolution.

The first test was to find out if the calculation of the speed of sound was correct. The speed of sound in the Verasonics terminal was set to the calculated value and an image was created. The resulting

image can be seen in the following figure and showed the echo of the backplate at 7mm, validating our calculated speed of sound and the model used. The red arrow points at the scale of depth and the red ellipsoid shows the backplate echo. Even though gain and contrast were set to the maximum possible values, the image was still rather dark which is due to ne non optimized probe that produced a very strong echo on the surface.

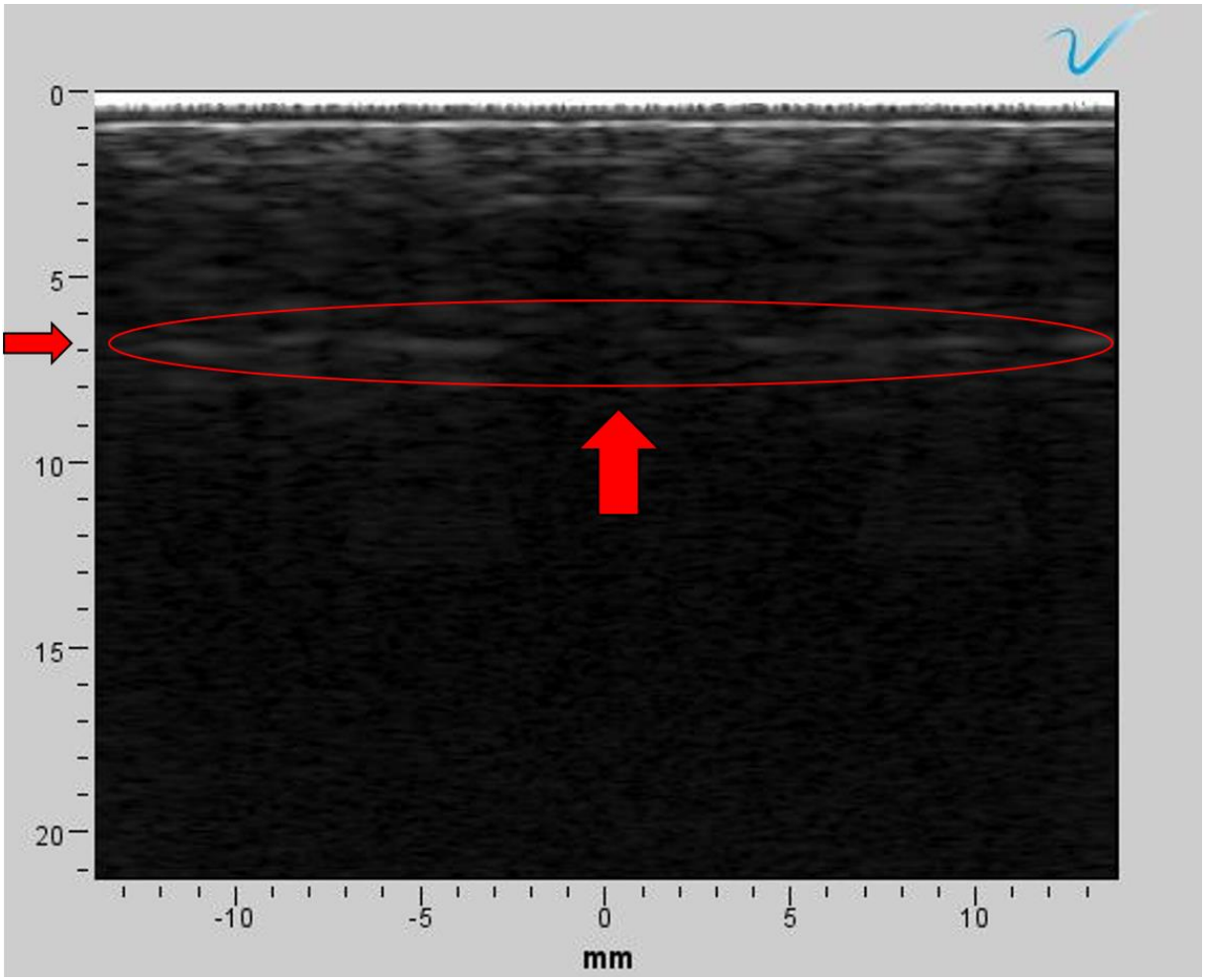

FIGURE 25: THE FIRST IMAGE ACQUIRED BY THE COMBINATION OF VERASONICS AND KOLO PROBE.

The next test included the defects in the test plate provided by the DLR. When the plate was manufactured different sized pieces of PP foil were put into different layers of the plate. PP foil has a significantly different density to CFRP with

$$\rho_{\mathrm{pp}} = 0.91 \frac{\mathrm{g}}{\mathrm{cm}^3} \quad \text{and} \quad \rho_{\mathrm{CFRP}} = 1.576 \frac{\mathrm{g}}{\mathrm{cm}^3}$$

This will create a big enough difference in the material to appear as a defect in NDE. To validate the test method according to industry standards defects are placed in different sizes and different heights. The general layout of the defects can be seen in the following figure. All foil patches are placed in the white grid on the plate shown in Fig. 20. The smallest size of 5mm was chosen to the industries standard, stating that a flaw size above 6mm must be detectable to consider the NDE technique for future use (GE regulation EC-SRC-0003)

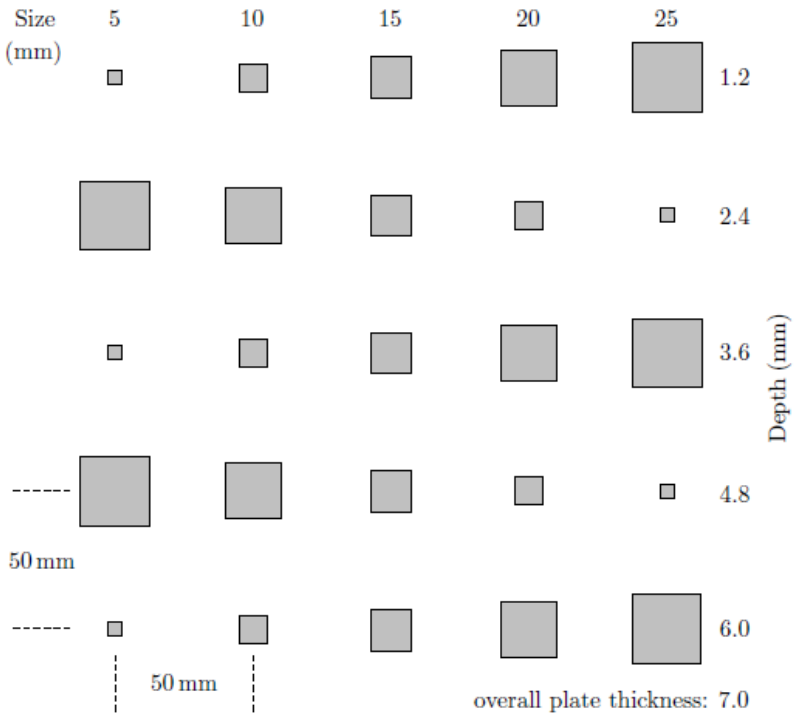

FIGURE 26: THE FLAWS IN THE TEST PLATE AND THEIR POSITIONS

In the following tests all flaws could be detected. The following picture shows the 10 mm flaw in 2 mm depth. Clearly visible is the missing backplate echo at the point of the defect and a little harder to spot, the delamination itself.

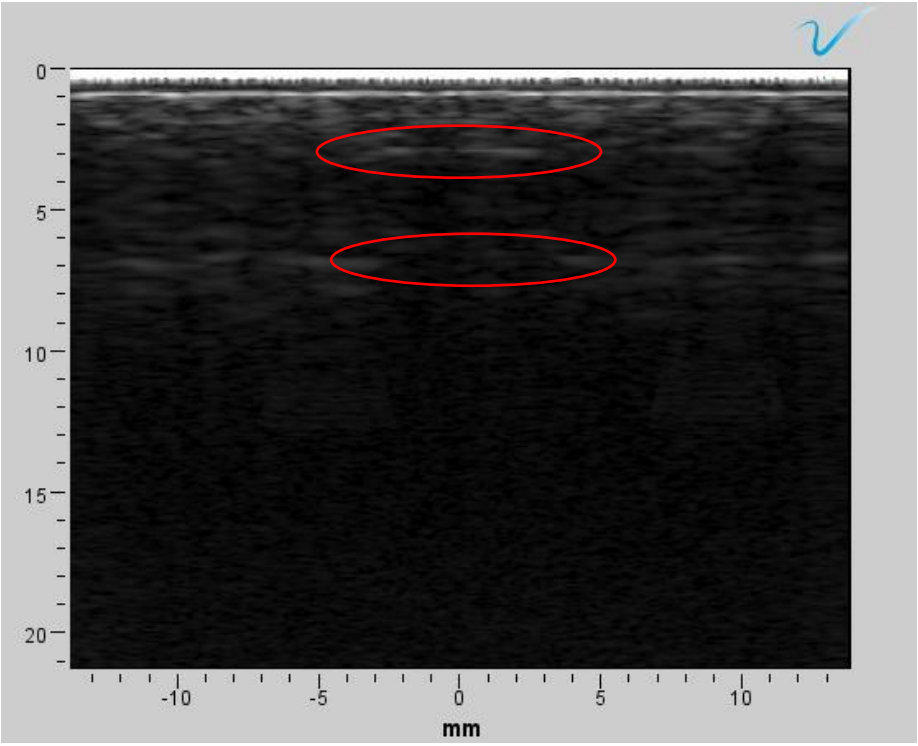

FIGURE 27: THE ACQUIRED SCAN WITH THE LOWER RED CIRCLE AT THE MISSING BACKPLATE ECHO.

Although it was shown in the aforementioned experiment that the Verasonics can be used to obtain the location and size of flaws in CFRP, some more changes to the system have to be made. First a new software for signal processing has to be written and although it can be based on the original Verasonics CMUT software it will still be considerable work. The second thing that has to be engineered is the connection of the CMUT probes to the Verasonics connector. Both tasks are helped a lot by the very open architecture of Verasonics, and that the company does sell a special connector board for research purposes.

These remaining problems are mentioned for the sake of thoroughness but as both are very time consuming and not important for the general feasibility of the project they will be addressed at a later point.

FIGURE 28: THE CHOSEN PROTOTYPE RIBBON CABLE BREAK-OUT BOARD MANUFACTURED BY VERASONICS

3.4 Fabrication and its many difficulties

For the very first prototypes a center frequency of 40 kHz was chosen. This had several different reasons. Because of the inherent loss of wave energy through the impedance mismatch, even current air coupled NDE methods use fairly low frequencies with examples from the DLR being 570 kHz (transmission method) and 200 kHz (Lamb wave method). This meant that the lower the center frequency of the produced PolyCMUTs the better, as it would possibly show the limits of the technology. The specific number of 40 kHz was chosen because there were already commercial 40 kHz piezo transducer available, which would have been a great receiver for a pitch catch test scheme.

The first PolyCMUTs produced had a center frequency of 2.83 MHz at a membrane diameter of 100 µm. The needed diameter for a center frequency of 40 kHz was calculated to be 1044 µm. This was both, the lowest frequency and the largest diameter ever produced for a PolyCMUT. As PolyCMUTs are based on plate vibration phenomena and membrane thickness, air gap and diameter can be changed, there are several different possible sizes for this frequency. A simplification is the choice between small and thin or large and thick membranes. The large and thick membranes have higher pull in voltages, and the risk of collapsing under their own weight during fabrication is considerably higher. The benefits although are: Higher output power, a higher bandwidth, better control of the pull in voltage as the layer thickness is easier to control, low risk of electrical short circuits as the isolation layer is thicker, a simpler fabrication process and the theoretical possibility to try and create PolyCMUTs in the audible range. This all led to the choice of producing the thick and large variant. To have a control group and, if fabrication fails to show at which diameter it started, it was decided to fill the 10 mm by 10 mm chip with different sizes of membranes and to test them all. The used diameters and their responding frequencies were are shown in Table 3.

Diameter [um]	f_R [kHz]	Aspect ratio
200	1,000	7.9
400	250	15.9
600	111	23.9
800	63	31.9
1,000	40	39.9
1,200	28.2	47.9
1,400	21.0	55.9
1,600	16.2	63.9
1,800	12.1	71.9
2,000	10.9	79.9
2,200	8.2	87.9
2,400	6.9	95.8
2,600	5.9	103.8
2,800	5.1	111.8
3,000	4.4	119.8

TABLE 3: THE CHOSEN DIAMETERS AND THEIR FREQUENCIES AND ASPECT RATIOS

The chosen diameters and the principle of using large, thick membranes instead of small ones produced a further problem. The very first batch of PolyCMUTs used Chromium as the metal for the upper contact, this however has several drawbacks. Chromium has a relatively low electrical conductivity (see Table 4) compared to other metals which necessitates a thicker metal layer. The thickness of the layer in combination with its high Youngs Modulus results in a very stable membrane, which in return means a higher resistivity against deformation and therefore a higher pull in voltage.

Material	Conductivity [S/m]	Young's modulus [GPa]	Poisson's Ratio	Density [Kg/m3]
Chromium	7.90e6	250	0.22	7,190
Aluminum	3.77e7	70	0.35	2,700
Gold	4.10e7	79	0.40	19,300
Silver	6.30e7	83	0.37	10,490
Copper	5.96e7	115	0.34	8,960

TABLE 4: THE DIFFERENT METALS POSSIBLE FOR EVAPORATION AND THEIR PROPERTIES.

The possible alternatives for Chromium are shown in table 4. These were the only practical choices as these are the metals available for the used e beam evaporator. With the given conductivities the resulting film thicknesses are: 261 nm for chromium, 49 nm for gold and 53 nm for aluminium. Silver and Copper were not chosen due to their reduced adhesive properties to SU8 [65] and the fact that the metal evaporator was not loaded with silver. Aluminium was chosen as the new contact metal, as it is light, flexible, very conductive but also cheaper then gold.

The next step in production was to draw a fabrication mask for the maskless aligner system containing all the chosen diameters and their respective etch channels. The resulting mask can be seen in the following figure.

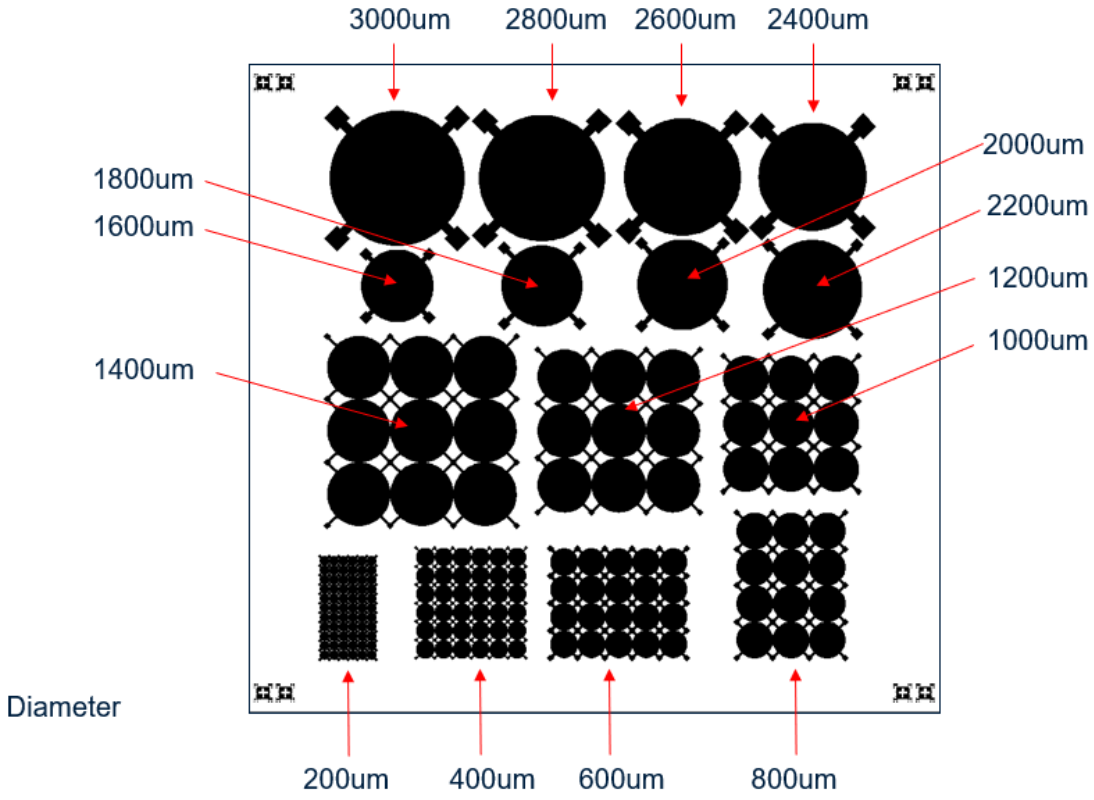

FIGURE 29: THE RESULTING FABRICATION MASK

The first step in production was the spin coating of Omnicoat [66] onto the waver which is then baked at 150° C for 3 min. The next step is to spin coat a layer of S1813, a positive photo resist. The resist is patterned by using the SF-100 maskless lithography system (St. Petersburg, USA). The UV-light of the system hardens the resist in specific areas. Afterwards the sample is immersed in MF319, an alkaline based developer, which etches both the S1813 [67] and the Omnicoat. The etching is stopped by rinsing the waver in deionized (DI) water. The paper by Carlos Gerardo mentions plasma etching as the next step to remove residues of Omnicoat. [57] This was not necessary as the etching process was already very clean.

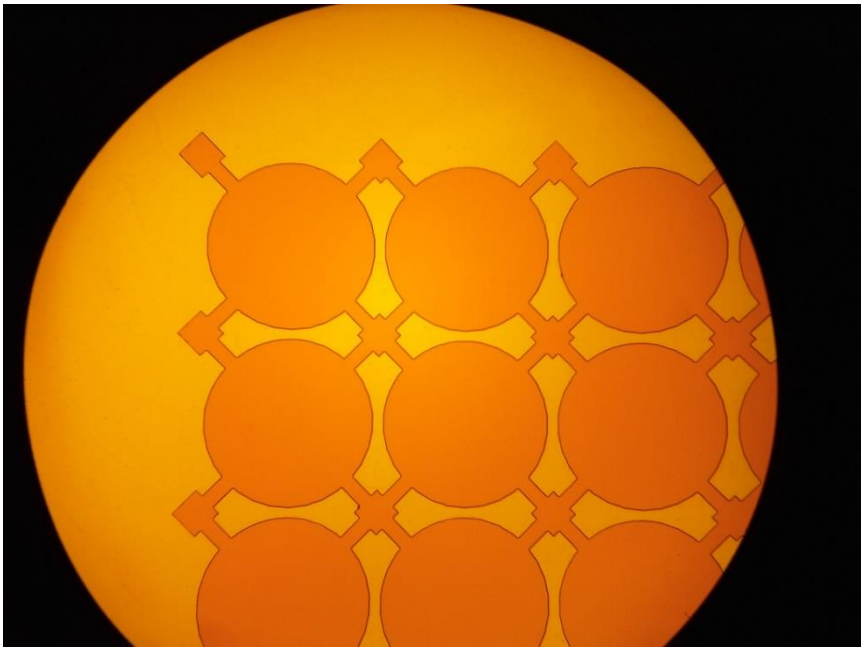

FIGURE 30: THE SACRIFICIAL LAYER OF OMNICOAT AFTER ETCHING

Following is the spin coating of the first layer of SU8 onto the sample. This acts as mechanical support for the top electrode and protects the CMUT from short circuits should the membrane collapse. The SU8 is then prebaked at 95 °C and patterned by the lithography system to further built up the etch channels. After developing in Acetone and rinsing in DI water, the sample is post exposure baked.

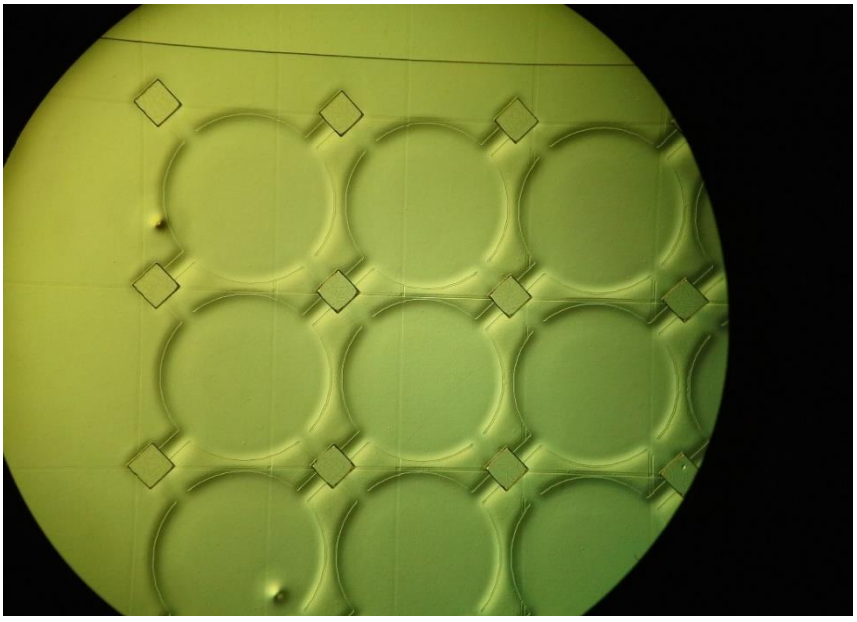

FIGURE 31: THE FIRST LAYER OF SU8

The next layer is the aluminium electrode. To be able to pattern the metal a lift off process is needed which can be achieved by depositing and patterning a layer of AZP 4110 photoresist [68]. The following evaporation is done in an electron beam evaporator manufactured by AJA International. The model is called ATC-ORION-8E UHV (Scituate, MA, USA).

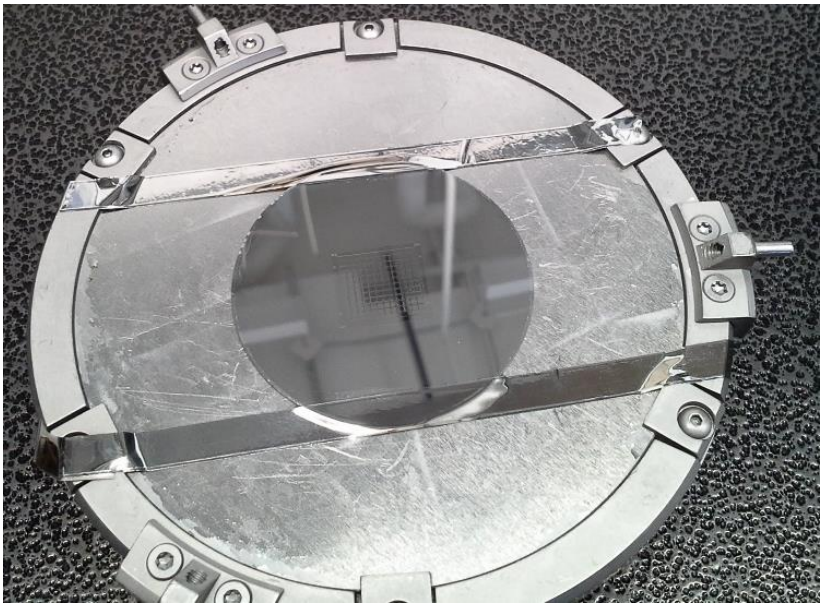

FIGURE 32: THE SAMPLE WITH THE EVAPORATED 50 NM ALUMINIUM LAYER

After the sample was again developed to form the electrodes, a second SU8 layer is deposited by spin coating, this time with a much lower spin rate to create a thicker layer. The SU8 is then again prebaked and patterned with the maskless lithography system. After removing the non patterned SU8, the sample is hard baked at 150 °C for 5 minutes and then gradually cooled down to room temperature. This baking process helps to release possible cracks (see Fig. 34) in the SU8 film formed by the residual stresses of the underlying layers.

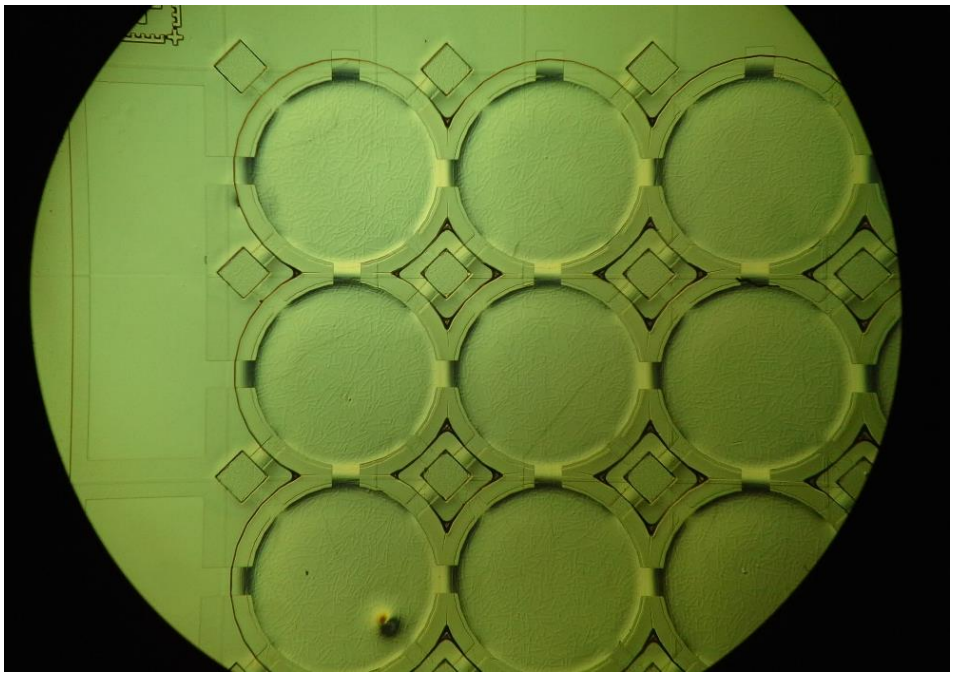

FIGURE 33: THE SECOND LAYER OF SU8 AFTER PATTERNING. THE MICROCRACKS BEFORE HARD BACKING ARE VISIBLE.

Figure 33 shows the layered membranes with the sacrificial layer still intact. The horizontal and vertical connections between the membranes are part of the aluminium electrodes. The diagonal connections and the diamonds in between are the etch channels for the sacrificial layer. The large rectangle on the left is the electrode for connection of the chip with the outside. Clearly visible (as mentioned above) are the microcracks that formed in the SU8 after patterning and prebaking. The structure seen in the top left corner is a simple alignment marker, to check if the different patterning steps were aligned to each other.

After the curing of the second layer the chip has to be diced to fit in the critical point dryer available to the lab. The maximum size usable is a chip of 10 mm by 10 mm. The dicing is done by creating grooves in the substrate with a laser cutter. The depth of the grooves is about one third of the thickness of the substrate. After laser cutting it is then broken manually. The milling of the grooves is a rather critical process as it can leave a lot of debris on the surface of the chip. Measures to prevent harm to the sample are either the usage of very low laser energy and subsequently more passes or a protective layer can be spin coated onto the sample and later be removed with acetone. As the low energy procedure is very time consuming the second option is chosen. Figure 34 shows the diced sample before drying. Clearly visible are the grooves milled by the laser in the left and right piece and the structure on the chip in the middle. A wafer this size can usually fit up to 4 chips, but as the metal evaporation is not perfectly even on the outer sides it was chosen to produce only one sample on the wafer.

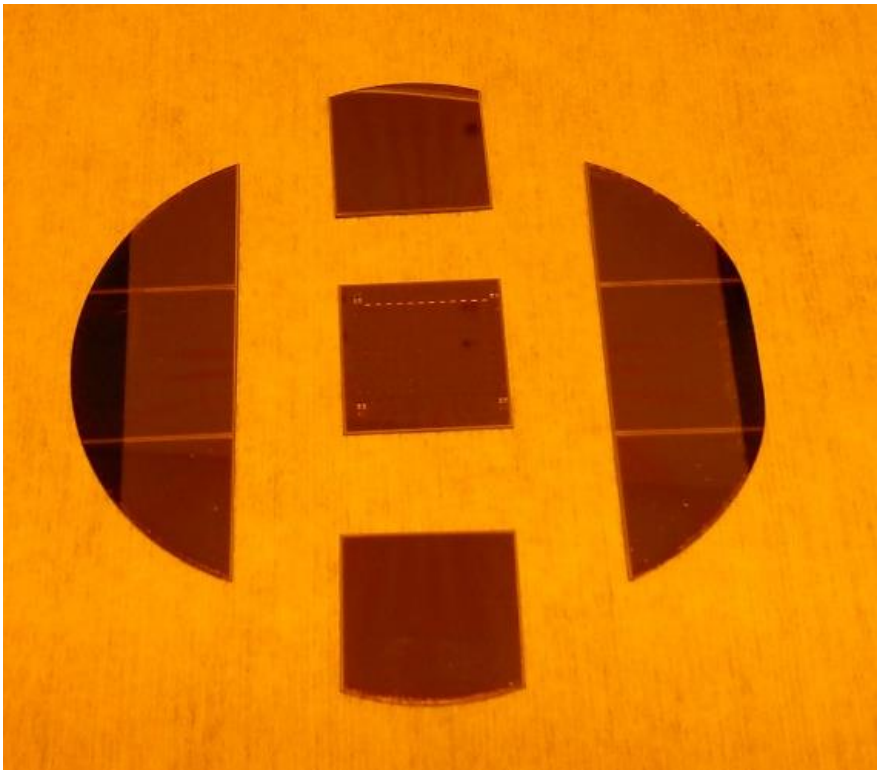

FIGURE 34: THE SAMPLE AFTER LASER CUTTING AND DICING

After dicing the chip was immersed in MF319 developer to etch the sacrificial Omnicoat layer. This process usually takes several hours, and its progress can be visually controlled under the microscope as the already etched parts appear darker. The darker coloration can be seen in the following figure which shows the etchant penetrating the channels and starting to etch the Omnicoat. However, there was a problem in the process. The large dark flake visible at the top of the microscope is a residue of

the aluminium contact floating away. It was discovered that the MF319 developer etches not only Omnicoat but also aluminium at a rate of several nanometers a second [69]. The etching of the aluminium electrode led to the destruction of the sample. The center membrane visible in Figure 35 did not possess an electrode from the start to be able to see through it and monitor the etching process.

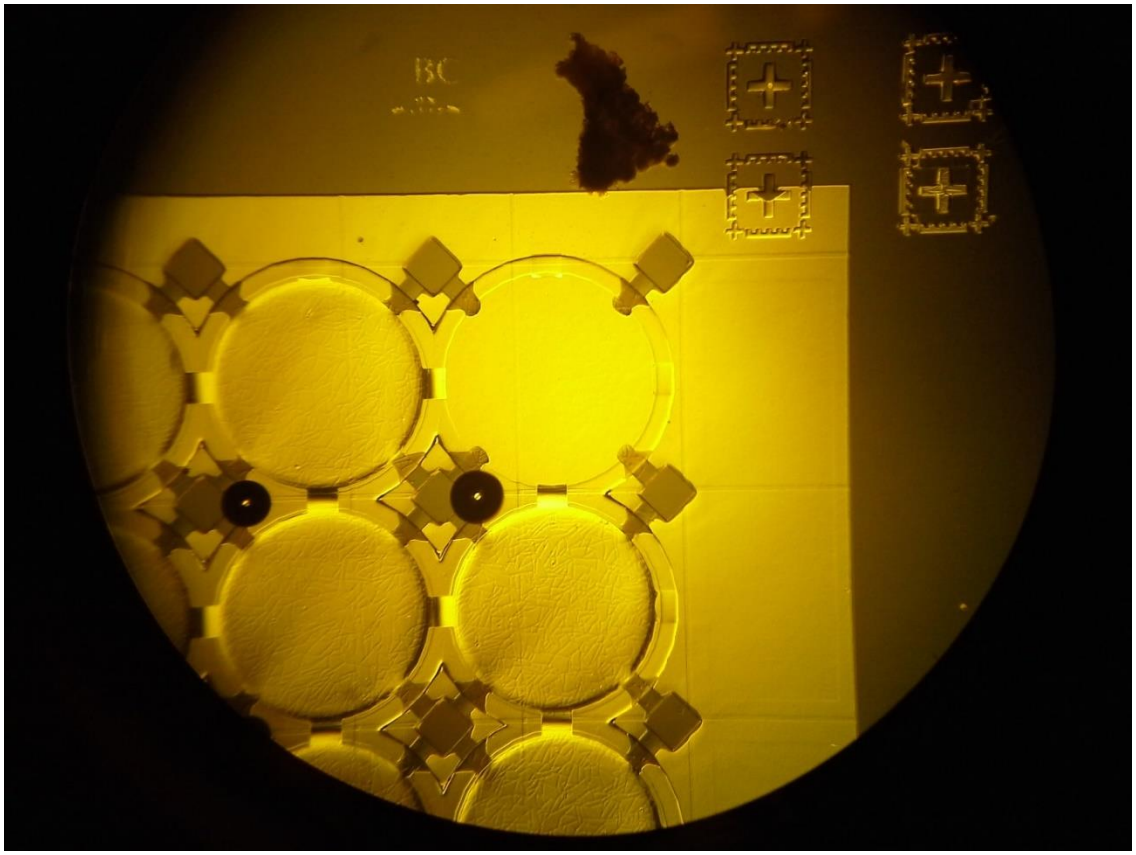

FIGURE 35: THE ETCHING SAMPLE WITH THE ALREADY MISSING ELECTRODES.

After the failure with the MF319 developer and the aluminium the discarded pieces of the dicing process were used to test different developers. The problem was that MF319 is based on tetramethylammonium hydroxide (TMAH) which etches aluminium. The new developer chosen was Microdeposit 1165, a developer based on N-methyl-2-pyrolidinone [70].

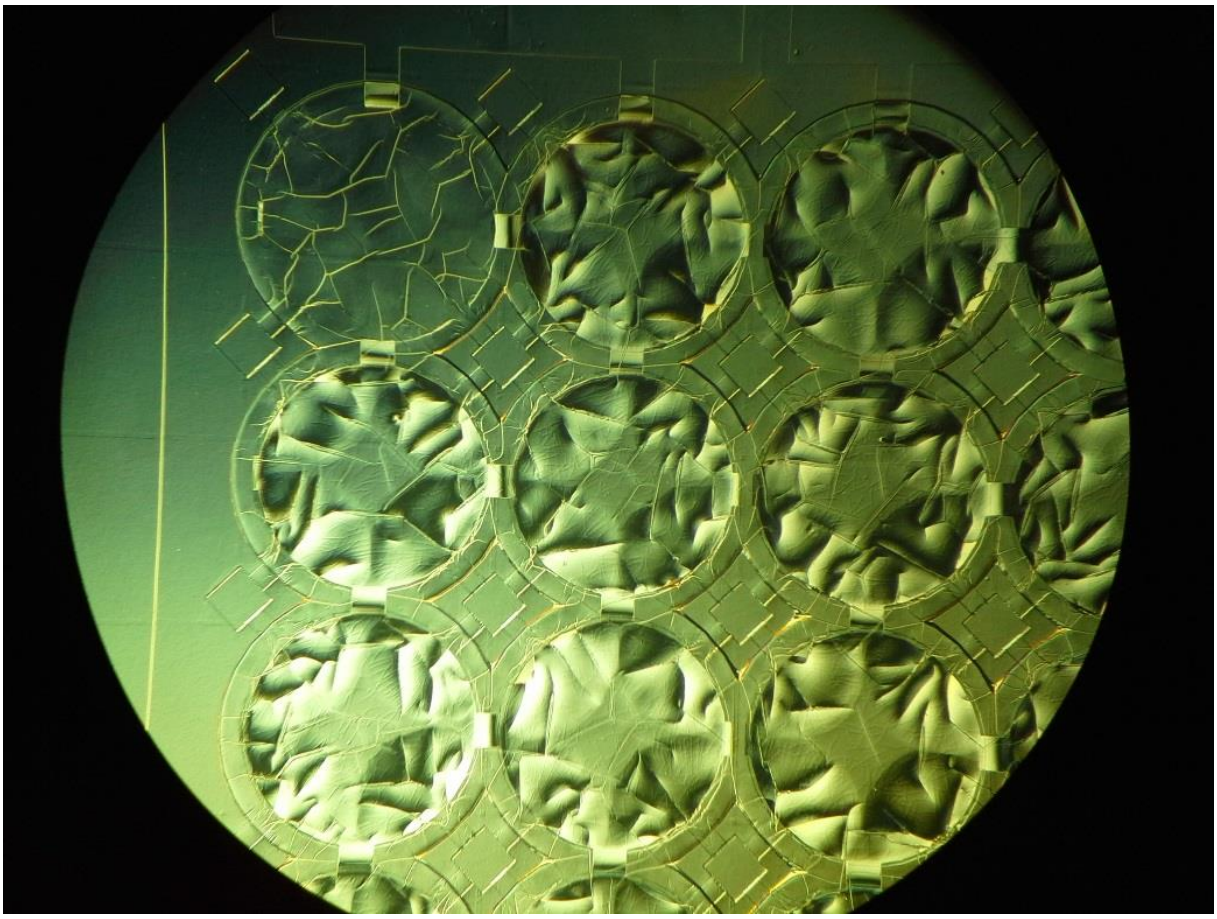

FIGURE 36: THE SECOND SAMPLE EDGED WITH MICRODEPOSIT 1165.

After edging the sample for 3 hours the Omnicoat underneath was removed but the SU8 absorbed a significant amount of developer and started swelling. The swelling was so significant that it started to crack the top electrode which can clearly be seen in Figure 36. This also destroyed the sample and the search for another method continued.

The next choice was to replace aluminium with gold. Although it is more expensive it possesses nearly the same mechanical properties and it was proven to be adhesive to SU8 [65] in older studies.

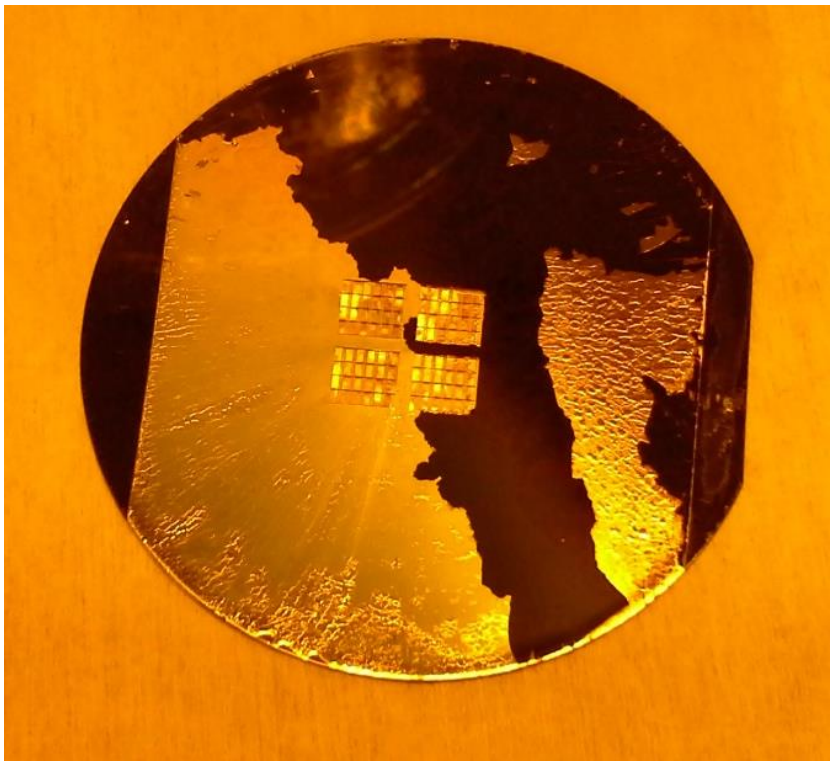

FIGURE 37: THE PEELED OFF GOLD LAYER IN ONE OF THE SAMPLES OF ROUND 3-6

Although Dai et al. [65] showed that it is possible to adhere gold to cured SU8 several different methods failed to produce the desired sample. Samples 3, 4 and 5 were all destroyed when the gold peeled off in the lift of process. Different methods included the use of titanium as an adhesion layer and the use of different developers and photo resists. It has to be mentioned that after the research period for this thesis ended a uniform gold layer was actually achieved but as it was already to late no working samples could find recognition in this thesis.

After gold failed to show the desired results the decision was made to accept the higher pull in voltages in the prototype stage and to switch back to chromium as this was an already proven process. The problem that surfaced this time was a very long etching time for the samples (more than 24 hours). This led the developer to start attacking the outer edges of SU8 as well, again destroying the sample. In Figure 38 the dark spots of attacked SU8 are clearly visible.

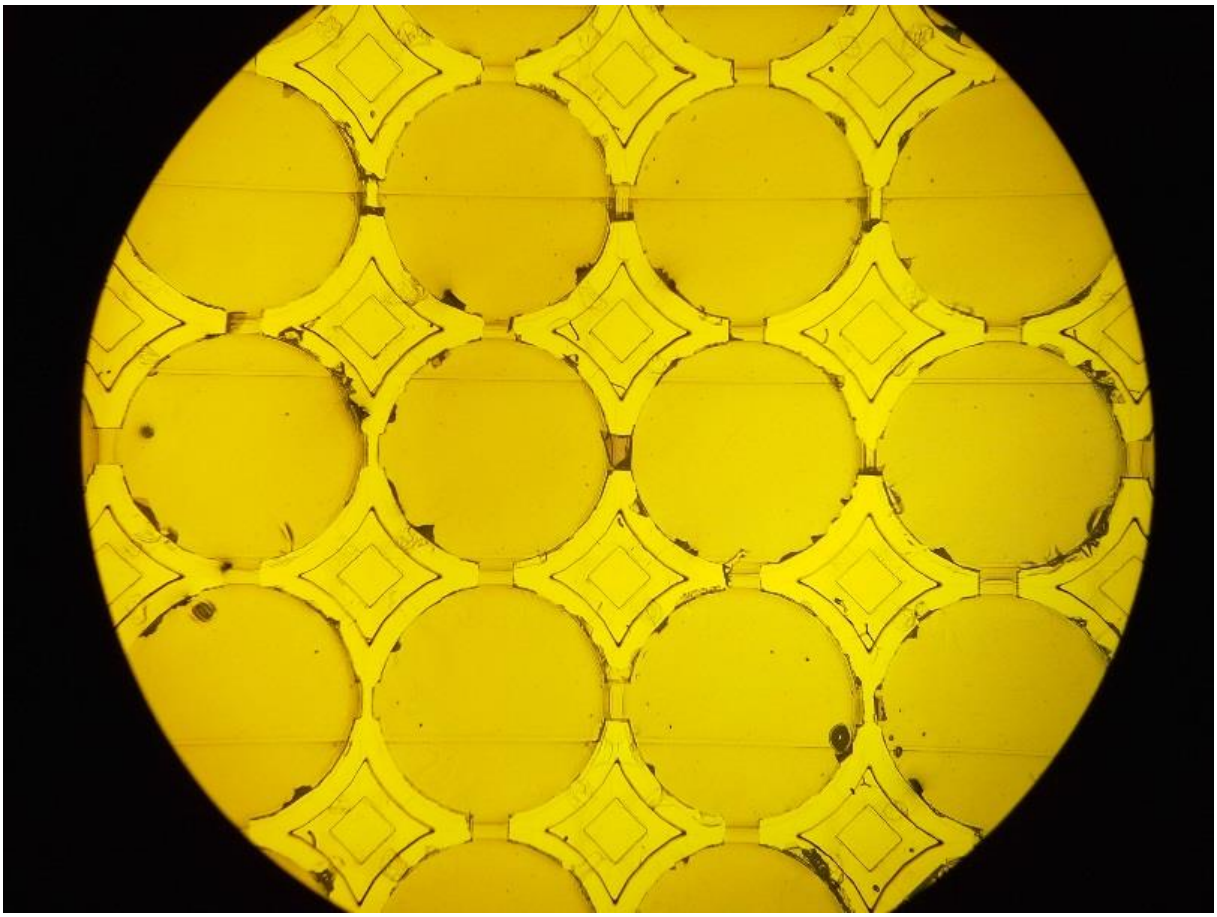

FIGURE 38: THE SAMPLE WITH THE ATTACKED SU8 LAYER AFTER 24 HOURS OF ETCHING.

As the process in itself was proven to work for smaller membrane sizes, and the problem clearly was the long etching time, it was decided to produce a new fabrication mask with holes in the membranes to allow the developer to penetrate through the membrane and not only through the channels. This however brought another change: The samples could not be sealed by Parylene C anymore as it would penetrate the holes and fill the cavity needed for vibration. The missing coating was suspected to have no major impact as the membranes were intended for air coupled instead of water coupled operation. A new fabrication mask with the frequencies already given in Table 3 was created.

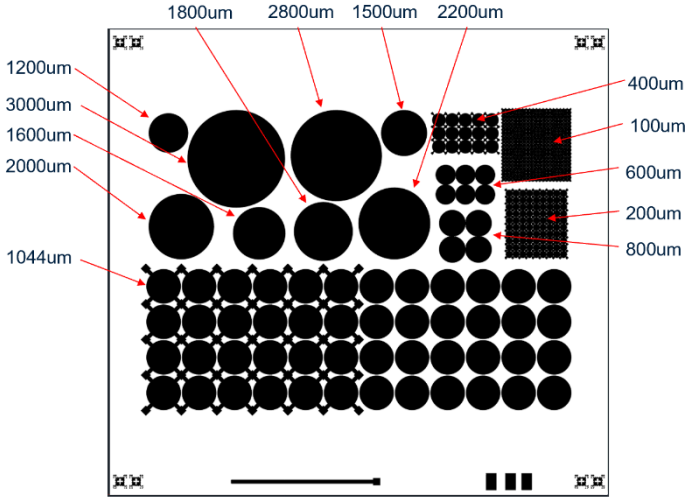

FIGURE 39: THE NEW FABRICATION MASK WITH THE ETCH HOLES

Before dicing and drying the resulting sample looked perfect as shown in Fig. 41. The etch holes were clearly defined and alignment of the different layers was perfect.

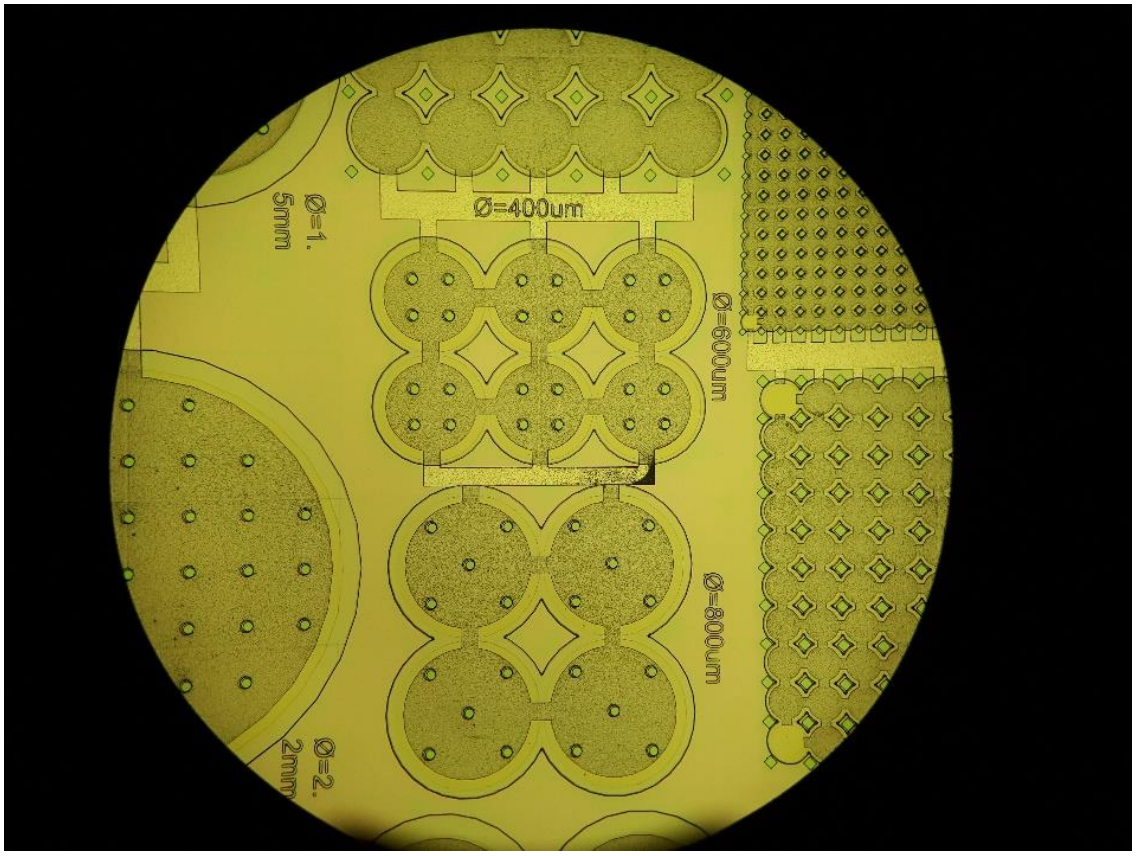

FIGURE 40: SAMPLE 7 WITH THE NEW FABRICATION MASK AND THE ETCH HOLES IN THE MEMBRANE.

The last steps remaining were the dicing, etching and then drying of the sample. However, when dicing was attempted the sample broke due to some manufacturing impurities in the wafer.

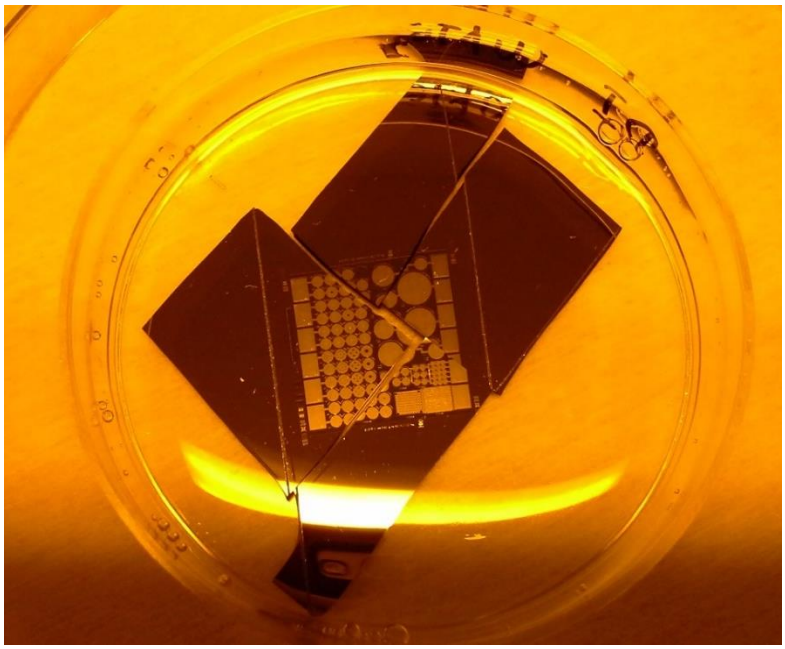

FIGURE 41: THE BROKEN SAMPLE 7 AFTER DICING.

The fabrication of sample 8 finally worked. After dicing and etching it was put in a critical point dryer (Tousimis, Rockville, MD, USA) were the remaining etchant is replaced by liquid CO_2 which evaporates at room temperature. During the critical point drying the membranes seemed to be deflected outwards. This let to a slight buckling effect further increasing the needed pull in voltage, however older samples showed no significant reduction in performance due to this effect. The buckling in the dryer can be seen in Fig. 43.

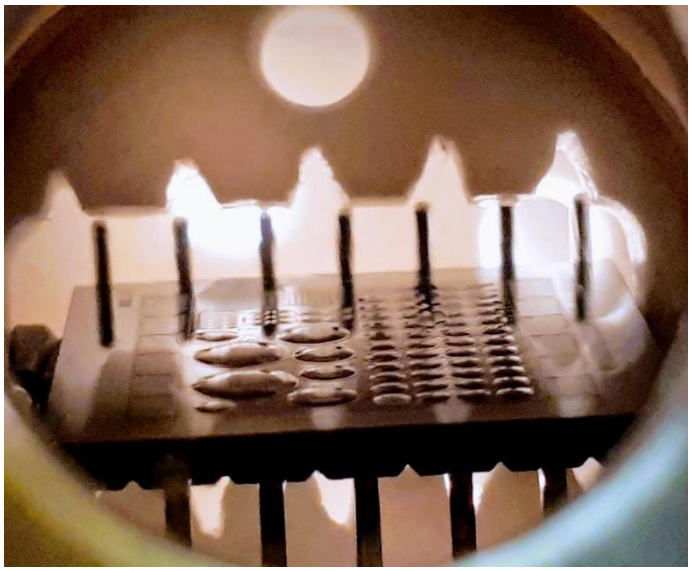

FIGURE 42: THE BUCKLED MEMBRANES INSIDE THE CRITICAL POINT DRYER.

After the drying the resulting chip was mounted on a PCB for further testing. The chip was glued onto the PCB with Kapton tape and the contacts were connected with silver ink.

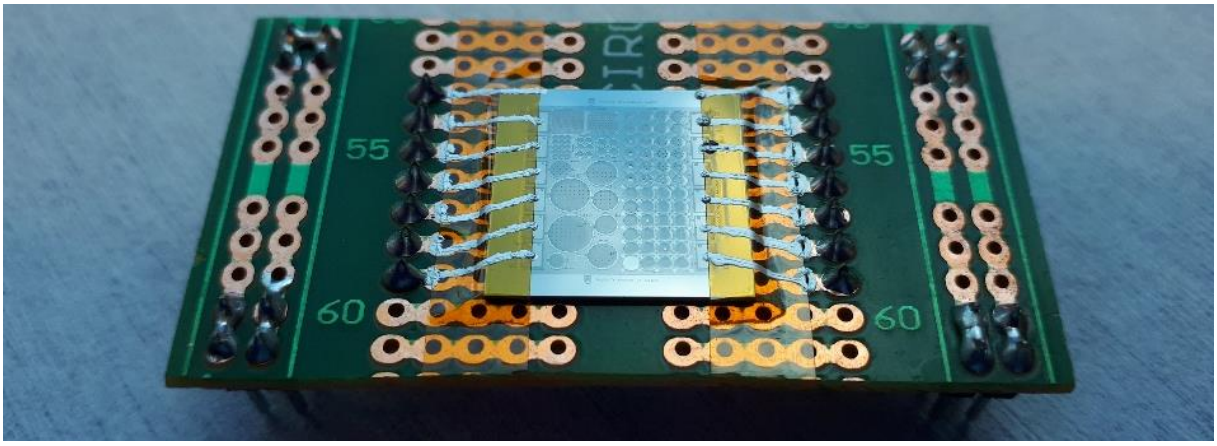

FIGURE 43: THE FINISHED SAMPLE READY FOR FURTHER TESTING.

3.5 The Laser Doppler Vibrometer and what it is used for

After fabrication the produced sample has to be analysed and tested. The main parameter in question is its center frequency. To characterize this frequency a so-called laser doppler vibrometer or LDV is used. The LDV used in this thesis is manufactured by Polytech (Waldbronn, Baden-Württemberg, Germany) and its operating principle is perfectly explained on their website:

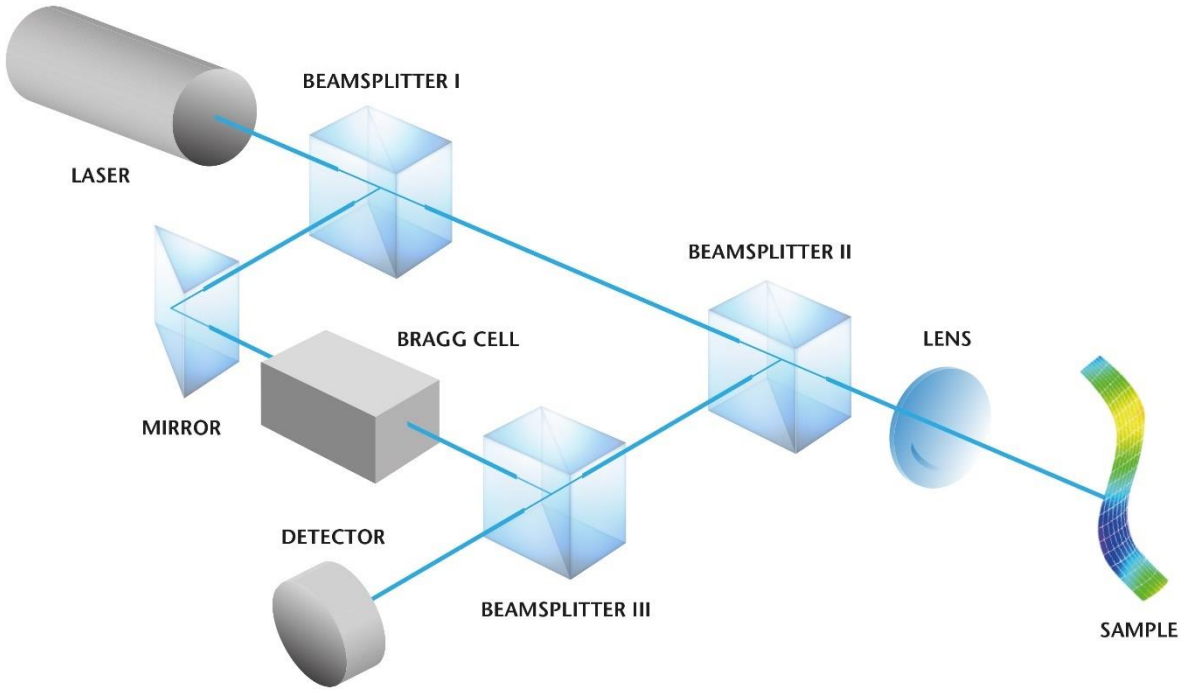

FIGURE 44: THE GENERAL OPERATING PRINCIPLE OF A LDV

The beam of a laser is split by a beam splitter (BS 1) into a reference beam and a measurement beam. After passing through a second beam splitter (BS 2), the measurement beam is focused onto the sample, which reflects it. This reflected beam is now deflected downwards by BS 2 (see figure) and is then merged with the reference beam onto the detector.

As the optical path of the reference beam is constant over time (r_2 = const.) *(with the exception of negligible thermal effects on the interferometer), a movement of the sample* ($r_1 = r(t)$) *generates a light / dark pattern, typical of interferometry, on the detector. One complete light / dark cycle on the detector corresponds to an object displacement of exactly half of the wavelength of the light used. In the case of the helium neon laser often used for vibrometers, this corresponds to a displacement of* 316 nm.

Changing the optical path length per unit of time manifests itself as the measurement beam's Doppler frequency shift. In metrological terms, this means that the modulation frequency of the interferometer pattern determined is directly proportional to the velocity of the sample. As object movement away from the interferometer generates the same modulation pattern (and modulation frequencies) as object movement towards the interferometer, this set-up alone cannot unambiguously determine the direction the object is moving in. For this purpose, an acousto-optic modulator (Bragg cell) that typically

shifts the light frequency by 40 MHz is placed in the reference beam (for comparison purposes, the laser light's frequency is $4.74 \cdot 10^{14}$ Hz). *This generates a typical interference pattern modulation frequency of 40 MHz when the sample is at a standstill. If the object then moves towards the interferometer, this modulation frequency is increased, and if it moves away from the interferometer, the detector receives a frequency less than* 40 MHz*. This means that it is now possible to not only clearly detect the path length, but also the direction of movement too.* [71]

With the help of the attached microscope and the corresponding software it is able to show movements and accelerations in the picometer range. For our purposes the LDV is used to measure the reaction of the membrane to excitation signals with different frequencies. The setup is as shown in Figure 45 and 46.

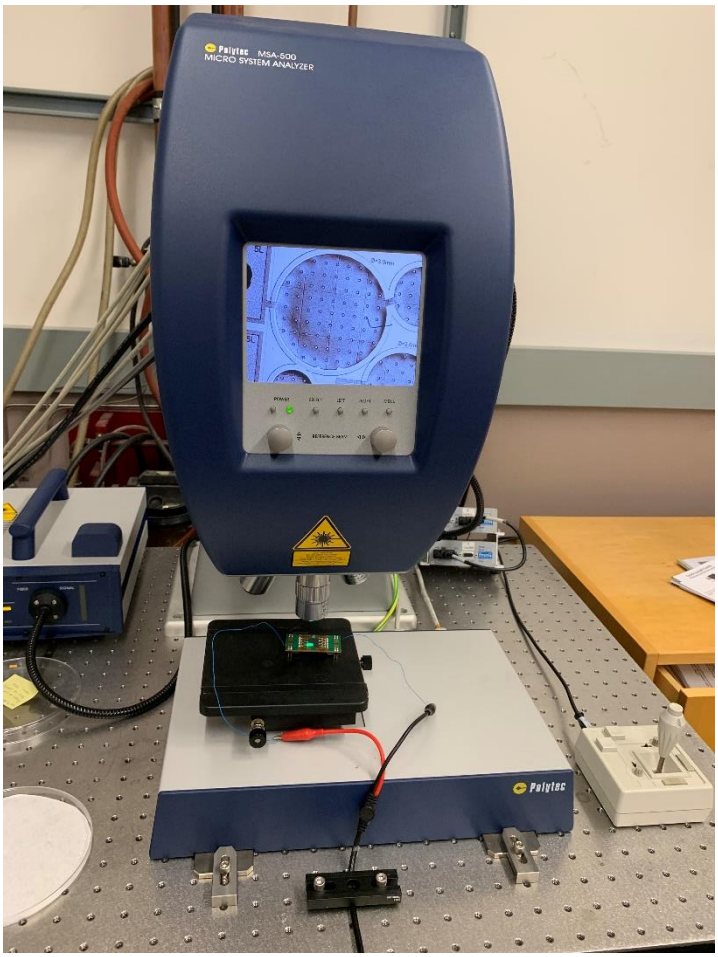

FIGURE 45: THE MICROSCOPE OF THE LDV SYSTEM WITH THE CONNECTED SAMPLE.

In the figure above the main measurement area is shown. Underneath the microscope the small green sample is visible, and it is connected to two cables leading to a function generator shown in the next figure. The small screen on top of the microscope is showing the current focus to help with positioning of the sample. The joystick on the right can move the black table in 2 dimensions but if the sample is large enough it can also be positioned by hand. Between the sample and the screen, the lens revolver for the microscope can be seen. The focussing mechanism is positioned at the back of the microscope and not shown. The black cable coming out of the small blue box on the left is an optical fiber leading the laser beam to the microscope. The laser itself is produced in the blue box. The whole built is

positioned on an air cushioned anti vibration table to get rid of any environmental vibrations. In Fig. 47 the electronic setup of the experiment is shown.

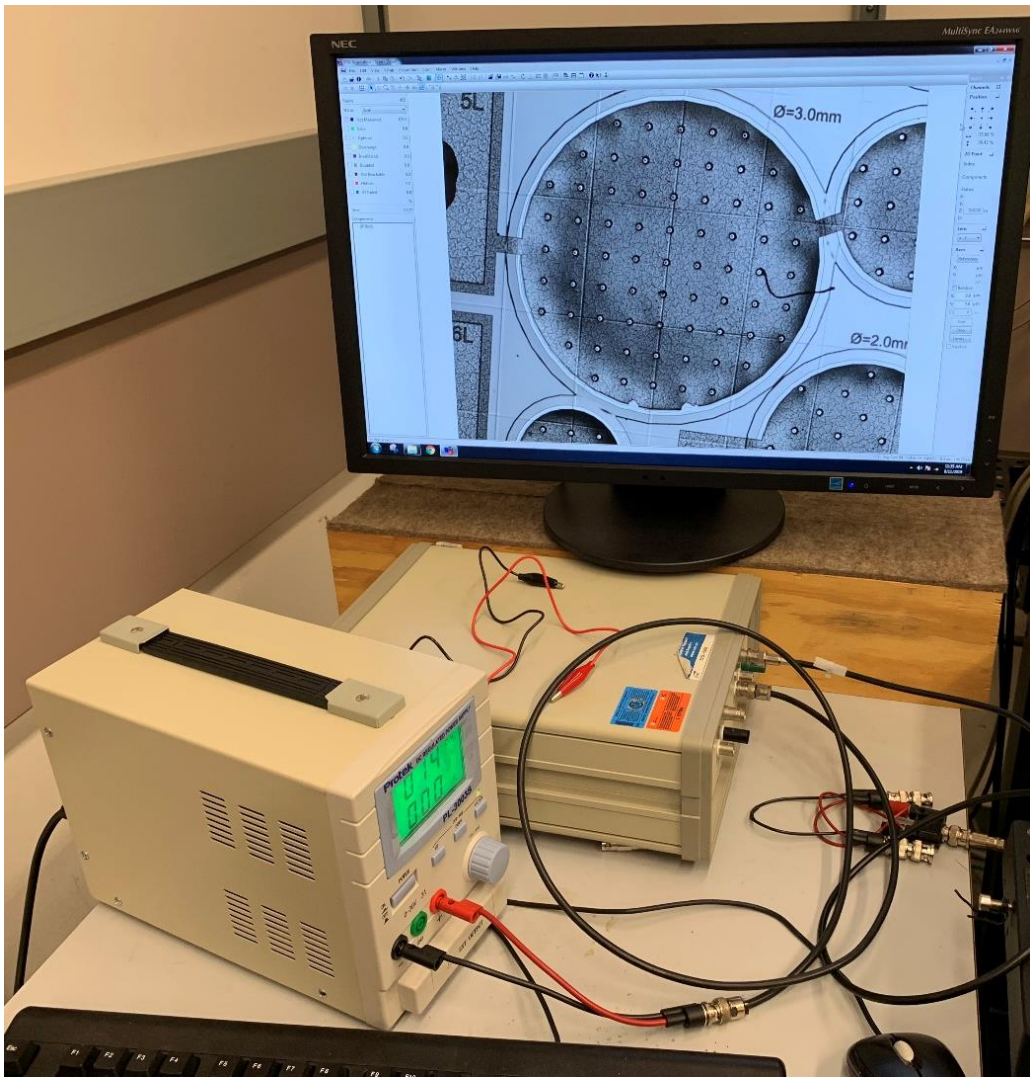

FIGURE 46: THE ELECTRONICS SETUP OF THE EXPERIMENT.

The screen shows the control terminal of the LDV where everything from basic positioning to measurement variables can be controlled. The flat box beneath the screen is an amplifier. This is necessary as the LDV built in function generator only supports up to 20 V, but because of the thick membranes and the chromium electrodes, the needed pull in voltages are in the area of 100 to 200 Volts. The amplifier has an amplification of 50 with a maximum output of 200 V. The box on the left is a direct current (DC) generator which is used to find the collapse voltage of the membranes and will be explained later on.

To actually test our sample for its center frequency we have to define certain parameters. First the scan points for the LDV need to be defined. As our membranes are usually parts of elements, it is advised to scan several membranes at once to be able to average the measured results. As the laser dot itself has a diameter of less than a micron and because different areas of the membrane will see different deflection, it makes sense to scan several points on the same membrane. The placement of scan points can be seen in the following figure. It shows the scan of 8 membranes at once with 40 scan points per membrane. The scan points can be placed in different patterns, but an even distribution was shown to yield the best results in past scans.

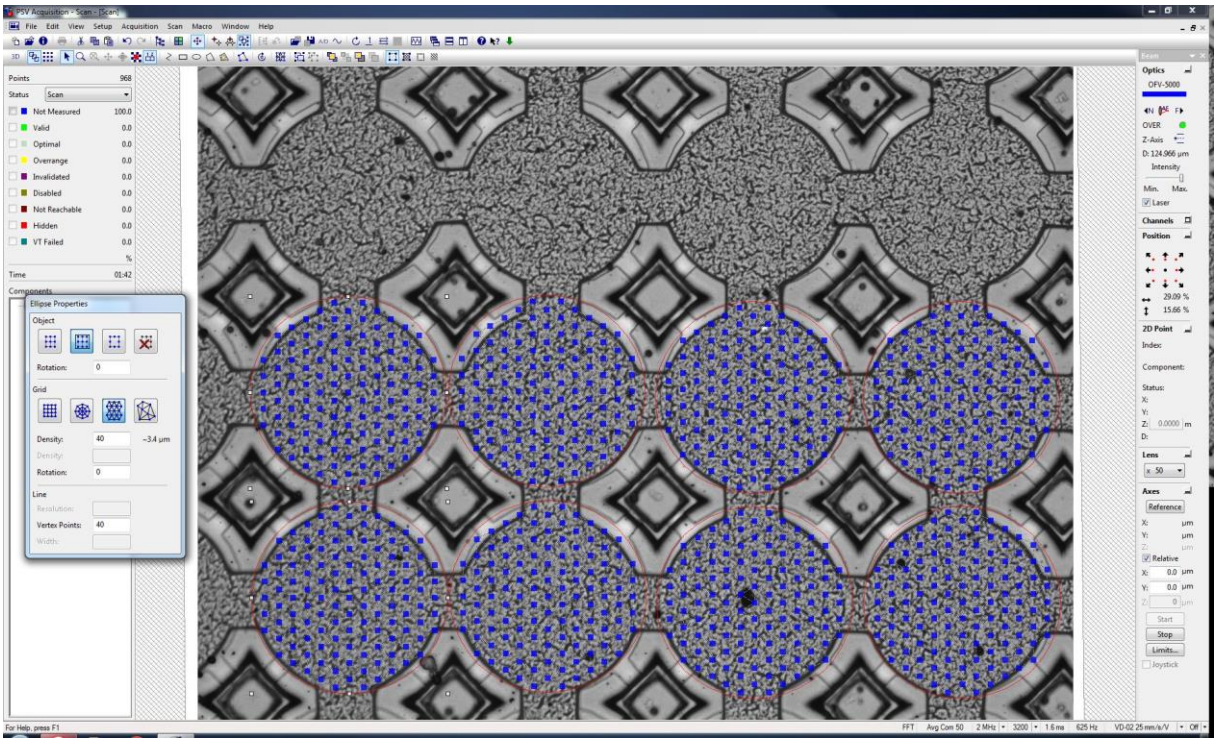

FIGURE 47: THE SCAN POINTS AS DEFINED IN THE CONTROL CENTER OF THE LDV

The other parameters that need to be defined are the following:

The excitation signal is chosen to be a periodic chirp. A chirp signal changes its frequency depending on the time. This allows for a deflection scan in different frequencies. The base signal amplitude is chosen to be 1 V with an offset of 0.8 V. Both are fed into the amplifier, so the actual current is 50 V with and offset of 40 V. The bandwidth of the measurements is set to 1 MHz starting at 10 kHz. The frequency resolution, or FFT number is set to 3200, resulting in a step size of roughly 310 Hz. An average of measurements is set to 50 meaning that every point is scanned 50 times and then the average result is shown. No further filters are used as the noise usually is not big enough to influence the measurements significantly.

After all the parameters are set the LDV can start its scan. This will (depending on the number of scan points and the average) take about 10 minutes per scan. A finished scan is shown and explained on the following page.

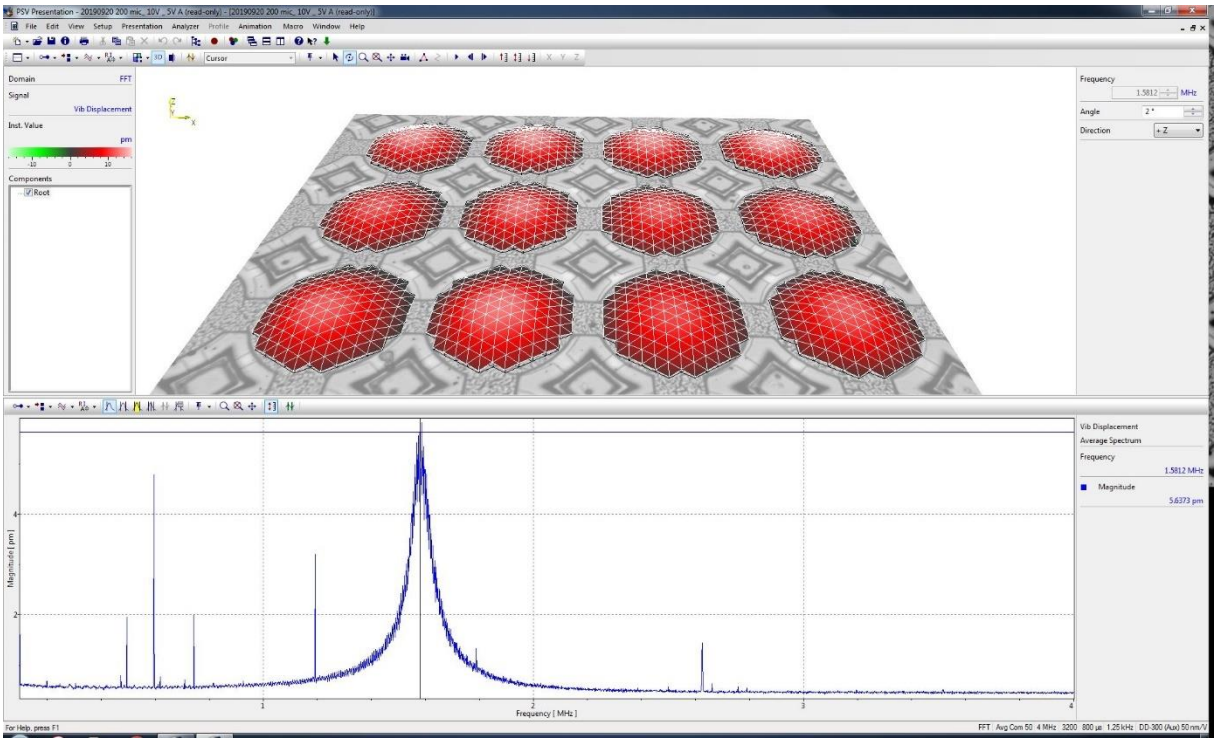

FIGURE 48: A FINISHED SCAN OF 12 MEMBRANES AND THEIR FREQUENCY RESPONSE.

The scan shown above is the typical result of a scan with the above-mentioned parameters. The top is a 3D model of the deflection that can also be animated to show the movement. This is particularly useful to show different vibration modes. The lower graph shows the deflection of the membrane in relation to the frequency of the excitation signal. The moment the excitation signal is the same as the resonance frequency of the membrane its deflection will increase significantly. This increase is the main peak in the graph above. The smaller spikes are noises that got picked up by the LDV as the measured deflection is just in the range of a few picometer. In this measurement the center frequency of the membranes was determined to be 1.58 MHz as shown by the number on the right.

3.6 Helmholtz and his frequency

As one may guess by the caption the scans of the produced, non-sealed sample did not resemble the perfect measurement shown above. All of the membranes were scanned but the scan of the 1044 µm diameter membrane will be shown. All the other scans can be found in the appendix.

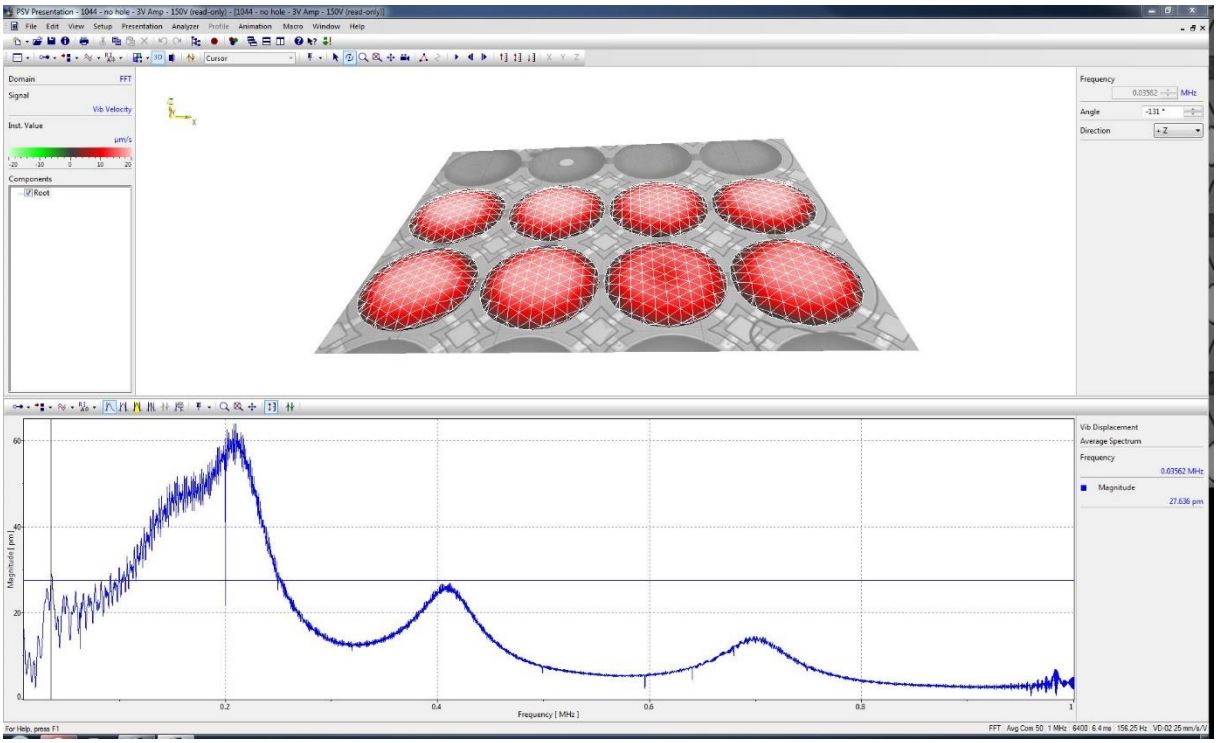

FIGURE 49: THE SCAN OF THE INTENDED 40KHZ MEMBRANES WITHOUT ANY ETCH HOLES AND THE CLASSIC CHANNELS

The scan in Fig. 50 shows the biggest problem that occurred with the new air-coupled sample. The different peaks show the different plate vibration modes. Plate vibration modes are the different resonance modes of a freely swinging plate. The first mode is the whole membrane moving up and down and should usually create the most movement and output power. The other vibration modes of a clamped circular plate are shown in Fig. 51 [72].

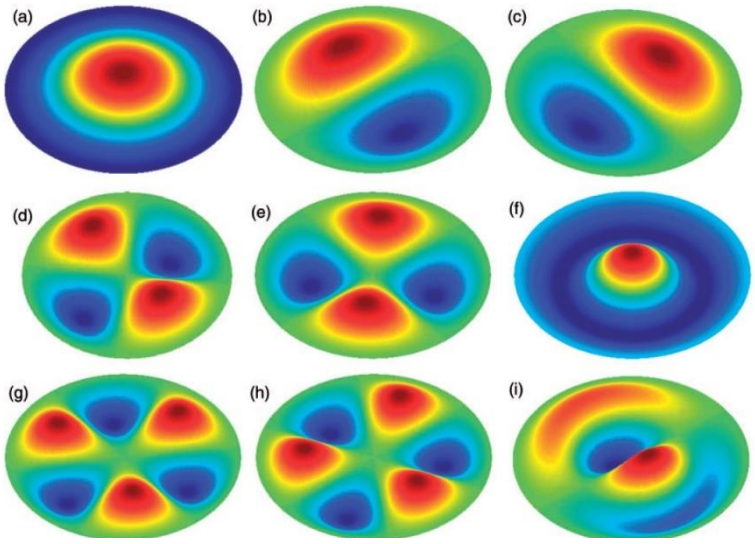

FIGURE 50: VIBRATION MODES 1-9 (A-I) OF A CIRCULAR PLATE

In the case of our scan the most dominant resonance frequency occurred at the second vibration mode. Another interesting phenomenon is the presence of further vibration modes in the bandwidth of 1 MHz. In a normal measurement the vibration modes are divided by several MHz and not just kHz. All of the other membrane sizes showed the same behaviour with the measured center frequencies in the table below.

Diameter [um]	f_R [kHz]	Measured f
100	4000	3756
200	1,000	1187
400	250	412
600	111	220
800	63	202
1,044	40	191-238
1,200	28.2	191
1500	17.78	179
1,600	16.2	179
1,800	12.1	186
2,000	10.9	180
2,200	8.2	186
2,800	5.1	192
3,000	4.4	186

TABLE 5: THE EXPECTED FREQUENCIES AND THE MEASURED ONES WITH THE RED NUMBERS BEING CLASSIC POLYCMUTS WITH ETCH CHANNELS.

The first 3 diameters were produced with the classic etch channel technique, as the diameters were too small to allow for etch holes in the membranes. Their measured frequencies are fairly accurate, with the slight deviations attributed to the buckled membranes. The larger membranes however show very similar results. The search for the reason began and it had to be some parameter in fabrication that stayed constant in the larger membranes. A thorough investigations showed the hole/membrane surface area ration was the only constant.

Diameter [um]	Etch hole diameter [um]	# holes	Total hole percentage to membrane	f_R Expected [kHz]	f_R Measured [kHz]
600	50	4	2.78%	111.0	220.0
800	50	5	1.95%	63.0	202.5
1,200	50	9	1.56%	28.2	191.9
1,500	50	13	1.44%	17.8	179.0
1,600	50	21	2.05%	16.2	179.0
1,800	50	21	1.62%	12.1	186.0
2,000	50	29	1.81%	10.9	180.0
2,200	50	37	1.91%	8.2	186.0
2,800	50	61	1.95%	5.1	192.5
3,000	50	69	1.92%	4.4	186.0

TABLE 6: THE DIFFERENT MEMBRANE SIZES AND THEIR HOLE PERCENTAGES.

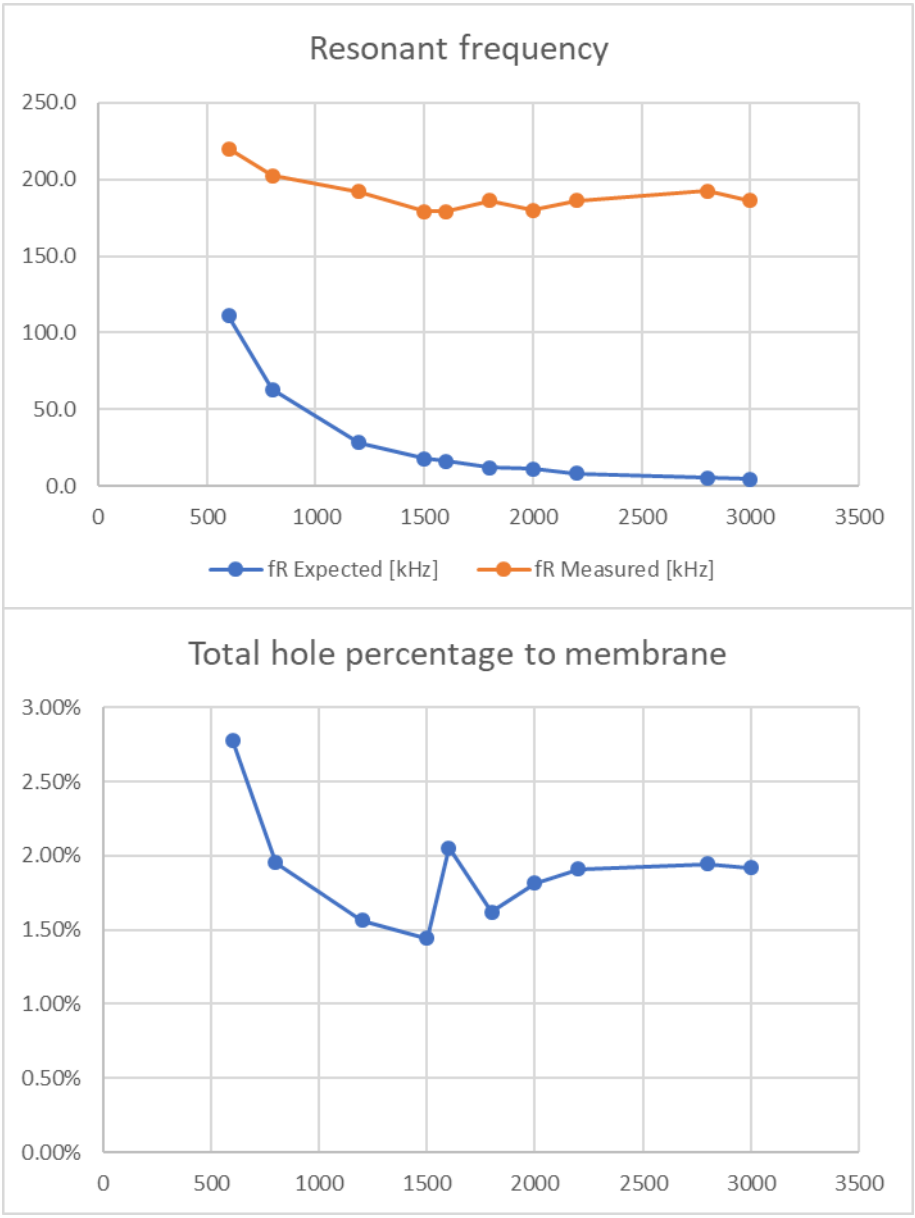

FIGURE 51: TWO DIAGRAMS SHOWING THE CORRELATION BETWEEN HOLE SIZES AND FREQUENCIES WITH THE X-AXIS SHOWING THE DIAMETERS IN MICRONS AND THE Y-AXIS SHOWING THE FREQUENCIES AND HOLE PERCENTAGES RESPECTIVELY

As can be seen in Fig. 52 and Table 6 the hole percentage stayed fairly constant with the curve of the measured frequencies following the curve of the hole percentage. The only possible explanation was that something had to dampen the vibration of the plate and amplify a certain resonance frequency attributed to the vent holes.

The answer came in form of a paper published in April 2019 by Liu et al. [73] In this paper the effect of a Helmholtz resonance was used to widen the bandwidth of the transducers produced. If a CMUT is produced and not properly sealed a so-called squeeze film effect is introduced. This dampens certain vibration modes. Another phenomenon introduced is a Helmholtz resonator. If a cavity with an opening, called a 'neck' is constructed and the air in this cavity is excited at a specific frequency it will start radiating waves to its surroundings. This effect is best known in the construction of speakers or musical instruments the best example being a guitar. In the paper mentioned both, the squeeze film effect and the Helmholtz resonance were used to enhance the performance of a classic CMUT. The used formulas could be traced back to allow for the calculation of the Helmholtz frequencies in the

sample PolyCMUTs and thus proof that the observed effect can really be traced back to Helmholtz and not only the deflection of the membranes while drying.

The basic model of the resonator was taken from the paper Liu et al. published and is shown in Fig. 53 [73].

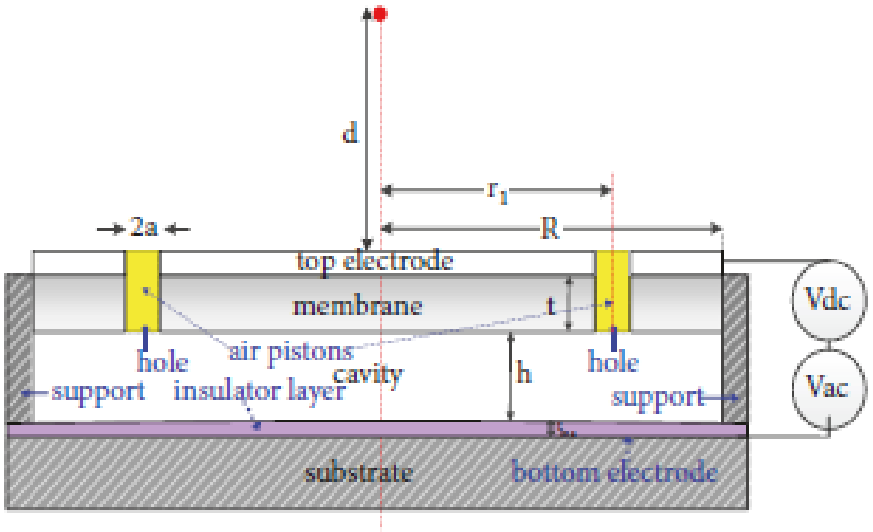

FIGURE 52: THE HELMHOLTZ RESONATOR CMUT MODEL FROM LIU ET AL.

The figure above shows a classic CMUT with vent holes. The yellow areas are the air pistons mostly contributing to the Helmholtz resonance. The variables used are the radius of the holes *a*, the thickness of the membrane *t,* the height of the cavity *h* and the radius of the membrane *R*.

The first equations needed are the resonant frequency of a clamped circular membrane ω_{P} [74]and the resonant frequency of the Helmholtz resonator ω_{H}. [75]

$$\omega_{\mathrm{P}} = 2\pi f_{\mathrm{P}} = 2\pi \cdot 0.47 \frac{t}{R^2} \sqrt{\frac{E}{\rho_{\mathrm{m}}(1-\nu^2)}} \tag{3.5}$$

$$\omega_{\mathrm{H}} = 2\pi f_{\mathrm{H}} = c\sqrt{\frac{S}{V(l+\delta)}} \tag{3.6}$$

With the combined poisons ratio of the membrane ν, the membrane Youngs modulus E, the membranes density ρ_m, the speed of sound in air c, with $t = l$ as the membrane/neck thickness and δ for the added end correction of the membrane. According to Ingard [75, 76] δ can be described as:

$$\delta = 0.48\sqrt{S}\left(1 - \frac{1.25\sqrt{n_{\mathrm{Hole}}}\cdot a}{R}\right) + 0.48\sqrt{S} \tag{3.7}$$

Withn_{Hole} being the number of holes and S the surface area of all holes combined.

The coupled resonance frequency can then be described as

$$\omega_{\pm}^2 = \frac{\omega_{\mathrm{P}}^2+\omega_{\mathrm{H}}^2}{2} \pm \frac{\sqrt{\left(\omega_{\mathrm{P}}^2-\omega_{\mathrm{H}}^2\right)^2+4\omega_{\mathrm{PH}}^4}}{2} \tag{3.8}$$

With

$$\omega_{\mathrm{PH}}^4 = \omega_{\mathrm{H}}^2 \frac{\mu A^2}{m_{\mathrm{P}}} \tag{3.9}$$

With A being the membrane surface area and m_{P} the mass of the membrane.

To reach the maximum performance boost we want the resonance frequencies of the Helmholtz resonator and the plate to be the same. If we use $f_{\mathrm{H}} = f_{\mathrm{P}}$ we can calculate the initial hole radius a_{ini}:

$$a_{\mathrm{ini}} = \frac{0.96*q_a*\sqrt{n_{\mathrm{hole}}*\pi}+\sqrt{0.96^2*n_{\mathrm{hole}}*\pi+q_{\mathrm{a}}^2-4(1+q_{\mathrm{a}}q_{\mathrm{b}})*(-q_{\mathrm{a}}*t)}}{2(1+q_{\mathrm{a}}q_{\mathrm{b}})} \tag{3.10}$$

Were

$$q_{\mathrm{a}} = \left(\frac{2\pi f_{\mathrm{p}}}{c}\right)^2 \left(\frac{\pi*R^2*h}{n_{\mathrm{Hole}}\cdot\pi}\right) \tag{3.11}$$

and

$$q_{\mathrm{b}} = \frac{0.6\cdot n_{\mathrm{Hole}}\sqrt{\pi}}{R} \tag{3.12}$$

The calculated Helmholtz frequencies are the following:

Diameter [um]	f_R [kHz]	Measured f	Helmholtz calc.
100	4000	3756	-
200	1,000	1187	-
400	250	412	-
600	111	220	580
800	63	202	427
1,044	40	191-238	309-385
1,200	28.2	191	333
1500	17.78	179	293
1,600	16.2	179	301
1,800	12.1	186	266
2,000	10.9	180	273
2,200	8.2	186	259
2,800	5.1	192	234
3,000	4.4	186	228

TABLE 7: THE CALCULATED HELMHOLTZ FREQUENCIES.

All those frequencies are curiously close together and they also would explain the effect of the widened bandwidth observed in the measurement in Fig. 50.

One interesting observation is that one batch of 1044 µm membranes had the normal etch channels instead the vent holes, but it still showed the shifted frequency. A reason for this could be that the unsealed etch channels act as Helmholtz resonators as well. To proof this theory another physical test was conducted: What would happen if the sample was sealed with Parylene C? All the samples with vent holes would be destroyed, but the elements with etch channels could be still usable. Another problem would be that the larger membranes would collapse due to atmospheric pressure as the sealing creates a vacuum in the cavity. The resulting resonances would not resemble the ones calculated as the Parylene changes the thickness of the membrane and adds to its stability, but the resulting LDV measurements could still show if the dominant vibration mode would be the first one again.

After the sealing the following results were obtained:

Diameter [um]	f_R [kHz]	Measured f	After sealing
100	4000	3756	4780
200	1,000	1187	1581
400	250	412	491
600	111	220	D
800	63	202	D
1,044	40	173	343
1,200	28.2	191	D
1500	17.78	179	D
1,600	16.2	179	D
1,800	12.1	186	D
2,000	10.9	180	D
2,200	8.2	186	D
2,800	5.1	192	D
3,000	4.4	186	D

TABLE 8: THE MEASURED RESULTS OF THE SEALED SAMPLE.

As expected, the frequencies of the membranes were further increased and the ones without etch channels were destroyed. What was the real breakthrough however were the obtained LDV measurements of the 1044 µm membranes with etch channels.

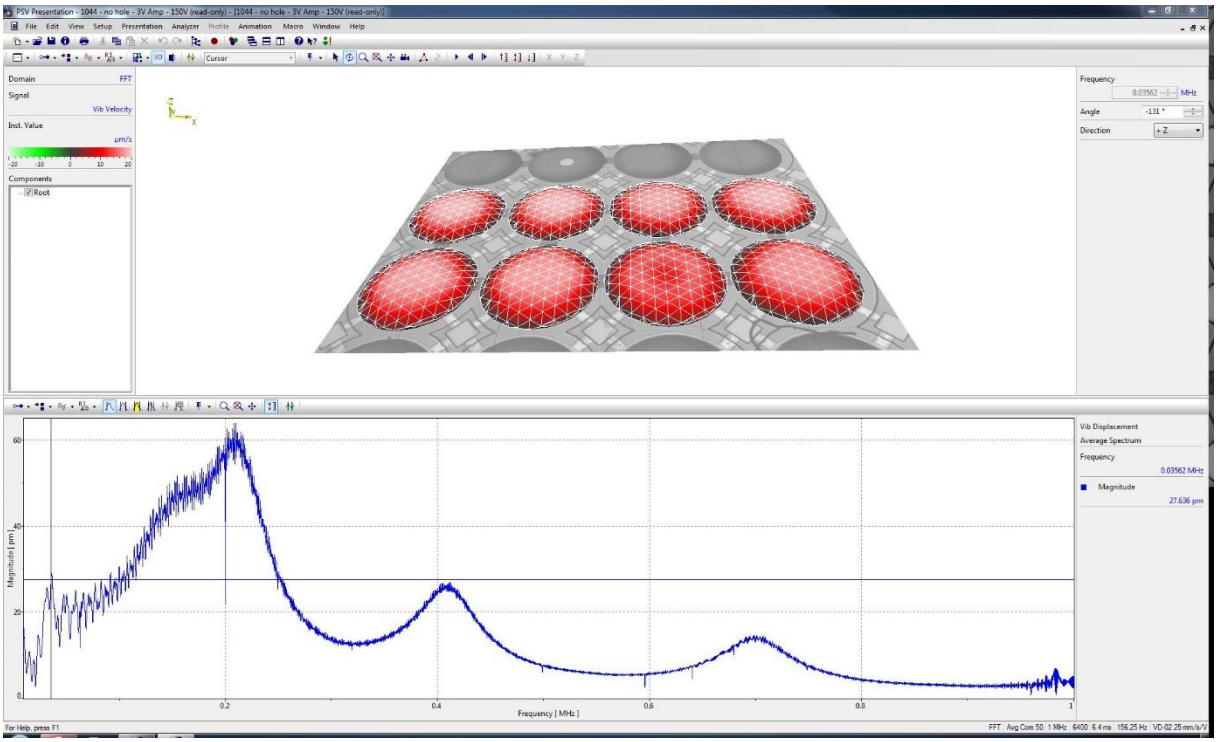

FIGURE 53: THE 1044 MICRON MEMBRANES BEFORE SEALING WITH THE WIDE BANDWIDTH AND SEVERAL VIBRATION MODES

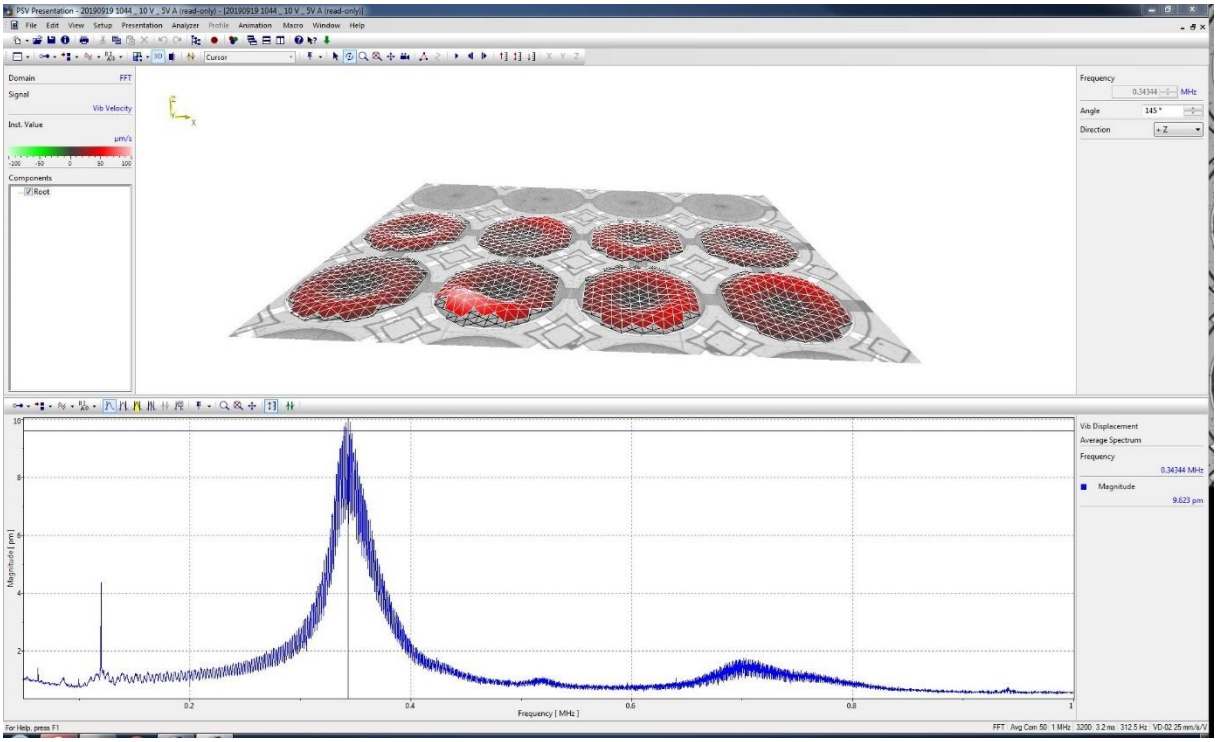

FIGURE 54: THE MEASUREMENT OF THE SEALED 1044 MICRON MEMBRANES

As expected, Fig. 55 shows that the membranes have collapsed due to the atmospheric pressure. The remaining suspended plate can still be used as a vibrating element though. The first SU8 layer acts as an insulator and protects the CMUT from a short circuit. This only shifts the frequency, but does not impact the basic functionality as mentioned by Shi et al. [72]. The measured frequency response shows

that there are still other vibration modes visible, but they are a lot less dominant, with the highest response at the first mode. The same can be observed with the other measurements shown in the appendix.

The calculation of the Helmholtz hole sizes was included into the calculation tool for the PolyCMUTs, but for confidentiality reasons this tool can not be published.

4. The results

4.1 The results of the Helmholtz experiments

The results of the Helmholtz experiments were the following:

First it was shown that PolyCMUTs can work in air although there are certain difficulties in fabricating the air coupled variants. The very low gap size of only 1 µm is too small for a sealed sample, as membranes of the needed diameter are not rigid enough to withstand atmospheric pressure. The gap size can be increased but this significantly increases the pull in voltage, negating one of the PolyCMUTs biggest strength, the energy efficiency. The maximum gap size that would still yield a reasonable pull in voltage was calculated to be no greater than 5 µm. The remaining time sadly did not allow for the fabrication and testing of such a sample. It has to be investigated in later research.

The Helmholtz frequency itself is hard to control, especially with the hole sizes needed for lower frequencies. The diameters are usually in the area of a few microns, which is too small a diameter to be properly fabricated with a maskless lithography system and through spin coating. The coating of the different layers will interfere with the holes and the developers can not properly penetrate them due to squeeze film effects. With the increase of the cavity size to about 5 microns, the hole size increases to more realistic levels in the area of 10 microns. This again could not be tested as the remaining time sadly was too short. For the near future air coupled PolyCMUTs seem to be sealed, but the paper of Liu et al. [73] shows enormous potential as an increase in bandwidth means also an increase in sensitivity.

The output pressure could sadly not be measured as the produced low frequency sample was collapsed and the resulting acoustic pressure is just too low for any evaluation. As CMUTs inherently suffer from low output pressure again the usage of Helmholtz resonances could boost the sensitivity of the whole system thus needing a lower acoustic pressure from the start.

All in all, the experiments showed a need for further research and development. The initial idea of this thesis, to test several air coupled specimen of different frequencies in experiments involving the CFRP plate could just not be realized as fabrication itself was not at a state were this was realistic. Nevertheless, the research conducted for this thesis meant a significant increase in the understanding of air coupled PolyCMUTs, their production and the phenomena associated with the air coupling. This actually leads us to the last chapter:

4.2 Are PolyCMUTs usable for NDE of CFRP?

The general answer to this question has to be yes. The Verasonics experiment showed that CMUTs in general can be used in contact measurements to obtain usable results, even though the probe itself was not even optimized for this kind of application. PolyCMUTs are not very different to normal CMUTs and in the meantime the research group surrounding Edmond Cretu has managed to connect a PolyCMUT to Verasonics and obtain B-mode images. Another big factor is the mentioned improvement of the impedance mismatch. The increase in transmitted power just because of a different material is significant and its effects were shown in the simulation. The deciding factor is still if the theoretical output power in air can be achieved or at least closely reached with a fabricated prototype.

The theoretical value used for the output power was calculated as being as high as 1 MPa using a gab size of 5 microns and a perfect management of the Helmholtz effect. As literature has shown both can be achieved with normal CMUTs [77], so there is no reason to believe PolyCMUTs can not do the same. The many problems with fabrication can be fixed over time but this is what is needed the most: More research on the fabrication method to be able to produce prototypes in usable qualities and quantities. The usage for a pulse echo air coupled PolyCMUT for now is unrealistic as fabrication is not proven.

Another usage however is more realistic: Carlos Gerardo was able to produce water coupled PolyCMUTs and the fact that PolyCMUTs are cheaper by a factor of 10 makes them interesting as replacements for normal transducers in current water coupled NDE methods. Another field of use could be new hybrid systems for example a PolyCMUT array as the receiver for a Lamb wave based NDE system. The spatial resolution of the array could be used for a better overall resolution.

For now, the technology of PolyCMUTs is highly experimental and it will still take several years till the first commercial products in the NDE world emerge. The conducted experiments however show the enormous potential the technology has, and the author of this thesis is convinced that PolyCMUTs have a glorious future in the world of ultrasound in general.

5. Acknowledgements

The process of writing this thesis was a long and very exciting journey. From learning about microfabrication and all its many facets to rediscovering my love for electrical engineering, the challenges were countless and came in many different shapes and sizes. All of this would not have been possible without the help and support of a group of extraordinary people. In the following sentences I will try to recognize and thank them all.

First of all, thank you to my family. When I told you, I was going to leave for 6 months to write my thesis in Canada all I heard was excitement, support, encouragement and several jokes about me not coming back to Germany. When I told you that I am going to stay in Vancouver 4 more years to pursue a PhD the only answer was 'we told you so'. Thank you for everything you are the best and I love you.

Thank you to Edmond Cretu and Robert Rohling, who without even knowing me, put their trust in me not only to write a master thesis in their research group about a topic I had never worked with but also to continue this work for 4 more years. I am looking very much forward to our future work and I am excited to return in January as your PhD student.

To Carlos. You took your time and explained everything microfabrication to me. You took me to the cleanroom, fabricated my samples, helped with my paperwork and so much more. Without you this would have been simply impossible. I am really looking forward to being your colleague once again for my PhD.

To Armin and the team of the DLR Augsburg for always answering my questions, taking me into your institute with open arms and supporting me in any way possible. Armin, your support was vital for this thesis. Thank you. I am looking forward to seeing you all again at the following conferences of our cooperation.

To my friends at home who called, talked to me and endured several rants about the hardships of scientific writing. You guys rock! I hope you all can make it to Vancouver one time or another. I would love to show you around.

To my colleagues in Kaiser 3030. You made work a fun place that I was looking forward to every single morning. I will see you all in January and I am looking forward to my return into the madhouse we call office.

To the people from Kings Night 💛🍻💛. All the hikes, the nights on the beaches, the talks, Bingo and all the other things that we did, made these 6 months unforgettable. I feel like I've known you all for years not months, and I will miss all of you in Vancouver. You guys made the difference and this into my best summer ever. I will make sure to visit all of you as much as I can.

And last but not least, thank you Heinz. I don't even know where to start and I don't think I can ever express how much you changed my live with a simple question. You asked us 'who wants to go to Canada to write their thesis?' and that was all it took to turn my whole life around. I found a city I love, a renewed passion of hiking and nature, a job for the next 4 years, many new friends from all over the world and so much more just because you asked that simple question. Thank you for always making time and having an open ear even though you have the busiest schedule I have ever seen. Thank you for putting your trust in me and the other DLR@UBC students. You are the best professor I have ever had in my 9 years of studying.

I sincerely hope I did not forget anybody and if I did, please know that I am grateful for all of this.

6. Sources

1. *The Popular science monthly* [online]. [New York, Popular Science Pub. Co., etc.], 1873. [Accessed 5 December 2019]. Available from: http://archive.org/details/popularsciencemo03newy01762662

2. GRAFF, Karl F. A History of Ultrasonics. In : *Physical Acoustics* [online]. Elsevier, 1981. p. 1–97. [Accessed 2 December 2019]. ISBN 978-0-12-477915-0. Available from: https://linkinghub.elsevier.com/retrieve/pii/B9780124779150500063

3. HELMHOLTZ, Hermann von. *Theorie der Luftschwingungen in Röhren mit offenen Enden*. 1. Auflage. Berlin : Reimer, 1860. Journal für die reine und angewandte Mathematik. In zwanglosen Heften.

4. KUNDT, A. IV. On the velocity of sound in tubes. *The London, Edinburgh, and Dublin Philosophical Magazine and Journal of Science*. July 1868. Vol. 36, no. 240, p. 22–26. DOI 10.1080/14786446808640018.

5. GALTON, Francis. Whistles for audibility of shrill notes. In : GALTON, Francis, *Inquiries into human faculty and its development.* [online]. New York : MacMillan Co, 1883. p. 38–40. [Accessed 5 December 2019]. Available from: http://content.apa.org/books/14178-008

6. CURIE, Jacques and CURIE, Pierre. Développement par compression de l'électricité polaire dans les cristaux hémièdres à faces inclinées. *Bulletin de la Société minéralogique de France*. 1880. Vol. 3, no. 4, p. 90–93. DOI 10.3406/bulmi.1880.1564.

7. KATZIR, Shaul. *The beginnings of piezoelectricity: a study in mundane physics*. Dordrecht : Springer, 2006. Boston studies in the philosophy of science, v. 246. ISBN 978-1-4020-4669-8. QC595.5 .K37 2006

8. LECONTE, John. ART. IX.--On the Influence of Musical Sounds on the Flame of a Jet of Coal-gas; *American Journal of Science and Arts (1820-1879); New Haven*. May 1858. Vol. 25, no. 73, p. 62.

9. TYNDALL, John. *Sound* [online]. New York : D. Appleton and company, 1903. [Accessed 5 December 2019]. Available from: https://catalog.hathitrust.org/Record/101821486

10. SPINDLER, Paul (de Chemnitz) Auteur du texte, MEYER, Georg (1857-1950) Auteur du texte and MEERBURG, Jacob Hendrik Auteur du texte. Annalen der Physik. *Gallica* [online]. 1866. [Accessed 5 December 2019]. Available from: https://gallica.bnf.fr/ark:/12148/bpt6k15212x

11. HELMHOLTZ, Hermann L. F. and ELLIS, Alexander J. *The sensations of tone: As a physiological basis for the theory of music, 6th ed*. New York, NY : Peter Smith, 1885. 2009-03173-000

12. RAYLEIGH, John William Strutt. *The theory of sound* [online]. London, Macmillan and co., 1877. [Accessed 5 December 2019]. Available from: http://archive.org/details/theorysound06raylgoog

13. RAYLEIGH, L. *On the Circulation of Air Observed in Kundt's Tubes, and on Some Allied Acoustical Problems* [online]. Royal Society of London, 1884. [Accessed 5 December 2019]. Available from: http://archive.org/details/philtrans00491697

14. RAYLEIGH, L. *Note on the Free Vibrations of an Infinitely Long Cylindrical Shell* [online]. Royal Society of London, 1888. [Accessed 5 December 2019]. Available from: http://archive.org/details/philtrans03541714

15. RAYLEIGH, L. *On the Bending and Vibration of Thin Elastic Shells, Especially of Cylindrical Form* [online]. Royal Society of London, 1888. [Accessed 5 December 2019]. Available from: http://archive.org/details/philtrans02342918

16. RAYLEIGH, L. *On the Bending of Waves Round a Spherical Obstacle* [online]. Royal Society of London, 1903. [Accessed 5 December 2019]. Available from: http://archive.org/details/philtrans09625840

17. RAYLEIGH, L. and SIDGWICK, M. *On the Specific Resistance of Mercury.* [online]. Royal Society of London, 1882. [Accessed 5 December 2019]. Available from: http://archive.org/details/philtrans03889441

18. RAYLEIGH, Lord. On Waves Propagated along the Plane Surface of an Elastic Solid. *Proceedings of the London Mathematical Society*. November 1885. Vol. s1-17, no. 1, p. 4–11. DOI 10.1112/plms/s1-17.1.4.

19. FOREST, Lee De. Device for amplifying feeble electrical currents [online]. US841387A. 15 January 1907. [Accessed 5 December 2019]. Available from: https://patents.google.com/patent/US841387A/en

20. VOIGT, Woldemar. *Lehrbuch der kristallphysik (mit ausschluss der kristalloptik)* [online]. Leipzig, Berlin, B.G. Teubner, 1910. [Accessed 5 December 2019]. Available from: http://archive.org/details/bub_gb_SvPPAAAAMAAJ

21. FESSENDEN, Reginald A. Apparatus for the transmission of energy by electric oscillation [online]. US1156677A. 12 October 1915. [Accessed 6 December 2019]. Available from: https://patents.google.com/patent/US1156677/enUS22229904A

22. FESSENDEN, Reginald A. Signaling by sound and other longitudinal elastic impulses [online]. US1108895A. 1 September 1914. [Accessed 6 December 2019]. Available from: https://patents.google.com/patent/US1108895/enUS81142814A

23. FESSENDEN, Reginald A. Apparatus for producing high-frequency oscillations [online]. US1166892A. 4 January 1916. [Accessed 6 December 2019]. Available from: https://patents.google.com/patent/US1166892/enUS522092A

24. FROST, Gary L. Inventing Schemes and Strategies: The Making and Selling of the Fessenden Oscillator. *Technology and Culture*. 2001. Vol. 42, no. 3, p. 462–488. DOI 10.1353/tech.2001.0109.

25. LANGEVIN, Paul. Piezoelectric signaling apparatus [online]. US2248870A. 8 July 1941. [Accessed 6 December 2019]. Available from: https://patents.google.com/patent/US2248870A/enUS390542A

26. SHAUL KATZIR. War and Peacetime Research on the Road to Crystal Frequency Control. *Technology and Culture*. 2009. Vol. 51, no. 1, p. 99–125. DOI 10.1353/tech.0.0413.

27. ZIMMERMAN, David. 'A more creditable way': The discovery of active sonar, the Langevin–Chilowsky patent dispute and the Royal Commission on Awards to Inventors. *War in History*. January 2018. Vol. 25, no. 1, p. 48–68. DOI 10.1177/0968344516651308.

28. Sergei Sokolov. [online]. [Accessed 9 December 2019]. Available from: http://www.ob-ultrasound.net/sokolov.html

29. KRAUTKRÄMER, Josef and KRAUTKRÄMER, Herbert. *Ultrasonic Testing of Materials* [online]. Berlin, Heidelberg : Springer Berlin Heidelberg, 1990. [Accessed 4 November 2019]. ISBN 978-3-662-10680-8. Available from: http://public.ebookcentral.proquest.com/choice/publicfullrecord.aspx?p=3099756

30. ROKHLIN, S. I., CHIMENTI, Dale E. and NAGY, P. B. *Physical ultrasonics of composites*. Oxford ; New York : Oxford University Press, 2011. ISBN 978-0-19-507960-9. TA418.9.C6 R65 2011

31. FIRESTONE, Floyd A. Flaw detecting device and measuring instrument [online]. US2280226A. 21 April 1942. [Accessed 9 December 2019]. Available from: https://patents.google.com/patent/US2280226A/enUS337419A

32. SPROULE, Donald Orr. Ultrasonic flaw detecting apparatus [online]. US2969671A. 31 January 1961. [Accessed 9 December 2019]. Available from: https://patents.google.com/patent/US2969671A/enUS638719A

33. History of NDT-Instrumentation. [online]. [Accessed 9 December 2019]. Available from: https://www.ndt.net/article/wcndt00/papers/idn378/idn378.htm

34. Early history of metal flaw detectors. [online]. [Accessed 9 December 2019]. Available from: http://www.ob-ultrasound.net/ndt.html

35. APTE, Nikhil, PARK, Kwan Kyu, NIKOOZADEH, Amin and KHURI-YAKUB, Butrus T. Bandwidth and sensitivity optimization in CMUTs for airborne applications. In : *2014 IEEE International Ultrasonics Symposium* [online]. Chicago, IL, USA : IEEE, September 2014. p. 166–169. [Accessed 13 August 2019]. ISBN 978-1-4799-7049-0. Available from: http://ieeexplore.ieee.org/document/6932362/

36. MA, B., FIROUZI, K., BRENNER, K. and KHURI-YAKUB, B. T. Wide Bandwidth and Low Driving Voltage Vented CMUTs for Airborne Applications. *IEEE Transactions on Ultrasonics, Ferroelectrics, and Frequency Control*. 2019. P. 1–1. DOI 10.1109/TUFFC.2019.2928170.

37. HOHM, Dietmar and HESS, Gisela. A subminiature condenser microphone with silicon nitride membrane and silicon back plate. *The Journal of the Acoustical Society of America*. January 1989. Vol. 85, no. 1, p. 476–480. DOI 10.1121/1.397699.

38. ORALKAN, O., ERGUN, A.S., JOHNSON, J.A., KARAMAN, M., DEMIRCI, U., KAVIANI, K., LEE, T.H. and KHURI-YAKUB, B.T. Capacitive micromachined ultrasonic transducers: next-generation arrays for acoustic imaging? *IEEE Transactions on Ultrasonics, Ferroelectrics and Frequency Control*. November 2002. Vol. 49, no. 11, p. 1596–1610. DOI 10.1109/TUFFC.2002.1049742.

39. ACHENBACH, J. D. *The Evaluation of Materials and Structures by Quantitative Ultrasonics* [online]. Vienna : Springer Vienna, 1993. [Accessed 6 November 2019]. CISM International Centre for Mechanical Sciences. ISBN 978-3-211-82441-2. Available from: http://link.springer.com/10.1007/978-3-7091-4315-5

40. HEDRICK, Wayne R., HYKES, David L. and STARCHMAN, Dale E. *Ultrasound Physics and Instrumentation*. Elsevier Mosby, 2005. ISBN 978-0-323-03212-4. Google-Books-ID: QoVsQgAACAAJ

41. BHARDWAJ, M C. HIGH EFFICIENCY NON-CONTACT TRANSDUCERS AND A VERY HIGH COUPLING PIEZOELECTRIC COMPOSITE. . 2004. P. 8.

42. COLLABORATION FOR NONDESTRUCTIVE TESTING. Wave Propagation. [online]. [Accessed 11 December 2019]. Available from: https://www.nde-ed.org/EducationResources/CommunityCollege/Ultrasonics/Physics/wavepropagation.htm

43. COLLABORATION FOR NONDESTRUCTIVE TESTING. Modes of Sound Wave Propagation. [online]. [Accessed 3 December 2019]. Available from: https://www.nde-ed.org/EducationResources/CommunityCollege/Ultrasonics/Physics/modepropagation.htm

44. HUBER, Armin. Non-destructive Testing of Future Rocket Boosters Using Air-Coupled Ultrasound. . P. 9.

45. HUBER, Armin and THELLMANN, Arthur-Hans. Quality Assurance of Carbon Fibre Reinforced Plastics Using Air- and Water-coupled Ultrasound - a Comparison. . P. 19.

46. LEMPRIERE, Brian M. 3 - Wave Propagation Concepts. In : LEMPRIERE, Brian M. (ed.), *Ultrasound and Elastic Waves* [online]. Burlington : Academic Press, 2003. p. 25–44. ISBN 978-0-12-443345-8. Available from: http://www.sciencedirect.com/science/article/pii/B9780124433458500299

47. SHULL, Peter J. Nondestructive Evaluation. . P. 841.

48. DÖRING, Daniel. *Luftgekoppelter Ultraschall und geführte Wellen für die Anwendung in der zerstörungsfreien Werkstoffprüfung*. Universitätsbibliothek der Universität Stuttgart, 2011. Google-Books-ID: 3dfAtAEACAAJ

49. SCHULLER, J, BOSSE, J, HILLGER, W and OSTER, R. Luftultraschallprüfung in der Luftfahrt. . P. 6.

50. LEISSA, Arthur W. *Vibration of Plates*. Scientific and Technical Information Division, National Aeronautics and Space Administration, 1969. Google-Books-ID: TfsfAAAAIAAJ

51. SAFARI, Ahmad and AKDOĞAN, E. Koray (eds.). *Piezoelectric and Acoustic Materials for Transducer Applications* [online]. Boston, MA : Springer US, 2008. [Accessed 18 December 2019]. ISBN 978-0-387-76538-9. Available from: http://link.springer.com/10.1007/978-0-387-76540-2

52. Products. [online]. [Accessed 18 December 2019]. Available from: http://www.kolomedical.com/products.html

53. EMADI, Arezoo and BUCHANAN, Douglas. Performance enhancement of an air-coupled multiple moving membrane capacitive micromachined ultrasonic transducer using an optimized middle plate configuration. *Journal of Micro/Nanolithography, MEMS, and MOEMS*. 20 December 2016. Vol. 15, no. 4, p. 045004. DOI 10.1117/1.JMM.15.4.045004.

54. KUPNIK, Mario, MIN-CHIEH HO, VAITHILINGAM, Srikant and KHURI-YAKUB, Butrus T. CMUTs for air coupled ultrasound with improved bandwidth. In : *2011 IEEE International Ultrasonics Symposium* [online]. Orlando, FL, USA : IEEE, October 2011. p. 592–595. [Accessed 13 September 2019]. ISBN 978-1-4577-1252-4. Available from: http://ieeexplore.ieee.org/document/6293544/

55. WYGANT, Ira O., KUPNIK, Mario and KHURI-YAKUB, Butrus T. CMUT design equations for optimizing noise figure and source pressure. In : *2016 IEEE International Ultrasonics Symposium (IUS)* [online]. Tours, France : IEEE, September 2016. p. 1–4. [Accessed 18 December 2019]. ISBN 978-1-4673-9897-8. Available from: http://ieeexplore.ieee.org/document/7728819/

56. Breakthrough Revolutionizes Ultrasound using Mechanical Engineering, Microfabrication and Novel Printing Process | UBC Mechanical Engineering. [online]. [Accessed 14 December 2019]. Available from: https://mech.ubc.ca/2018/10/17/breakthrough-revolutionizes-ultrasound/

57. GERARDO, Carlos D., CRETU, Edmond and ROHLING, Robert. Fabrication and testing of polymer-based capacitive micromachined ultrasound transducers for medical imaging. *Microsystems & Nanoengineering*. December 2018. Vol. 4, no. 1, p. 19. DOI 10.1038/s41378-018-0022-5.

58. JOSEPH, Jose, SINGH, Shiv Govind and VANJARI, Siva Rama Krishna. Fabrication of SU-8 based Capacitive Micromachined Ultrasonic Transducer for low frequency therapeutic applications. In : *2015 37th Annual International Conference of the IEEE Engineering in Medicine and Biology Society (EMBC)* [online]. Milan : IEEE, August 2015. p. 1365–1368. [Accessed 14 December 2019]. ISBN 978-1-4244-9271-8. Available from: https://ieeexplore.ieee.org/document/7318622/

59. CALIANO, Giosue, MATRONE, Giulia and SAVOIA, Alessandro Stuart. Biasing of Capacitive Micromachined Ultrasonic Transducers. *IEEE Transactions on Ultrasonics, Ferroelectrics, and Frequency Control*. February 2017. Vol. 64, no. 2, p. 402–413. DOI 10.1109/TUFFC.2016.2623221.

60. ERGUN, Arif S., YARALIOGLU, Goksen G. and KHURI-YAKUB, Butrus T. Capacitive Micromachined Ultrasonic Transducers: Theory and Technology. *Journal of Aerospace Engineering*. April 2003. Vol. 16, no. 2, p. 76–84. DOI 10.1061/(ASCE)0893-1321(2003)16:2(76).

61. CYCOM® 977-20 RTM - Solvay - datasheet. [online]. [Accessed 15 December 2019]. Available from: https://omnexus.specialchem.com/product/r-solvay-cycom-977-20-rtm

62. PICKETT, Anthony. *Process and Mechanical Modelling of Engineering Composites*. IFB, University Stuttgart, 2018. ISBN 978-3-9819539-1-6.

63. DATTA, Subhendu K. *Elastic Waves in Composite Media and Structures: With Applications to Ultrasonic Nondestructive Evaluation* [online]. 0. CRC Press, 2019. [Accessed 8 May 2019]. ISBN 978-1-4200-5339-5. Available from: https://www.taylorfrancis.com/books/9781420053395

64. PMGROUP. Vantage Systems. *Verasonics* [online]. [Accessed 18 December 2019]. Available from: https://verasonics.com/vantage-systems/

65. DAI, Wen, LIAN, Kun and WANG, Wanjun. A quantitative study on the adhesion property of cured SU-8 on various metallic surfaces. *Microsystem Technologies*. July 2005. Vol. 11, no. 7, p. 526–534. DOI 10.1007/s00542-005-0587-4.

66. MICRO RESIST TECHNOLOGY GMBH, MCC PRODUCTS. Omnicoat. [online]. [Accessed 13 January 2020]. Available from: https://www.microresist.de/en/products/mcc-products

67. MCGILL NANOTOOLS - MICROFAB. S1813 Spin Coating. [online]. [Accessed 12 January 2020]. Available from: http://mnm.physics.mcgill.ca/content/s1813-spin-coating

68. MICRO- NANO-FABRICATION SERVICES AT UBC VANCOUVER'S ANF. AZP4110 Process. [online]. [Accessed 13 January 2020]. Available from: https://www.nanofab.ubc.ca/processes/photolithography/az-p4110-process/

69. LNF WIKI. MF 319. [online]. [Accessed 13 January 2020]. Available from: http://lnf-wiki.eecs.umich.edu/wiki/MF_319

70. Microposit remover 1165 - eth - FIRST. [online]. [Accessed 13 January 2020]. Available from: https://www.yumpu.com/en/document/view/44139769/microposit-remover-1165-eth-first

71. Vibrometry - Technology - Polytec. [online]. [Accessed 13 January 2020]. Available from: https://www.polytec.com/int/vibrometry/technology/$laser-doppler-vibrometry/$scanning-vibrometry/

72. SHI, Xianjie, SHI, Dongyan, LI, Wen L and WANG, Qingshan. A unified method for free vibration analysis of circular, annular and sector plates with arbitrary boundary conditions. *Journal of Vibration and Control*. February 2016. Vol. 22, no. 2, p. 442–456. DOI 10.1177/1077546314533580.

73. LIU, Xin, YU, Yuanyu, WANG, Jiujiang, PUN, Sio Hang, VAI, Mang I and MAK, Peng Un. An Analytical Model for Bandwidth Enhancement of Air-Coupled Unsealed Helmholtz Structural CMUTs. *Journal of Sensors*. 17 April 2019. Vol. 2019, p. 1–16. DOI 10.1155/2019/3896965.

74. ZHANG, Wen, ZHANG, Hui, JIN, Shijiu and ZENG, Zhoumo. A Two-Dimensional CMUT Linear Array for Underwater Applications: Directivity Analysis and Design Optimization. *Journal of Sensors*. 2016. Vol. 2016, p. 1–8. DOI 10.1155/2016/5298197.

75. INGARD, Uno. On the Theory and Design of Acoustic Resonators. *The Journal of the Acoustical Society of America*. November 1953. Vol. 25, no. 6, p. 1037–1061. DOI 10.1121/1.1907235.

76. INGARD, K. Uno. *Notes on acoustics*. Hingham, Mass : Infinity Science Press, 2008. Physics series. ISBN 978-1-934015-08-7. QC225.15 .I56 2008

77. YAMANER, F. Yalcin, OLCUM, Selim, OGUZ, H. Kagan, BOZKURT, Ayhan, KOYMEN, Hayrettin and ATALAR, Abdullah. High-power CMUTs: design and experimental verification. *IEEE Transactions on Ultrasonics, Ferroelectrics, and Frequency Control*. June 2012. Vol. 59, no. 6, p. 1276–1284. DOI 10.1109/TUFFC.2012.2318.

7. Appendix

Statutory declaration and copyright for student works[1]

Herewith I, Welsch, Jonas, student number 2797609, living in Im Unterfeld 15, 76547 Sinzheim, grant the University of Stuttgart, Institute of Aircraft Design, a free, temporally and spatially unlimited, simple right of use for the bachelor's thesis/master's thesis or other student work with the title

PolyCMUTs for ultrasonic nondestructive testing of carbon fiber reinforced plastics – A feasibility study.

and the results of this work. I declare to have written this work independently and to have complied in the preparation of this work with the relevant terms, in particular with the copyright protection of third-party contributions. As far as my work contains external contributions (e.g. pictures, drawings, text passages), I declare that these contributions are marked as such (e.g. quotation, indication of source) and that I have obtained any necessary author's consent for the use of these contributions in my work. In the event of infringement of the rights of third parties through my work, I agree to compensate the University of Stuttgart for any resulting damage or to indemnify the University of Stuttgart against any third-party claims.

The right of use hereby granted to the University of Stuttgart extends to all known types of use and, in addition, the right to use the work results in research, teaching and study. This includes in particular the right of duplication and distribution, the right to process, modify and use of modified results as well as the right to make them publicly accessible on the internet and the right to transfer them to a third party without my renewed consent.

I am aware that granting the right of making my work publicly accessible also means that my name can be mentioned in connection with the title of the above-mentioned work on the websites of the University of Stuttgart. I am also aware that - if my work itself is not made accessible on the internet - the granting of the right to use public access also means that the University of Stuttgart can mention my name on its websites in connection with the title of the above-mentioned work (e.g. in lists of student work completed at the institute).

In addition, I transfer the ownership of a copy of my above-mentioned work to the University of Stuttgart, which I make available to the library of the Institute of Aircraft Design free of charge and grant the University of Stuttgart the above-mentioned rights of use for this copy as well.

Stuttgart, 17.12.2019

.....

Place, date, signature

[1] Based on the document „Einräumung von Nutzungsrechten an einer studentischen Arbeit“ of the central administration of the University of Stuttgart from 29.09.2016.